Non-intrusive Methods for Mode Estimation in Power Systems using Synchrophasors

Vedran Perić

UNIVERSIDAD PONTIFICIA
ICAI ICADE
COMILLAS
MADRID

TUDelft
Delft University of Technology

KTH
VETENSKAP
OCH KONST

Non-intrusive Methods for Mode Estimation in Power Systems using Synchrophasors

Vedran Perić

Thesis supervisors:

Dr. Luigi Vanfretti,   KTH Royal Institute of Technology

Dr. Xavier Bombois, Laboratoire Ampère UMR CNRS 5005, Ecole Centrale de Lyon

Dr. Cristian Rojas,   KTH Royal Institute of Technology

Members of the Examination Committee:

Prof. dr. Hans-Peter Nee, Chairman, KTH Royal Institute of Technology

Prof. dr. Luis Rouco,   Comillas Pontifical University

Dr. Marjan Popov,   Delft University of Technology

Prof. dr. Kjetil Uhlen,   Norwegian University of Science and Technology

Prof. dr. Mathias Bollen,   Luleå University of Technology

Prof. dr. Mani Venkatasubramanian, Opponent, Washington State University

Non-intrusive Methods for Mode Estimation in Power Systems using Synchrophasors

Proefschrift

ter verkrijging van de graad van doctor
aan de Technische Universiteit Delft,
op gezag van de Rector Magnificus prof. ir. K.C.A.M. Luyben,
voorzitter van het College voor Promoties
in het openbaar te verdedigen op dinsdag 15 maart 2016 om 13:00 uur

door

Vedran PERIĆ

Master in Electrical and Computer Engineering,

University of Novi Sad, Servië

geboren te Tuzla, Bosnië en Herzegovina

This dissertation has been approved by the promotors:

Prof.dr.ir. P.M. Herder and Dr. Luigi Vanfretti,

Composition of the doctoral committee:
Prof. dr. Hans-Peter Nee, Chairman, KTH Royal Institute of Technology
Prof.dr.ir. P.M. Herder,   Delft University of Technology
Dr. Luigi Vanfretti,   KTH Royal Institute of Technology

Independent members:
Prof. dr. Luis Rouco,   Comillas Pontifical University
Dr. Marjan Popov,   Delft University of Technology
Prof. dr. Kjetil Uhlen,   Norwegian University of Science and
Technology
Prof. dr. Mathias Bollen, Luleå University of Technology
Prof. dr. Mani Venkatasubramanian, Opponent, Washington State
University

The doctoral research has been carried out in the context of an agreement on joint doctoral supervision between Comillas Pontifical University, Madrid, Spain, KTH Royal Institute of Technology, Stockholm, Sweden and Delft University of Technology, the Netherlands.

Keywords: Synchrophasors, Phasor measurement units, system identification, mode estimation, electromechanical oscillations, prediction error, signal selection, experiment design, probing.

SETS Joint Doctorate

The Erasmus Mundus Joint Doctorate in *Sustainable Energy Technologies and Strategies*, SETS Joint Doctorate, is an international programme run by six institutions in cooperation:

- Comillas Pontifical University, Madrid, Spain
- Delft University of Technology, Delft, the Netherlands
- KTH Royal Institute of Technology, Stockholm, Sweden
- Florence School of Regulation, Florence, Italy
- Johns Hopkins University, Baltimore, USA
- University Paris-Sud 11, Paris, France

The Doctoral Degrees issued upon completion of the programme are issued by Comillas Pontifical University, Delft University of Technology, and KTH Royal Institute of Technology.

The Degree Certificates are giving reference to the joint programme. The doctoral candidates are jointly supervised, and must pass a joint examination procedure set up by the three institutions issuing the degrees.

This thesis is a part of the examination for the doctoral degree. The invested degrees are official in Spain, the Netherlands and Sweden respectively.

Abstract

The power system industry has been going through dynamic infrastructural and operational changes in recent years that have caused more prominent lightly damped electromechanical oscillations. Real-time monitoring of electromechanical oscillations is of great significance for power system operators; to this aim, software solutions (algorithms) that use synchrophasor measurements have been developed for this purpose. Mode estimation is widely accepted as one of the most important applications of wide area and measurement systems. This thesis investigates different approaches for improving mode estimation process by offering new methods and deepening the understanding of different stages in the mode estimation process.

One of the problems tackled in this thesis is the selection of synchrophasor signals used as the input for mode estimation. The proposed selection is performed using a quantitative criterion that is based on the variance of the critical mode estimate. This approach differs from the existing techniques based on heuristics or on the analysis of the observability matrix of the power system. The proposed criterion and associated selection method, offer a systematic and quantitative approach for PMU signal selection. It is shown that not only the power system model affects the decision on signal selection, but also the characteristics of the ambient noise excitation that is neglected in observability-based methods. In addition, it is shown that the signal selection problem is similar to the PMU placement problem for this particular application, which means that the proposed solution provides a way of including mode estimation requirements into a global PMU placement formulation.

The thesis also analyzes methods for model order selection used in mode estimation. Further, negative effects of forced oscillations and non-white noise load random changes on mode estimation results have been addressed by exploiting the intrinsic power system property that the characteristics of electromechanical modes are predominately determined by the power generation and transmission network.

An improved accuracy of the mode estimation process can be obtained by intentionally injecting a probing disturbance. It is shown that further improvement can be accomplished by adequately shaping the frequency spectrum of the probing signal. The thesis presents an optimization method that finds the optimal spectrum of the probing signals. In addition, the probing signal with the optimal spectrum is generated considering arbitrary time domain signal constraints that can be imposed by various probing signal generating devices.

Finally, the thesis provides a comprehensive description of a practical implementation of a real-time mode estimation tool. This includes description of the hardware, software architecture, graphical user interface, as well as details of the most important components such as the Statnett's SDK that allows easy access to synchrophasor data streams.

ii

Sammanfattning

Elkraftsbranschen har under de senaste åren undergått dynamiska förändringar som har orsakat tydligare elektromekaniska oscillationer med låg dämpning. Realtidsövervakning av elektromekaniska oscillationer är av stor betydelse för kraftsystemoperatörer och av denna anledning har mjukvarulösningar (algoritmer) utvecklats för detta ändamål. Det är allmänt erkänt att estimering av egenmoder är en av de mest viktiga tillämpningarna av WAMS, övervakningssystem för stora områden (engelska: wide-area measurement systems).

Ett av problemen i denna avhandling är hur insignaler från synkroniserade fasmätningar ska väljas för modestimeringen. Det föreslagna valet görs med ett nytt kriterium baserat på den mest kritiska modens varians. Denna tillnärmning på problemet medför ett paradigmskifte då tidigare föreslagna metoder för val av insignal har antingen baserats på ren heuristik eller på observerbarhetsanalys som har visat sig vara otillräcklig. Det påvisas att inte bara kraftsystemmodellen påverkar insignalvalet utan även karaktären på bruset i som exciterar systemet vilket bortses från i metoder som bygger på observerbarhet. Vidare visas det att insignalvalet liknar problemet med att placera fasmätningsenheter (PMUer) för detta ändamål, vilket betyder att den föreslagna lösningen ger ett sätt att inkludera behoven för modestimeringen i PMU-placeringsproblemet.

Denna avhandling analyserar också metoder för val av modellens ordningstal för modestimering. Vidare så behandlas även de negativa effekter på modestimering som tvungna svängningar och laständringar bestående av färgat brus innebär; dessa löses genom att utnyttja att karakteristiken hos de elektromekaniska egenmoderna är bestämda av transmissionsnätets egenskaper.

Förbättrad noggrannhet hos modestimeringen kan uppnås med att injicera systemet med en signal för sondering. Det visas att ökad noggrannhet kan uppnås med ett anpassat frekvensspektrum hos denna signal. Avhandlingen presenterar en optimeringsmetod som finner det optimala spektrumet för sondsignaler. I tillägg så genereras sondsignaler med optimala spektrum som tar hänsyn till godtyckliga begränsningar i tidsdomänen som kan orsakas av de apparater som generar signalen.

Slutligen så ger avhandlingen en fullödig beskrivning av en praktisk implementering av ett verktyg för modestimering i realtid. Detta inkluderar en beskrivning av den använda hårdvaran, mjukvaruarkitekturen och användargränssnittet samt detaljer av de viktigaste komponenterna, såsom Statnetts SDK för ett användarvänligt strömmande av synkroniserade fasvektormätningar.

Samenvatting

Recente veranderingen in de energie sector hebben tot gevolg dat er meer zwak gedempte electro-magnetische oscillaties voorkomen. Het real-time monitoren van dit soort oscillaties is erg waardevol voor electriciteitsnet beheerders. Voor dit doeleinde zijn algoritmen ontwikkeld die gebruik maken van synchrophasor metingen. Het is in het algemeen bekend dat de schatting van trillingsmodes een van de belangrijkste toepassingen is van meet systemen op grote schaal. In deze thesis worden verschillende technieken onderzocht om deze schatting te verbeteren door de oorzaak van mogelijke afwijkingen te identificeren. Daarnaast wordt in deze thesis de implementatie van de nieuwe methode uitgebreid behandeld.

Een van de problemen die worden behandeld is de selectie van synchrophasor signalen die worden gebruikt als ingrediënt voor de schatting van de trillingsmodes. De voorgestelde selectie wordt uitgevoerd aan de hand van een nieuw criterium dat is gebaseerd op de variantie van de schatting van de kritieke modes. Deze aanpak verschilt met de huidige procedures die gebaseerd zijn op ruwe schatting of op de analyse van de observability matrix van het elektrisch systeem. We laten zien dat niet alleen dit model van belang is bij de signaal selectie, maar ook de karakteristieken van de aanwezige ruis, hetgeen wordt genegeerd in de methoden gebaseerd op de observability matrix. Ook tonen we aan dat de signaal selectie lijkt op het probleem van PMU plaatsing, wat betekent dat de voorgestelde oplossing ook een manier voorziet om de eisen van de trillingsmodeschatting te omvatten in de globale PMU plaatsing.

De thesis analyseert ook methoden om de orde van het model dat voor de schatting van de trillingsmodes gebruikt wordt te kiezen. Ook worden de negatieve effecten van geforceerde oscillaties en gekleurde ruis aangepakt door gebruik te maken van de intrinsieke eigenschap van elektrische systemen dat de karakteristieke functies van elektromechanische systemen wordt gedomineerd door het transmissie gedeelte.

Een nauwkeurigheidsverbetering voor de schatting van trillingsmode kan worden behaald door opzettelijk verstoringen te veroorzaken met een sonde. We tonen aan dat verdere verbetering wordt behaald door het frequentie spectrum van deze verstoringen adequaat te kiezen. In de thesis wordt een optimalisatie methode uiteen gezet die het optimale frequentie spectrum van deze verstoringen bepaald. Daarnaast worden aanvullende beperkingen in het tijdsdomein (die voorkomen in dergelijke apparaten) ook beschouwd.

Ten slotte wordt een volledige beschrijving van de praktische implementatie van een real-time methode voor trillingsmodeschatting gegeven. Hierin wordt een beschrijving gegeven van de hardware, de software architectuur, de grafische user interface maar ook de benodigde details van de belangrijkste componenten, zoals Stattnet's SDK die gemakkelijke toegang verschaft tot de data van synchrophasors.

Acknowledgment

There are so many great people without whom this dissertation would not have been possible.

First and foremost, I would like to express my deepest gratitude to my supervisor Luigi Vanfretti, first for offering me this PhD position and later for the unconditional and friendly support throughout the studies. His unparalleled devotion to work and courageous approach to problems have taught me what leadership is all about. And the most important, he has shown me that being a good person is much more important that any research result or published paper. It was amazing having you as a supervisor.

I would like to thank my second supervisor Xavier Bombois for being a great friend from the first moment we met. It was a great experience working with someone who is so knowledgeable, organized and meticulous. Also, I have enjoyed our discussions about economy, politics and other social issues, even though we have not always agreed. Finally, I would like to thank my third supervisor, Cristian Rojas, for all the discussions that we had and for carefully reviewing the thesis. I really appreciate his impressive knowledge of mathematics and system identification, and moreover, his responsiveness and kind attitude.

I am thankful to Oleg for giving me the opportunity to continue the work in the area of wide area monitoring systems, which gave me additional motivation in the last several months.

Further, I would like to thank my professor Andrija Sarić for leading me through the first research steps, for encouraging me to pursue a research career and for offering his valuable help and advices whenever needed. I would like to thank my numerous friends from Brčko, Novi Sad and all around the world. It was always nice to make a break and meet up with the old friends.

It was great being a member of SmartTSLab. I would like to thank each and every one of you. I believe this is truly a unique research group. Especially, I am grateful to my office mates Almas and Tetiana for their sincere friendship and all the great time we have spent together. In addition, I would like to thank Hossein and Francisco for being great friends and for reviewing the thesis, and to Jan and Ronald for helping me with the Swedish and Dutch translations of the thesis abstract.

I express my gratitude to my Serbian friends from Stockholm who have made me feel more at home. Marina, Nemanja, Ognjen, Spasoje, Radovan, Tina and Jezidimir, thank you for your friendship. I am especially grateful to my relatives

"Knowledge is the golden ladder over which we climb to heaven; knowledge is the light which illuminates our path through this life and leads to a future life of everlasting glory."

— Mihajlo Idvorski Pupin

(A quation of Pupin's mother, Olimpiada Pupin, from his autobiography *From Immigrant to Inventor*)

x

Contents

Chapter 1

Introduction

1.1   Background

The power system industry has been going through dynamic infrastructural and operational changes in recent years, which have changed the way how the industry is functioning. Deregulation and competitive markets have been established with the aim to improve efficiency and to attract new investments. Fast developments in the semiconductor industry and Information and Communication Technology (ICT), together with the competitive market philosophy, have motivated research on how power system utilities can benefit from these new technologies. This research has opened opportunities for better monitoring and control of the system and consequently better efficiency. Last but not the least, an increased environmental awareness has brought large investments in renewable resources, which introduced dispersed and highly volatile power generation. All these changes impose new challenges that, in order to be adequately addressed, require a paradigm shift in power system operation.

One of the by-products of the ongoing changes in the power industry is that lightly damped electromechanical oscillations have become more pronounced. Electromechanical oscillations were initially caused by the introduction of high gain automatic voltage regulators, which are designed to overcome voltage stability problems in the power grid. Recently, the installation of large scale

renewable resources connected to the grid through power electronic converters has caused a reduction in the system's mechanical inertia. The reduced inertia makes the system more vulnerable to stability issues, including electromechanical oscillations. The volatile nature of renewable resources such as wind and solar power plants, together with uncertain market behavior, result in conditions that are often unpredictable for system operators. This means that the system might be operated in conditions for which it has not been designed, making it more vulnerable from the stability point of view. In order to ensure more reliable operation of the systems, large interconnected networks, such as Central European Grid (formerly UCTE grid), make plans for interconnections to other areas. These large areas, which are sometimes connected by relatively weak power lines, cause new electromechanical oscillations or boost the existing ones. Considering that lightly damped oscillations can be potentially dangerous, this has become a great concern for the power system community.

To analyze and control power system oscillations or even more generally, any other phenomenon in the system, it is necessary to obtain adequate models that describe the behavior of the phenomenon of interest. These models can be obtained in two ways:

1) Physical modeling,
2) Measurement based modeling.

This modeling classification is very general and can be applied for the analysis of arbitrary phenomena in arbitrary dynamical systems.

Physical modelling implies building models using laws of physics such as Kirchhoff's laws, Newton's law of motion, etc. These laws determine the model structure of the analyzed system, whereas the values of model parameters are determined from different experiments performed on each individual component of the system. These experiments are usually carried out by the component manufacturer and end-users are often supplied with the necessary parameter values.

Physical modelling is a well-studied area that provides deep insight into the actual nature of the dynamic system behavior such as electromechanical oscillations in power systems. However, this approach has the intrinsic weakness that the components change their properties (parameters) due to aging and/or changing operating conditions. This means that these models have to be updated frequently, which is a very cumbersome and costly procedure for power system utilities. Often, model updates are not economically feasible, which means that the available models are often inaccurate description of the reality. This weakness became obvious in power systems after the August 14, 2003 blackout in the Eastern US interconnection. During that blackout 50 million people were affected with a total load loss of 61,800 megawatts (MW). The estimated cost of the blackout was between 4 billion and 10 billion USD in the United States only

[1]. The post-mortem analyses with the existing models could not reproduce the event due to inaccurate modelling. This was especially the case for modelling of loads and generators. The result of this was that the utilities had to make large investments in obtaining more accurate models with the aim to analyze the incident and to design counter measures to prevent future blackouts. This was also the case in the 1996 outage on August 10 with more details provided in [2].

An alternative to physical modeling is measurement based modeling. Real time measurements provide accurate information about current system behavior. Consequently, this information can be used to obtain updated models that describe the current state of the system. This approach is relatively new and significantly less investigated in the literature, but it has a great potential to be used in power systems for analyses of complex phenomena, including but not limited to electromechanical oscillations. Generally, there are several challenges that the model estimation tools need to deal with (see also Fig. 1.1):

   1) *Large dimensions* of the problem,
   2) *Large amounts* of measurement data,
   3) *Uncertainty* in the estimated model,
   4) *Privacy* and data access,
   5) *Fast tracking* of model changes.

Most of these issues are coupled and contradictory by nature, i.e. the solution of one issue increases the complexity of the other. For instance, it is desirable to have models with high level of details, which requires large model dimensions, but this requirement implies that large amount of data is necessary for the estimation of such complex models. In the same fashion, a small model uncertainty implies that more information about the system is required, which leads to requiring a larger amount of data. A large amount of data makes data handling more difficult from the computational perspective but also from the cyber security perspective. The requirement of fast tracking on the other hand implies that fast numerical algorithms with shorter datasets should be used, which compromises the uncertainty of the estimated model. As a conclusion, it is obvious that an adequate solution will have to deal with large amounts of data collected in a short period of time, where the data is obtained by a potentially large number of sensors.

A breakthrough in power system operation was made by the development of synchrophasor technology. This technology provides vast amount of information about the system dynamics. Currently, in the US there are more than 1700 Phasor Measurement Units (PMUs) [3] while in China, full 500 kV transmission system observability has been accomplished for some years [4]. In addition, with further development of this technology it is reasonable to expect that even higher data reporting rates which will provide even more information about the system dynamics. However, it has to be noted that PMUs are not the only source of information to exploit and that other direct and indirect measurements, as well as

forecast techniques, can be used as an additional source of information that can contribute to better modeling of the system.
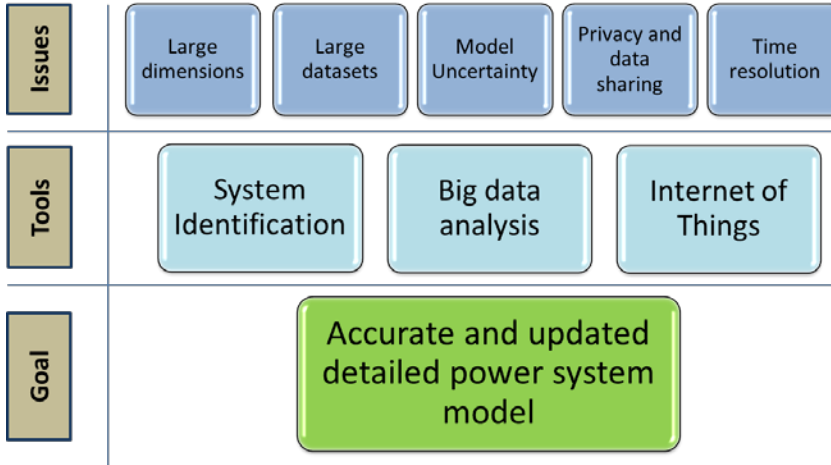
Fig. 1.1 Challenges and approaches in power system model estimation.

To solve the abovementioned issues a multidisciplinary approach is needed. Some of the research lines that are expected to give contribution in this field are big data analysis, internet of things, control theory and system identification, etc. Big data analysis is supposed to provide algorithms that are able to handle massive amounts of measured data. The Internet of Things concept might make access to these measured data even easier by solving privacy issues and making the deployment of different sensors easier.

This thesis, unfortunately, will not give answers to all the fundamental challenges raised in the previous paragraphs. However, there is a hope that the thesis will motivate further research in this very important area. In this thesis, the focus will be on electromechanical oscillations, which can be accurately described by low order models, thus significantly simplifying the overall problem. For instance, one oscillation is accurately described by one pole/mode of the dynamic system, which means that the sufficient model order for the description of inter-area modes in the system is two times the number of modes (the number of critical inter area modes is typically less than 5). The models that describe electromechanical oscillations are estimated using measured synchrophasor signals. The algorithms which use synchrophasor measurements to estimate critical modes (frequency and damping ratio) are often referred to as mode estimators.

Generally there are three groups of mode estimators:

1) Transient response (sometimes called ringdown),
2) Ambient response,
3) Probing.

This classification is based on the types of measured responses that are used for mode estimation. Transient response or ringdown mode estimators use data that are the result of some large disturbance in the system. This type of system response is called "natural system response" (or response due to initial conditions) and it is mainly determined by the poles of the system, which means that this response can be used for estimating the modes' frequency and damping. This can be achieved by fitting exponentially decayed sine waveforms to the measured response. Some of the popular approaches for this type of mode estimation are Prony analysis, the Eigenvalue Realization Algorithm (ERA), Matrix Pencil's etc. Under the assumption that only the linear part of the response is analyzed (appropriate data pre-processing is assumed) these methods are able to provide very accurate mode estimation results. The reason behind this fact is that given a strong system excitation, the measurement noise does not have significant effect on the mode estimator's accuracy.

However, in real-life operation, an occurrence of such a large disturbance is relatively rare, and moreover, unwanted. This means that operators cannot rely on this source of information for continuous mode tracking. Nevertheless, these methods are useful because they can provide fast and accurate estimates after a disturbance. These estimates can be used as the basis to take manual control actions or to trigger automated corrective actions. Another important application of these methods is post-mortem analyses, i.e. when analysis of past disturbances is needed, usually with the aim to develop long term actions that should prevent future disturbances of the same kind. These methods are extensively investigated in the literature and they will not be a topic of further discussion in this thesis.

Another approach to estimate modes is based on the system's *ambient response* that is omnipresent in all synchrophasor measurements. As it will be shown later, this ambient noise is *colored* by the system that creates it. This means that the ambient response carries information about the system, and consequently, information about the dominant system modes. A compromise between these two categories of mode estimation methods (ambient vs ringdown) has been found in methods that use a low magnitude probing signals as an excitation to the system. These methods are non-intrusive (do not jeopardize stability of the system by any means) but, due to the known excitation, are able to provide more accurate mode estimation results compared to ambient data-based methods. A low magnitude excitation (probing) can be generated by the following modulating signals:

1) Reference signals of automatic voltage regulators,
2) Reference signals in the control systems of FACTS devices (active and reactive power, voltage control, etc),
3) Reference signals of turbine governors.

The focus of this thesis is on non-intrusive mode estimation, meaning ambient data-based and probing methods. First, a literature review related to non-intrusive mode estimation methods will be provided, together with the gap analysis. Later, the thesis' contributions will be presented, whereas the following chapters will describe these contributions in detail.

1.2   Literature Review

This section describes state of the art of non-intrusive mode estimation methods. First, a short historical overview is provided, followed by a description of the basic principle of mode estimation algorithms. Further, different mode estimation algorithms are classified into several groups according to their properties, followed by a description of each group of methods. At the end, some challenges and alternative approaches are emphasized.

1.2.1   History of mode estimation in power systems

The need for obtaining power system models from measured data has been recognized in the industry for a long time. A substational effort has been put in understanding what information can be obtained from the measured data. This work was a basis for developing methods that are focused on the estimation of electromechanical oscillations.

In the late 1970s and 1980s, Bonneville Power Administration conducted field tests with the aim to gather more information about the dynamic behavior of the Western US power system. The first tests were conducted in 1977, when the system was intentionally perturbed by white noise disturbance signal [5]-[9]. The spectrum of the obtained measured signals was used to assess the dynamic behavior of the system. This assessment enabled an early detection of an emerged oscillation, which was reported in [8]. Further, these tests led to the development of tools for oscillation detection [10]. In parallel, more intrusive tests have been conducted with the aim to record system's response in case of a large disturbance. It was found that the Prony method is suitable for this application [11]. Other research also contributed to the solution of the model estimation problem. For example in [12], an ambient excitation is used to fit a simple model structure, and in [13] a transfer function of an individual element (a generator) was identified. In [14], a non-parametric method similar to the Empirical Transfer Function Estimate (EFTE) is used to fit the system response to a known excitation. In the second step of the proposed method the estimate is used for fitting to a model structure in the frequency domain. Online stability

assessment based on real time measurements was proposed quite early (in 1993) [15]. This initial approach exploited properties of the classical power system model. Later, online stability assessment has been investigated thoroughly, which will be described in detail in the sequel of this chapter.

In [16]-[19] ringdown signals were used for model identification. Soon, it was recognized that the models estimated from measurements can be used not only for stability assessment but also for power system control and controller design where the focus was on damping controller design. This application motivated research in this area with several notable results [20]-[25]. In addition to the classical control approaches, several authors investigated improving damping of the system by changing thy system operating points [26],[27]. As the significance of the mode estimation in power system became more relevant, an IEEE task force was established to provide a comprehensive treatment of different mode estimation approaches. A report produced as a result of the efforts of the task force has been published as a special IEEE publication [28]. Furthermore, the importance of dynamic system state tracking is emphasized in several general scope publications [20],[29]-[34]. An overview of possible applications (in addition to mode estimation) was presented in [35], where the FNET wide area measurement system developed at Virginia Tech and the University of Tennessee was used to analyze dynamic phenomena across North America.

1.2.2   Basic principles of ambient based mode estimation

Ambient mode estimation algorithms have been used in civil, aerospace and mechanical engineering since the 1970s [36]. But it was in 1997 when Pierre et al. published pioneering results about ambient based mode estimation [37], which established research foundation in this area. These methods gained popularity thanks to the introduction of synchrophasor technology that enabled an easy access to high sample-rate measurements [38]. In this subsection, the basic principle of ambient mode estimation methods is introduced, without describing particularities of different available methods.

During the steady state period, the power system behavior can be described by a linear Multiple Input Multiple Output (MIMO) model where the excitation driving the system is a product of random load switching. The assumptions of steady state and linearity are heavily exploited in the development of ambient mode estimation algorithms (even though there are methods that do not rely on this assumption). This assumption should not be seen as a limitation because in the case of non-steady state periods (presence of large disturbances), other methods developed for ringdown signals are more suitable. Therefore, the resulting power system model can be represented by Fig. 1.2.
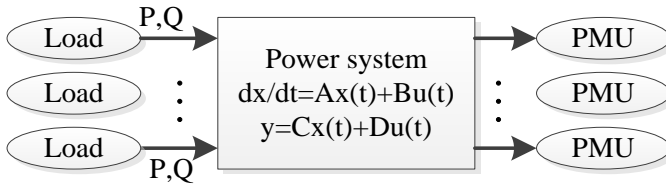
Fig. 1.2 Power system model during ambient condidtions.

If only one measurement variable is monitored (observed), it can be shown that the model can be described by a Single-Input Single-Output (SISO) model that has the same poles/modes as the original MIMO system (see Fig. 1.3).
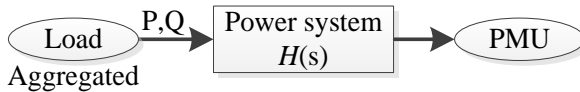
Fig. 1.3 Simplified SISO model of the system during ambient conditions.

This model is described by only one transfer function and the load represents the aggregated consumption of the whole power system. It can be assumed that this aggregated load has white noise characteristics. If observed in the frequency domain, this means that the power spectrum of the measured signal is proportional to the squared modulus of the system's frequency response.

Power spectrum of the aggregated load

Square of the frequency response of H(s)

Power spectrum of the measured signal
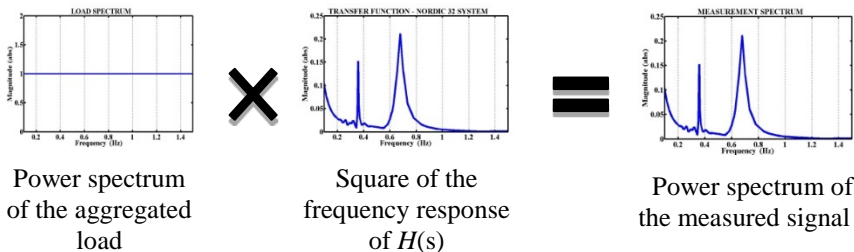
Fig. 1.4 Frequency domain representation of the system.

Furthermore, this means that it is possible to fit the coefficients of the transfer function to the measured power spectrum. Once the transfer function is determined, and using the property that the modes of the aggregated system (H(s)) are the same as the ones in the original MIMO system, it is easy to obtain values of the modes, i.e. their frequency and damping ratio. The only unanswered question here is how to carry out this fitting procedure. This can be

done in many ways, leading to different ambient based mode estimation algorithms.

In the case of probing, the only difference is that (in addition to the ambient excitation) at least one input signal is known (designed). Consequently, the underlying model of the system has to be fitted taking into account the probing (input) signals as well as the ambient response. As linearity has been implicitly assumed, the superposition principle can be exploited. This means that when probing, the measured (output) signal is composed of two components. The first component is a result of the ambient excitation (as explained above), and the second is a result of probing. This is illustrated in Fig. 1.5:
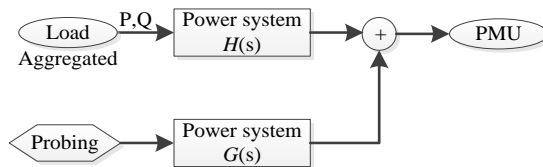
Fig. 1.5 Model of the sytem during probing tests.

It has to be noted that transfer functions H(s) and G(s) are not equal, which means that in order to obtain a full description of the system, both transfer functions have to be estimated.

1.2.3   Classification of mode estimation methods

As mentioned in the previous subsection, there are different approaches (i.e. algorithms) to obtain a mathematical description of the system, and consequently, critical electromechanical modes from measured data. These algorithms for mode estimation have different properties that can be used for their classification and analysis.

The first classification can be carried out by considering the method's ability to obtain modes when: 1) excitation is due to *ambient noise* and 2) the excitation is exactly known (*probing*). Further, signal processing and system identification algorithms can be generally categorized as *stationary* and *non-stationary*. Stationary methods assume that the properties of the underlying model do not change with time, while non-stationary methods attempt to capture how the system is changing in time, in addition to estimating the model parameters.

A model of the system can be obtained from a *block of data* (one model estimate is obtained with one data block) or the model can be *recursively* updated when a new measurement set becomes available. Recursive algorithms are in general more attractive for online applications due to their lower computational cost, however there is also a qualitative difference between these two groups of methods. In the case of recursive algorithms, a forgetting (penalty) factor is often applied to the data points that are further in the past, and thus, are

given exponentially lower importance. Conversely, block processing algorithms usually treat all the data in the block equally.

In addition to mode estimation (mode frequency and damping ratio) some algorithms are able to provide *estimates of mode shapes*. Information about modes shapes is useful to help determining which generators are involved in the observed oscillation. To be able to estimate mode shapes, it is necessary to use multiple measurements locations i.e. the estimated model must have multiple outputs. Some methods such as subspace identification provide this estimate at practically no additional cost, while in the case of other methods additional computation is required. The mode shape estimation topic will be covered separately in this chapter.

The main properties of different mode estimation algorithms are summarized in Table 1.1.

Table 1.1 Classification of mode estimation algorithms.

Property	Algorithm Type		
Excitation	Ambient	or	Probing
Stationarity	Stationary	or	Non-stationary
Computation type	Block Processing	or	Recursive
Mode shape estimation	Supported	or	Unsupported

It has to be noted that one group of mode estimation methods can have different properties (e.g. prediction error methods can have both block processing and recursive form, they can be designed either for probing or ambient excitation, provide mode shapes or not, etc). However, when considering stationarity, it is possible to clearly distinguish groups of methods that use the stationarity assumption from those that do not (because stationarity is an intrinsic property of the approach).

The following table (Table 1.2) lists different groups of methods classified as stationary or non-stationary methods.

Table 1.2 Stationary and non-stationary mode estimation algorithms.

Stationary	Non-stationary
Time-series analysis	Hilbert Huang Transform (HHT)
Subspace identification	Wavelet
Frequency domain analysis	Teager Kaiser operator
Ringdown from ambient	Koopman modes
Kalman filtering	Associate Hermite Expansion
Non-parametric methods	

These groups of methods will be discussed in more details in the sequel of this chapter.

1.2.4   Methods for mode estimation

The following paragraphs describe different methods and approaches for mode estimation. Namely, the following methods are covered:

1) Subspace identification methods,
2) Time series analysis,
3) Mode estimation algorithms based on Kalman filtering,
4) Frequency domain methods,
5) Non-parametric methods,
6) Ringdown mode estimation applied on signals constructed from ambient data,
7) Methods based on the Hilbert Huang Transform,
8) Methods based on Wavelets.

Each of these groups will be described shortly in the sequel and relevant references will be provided.

Subspace identification methods

Subspace identification methods have gained attention in the system identification community due to their robust implementations and the simplicity they offer in identifying MIMO systems. The main idea behind subspace methods is to extract a column space of the system's observability matrix. It can be shown that this column space contains information about the system that is, in the mathematical sense, similar to the original system (obtained using a similarity transformation). An important property that is exploited in mode estimation is that a similar system has the same eigenvalues as the original one.

The column space of the observability matrix is extracted from the data matrices that are created from measured data. The appealing property of subspace methods is that they provide the results by performing QR and SVD

decompositions, which are both numerically stable and efficient operations. This means that subspace methods are scalable, suitable for large models and large data sets. It is important to note that for ambient mode estimation stochastic subspace identification is used. This is due to the stochastic (ambient) excitation. A detailed theoretical description of subspace methods can be found in [39].

Application of subspace methods in power systems was proposed as early as 1996 [20], whereas the first application for mode estimation in power systems is presented in [40] and a more detailed analysis of subspace methods for this application is provided in [41]. Confidence intervals of the estimates obtained using subspace methods for ambient mode estimation are calculated using bootstrap methods in [42], whereas confidence intervals for probing mode estimation were proposed in [43]. A numerically efficient recursive method for subspace identification, where an SVD decomposition is not required in every iteration, is proposed in [44]. An improved bootstrap method is presented in [45]. A slightly modified stochastic subspace method is proposed in [46], while different subspace algorithms are tested in [47]; however, in these methods the stochastic part of the system was not considered.

Time series analysis

The theory of time series and spectral analysis is the basis for numerous mode estimation methods. One of the most popular approaches applied in power system mode estimation is to estimate AR(MA) models from the covariances that are estimated from data. The basis for these methods are the so called Yule-Walker equations, which are used to determine the coefficients of a rational transfer function of the underlying ARMA model, which can be written as:

$$y(k) = -\sum_{i=1}^{p} a_i y(k-i) + \sum_{j=0}^{q} b_j u(k-j) \,, \qquad (1.1)$$

where:

$y(k)$ – measured output signal at time point k;

$u(k)$ – random load input at time point k (assumed to be white noise);

a_i, b_j ($i=1,\dots,\ p$, and $j=0,\dots,\ q$) – unknown coefficients of the rational transfer function;

p, q – orders of the numerator and denumerator of the estimated rational transfer function, respectively.

Multiplying both sides of (1.1) by $y(k-q-l)$, $l=1,...,p$, taking the expected

value and using the definition of autocorrelation (r), the following matrix equation (known as the modified Yule-Walker equations) can be written:

$$\begin{bmatrix} r(q) & \cdots & r(q-p+1) \\ \vdots & & \vdots \\ r(q+p-1) & \cdots & r(q) \end{bmatrix} \begin{bmatrix} a_1 \\ \vdots \\ a_p \end{bmatrix} = - \begin{bmatrix} r(q+1) \\ \vdots \\ r(q+p) \end{bmatrix}. \tag{1.2}$$

Note that the following property is used in the derivation: $E\{u(k-j)\cdot y(k-q-l)\} = 0$, for $j<l+q$. The autocorrelations in (1.2) are estimated using (1.3):

$$r(n) = \frac{1}{N} \sum_{k=0}^{N-n-1} y(k+n)\,y(k). \tag{1.3}$$

The solutions of the system (1.2) are the autoregressive (AR) coefficients of the model, which are sufficient to compute the modes of the system. In case that the moving average (MA) part is also of interest, it can be computed using Durbin's method [48].

In power systems, this procedure has been the basis for development of a large number of methods. For instance, the first paper that uses estimation of AR model was published by Pierre [37]. In [49], the Yule-Walker and Burg methods were applied on low-voltage measurements. The use of block processing ARMA model estimation is demonstrated in [50]. In [51], the Yule-Walker method with Spectral analysis is proposed. This method differs from the original in the way how autocorrelation coefficients are calculated. Instead of (1.3), the autocorrelation coefficients in [51] are obtained as an inverse Fourier transform of the spectrum that is estimated using a non-parametric method such as Welch's method. The robust recursive least squares (RLS) method is introduced in [52], while a regularized robust RLS method is proposed in [53] where a dynamic regularization is introduced to help to include a priori knowledge about the system and reduce influence of under-determined problems. The robust approach helps to reduce the negative the influence of the so called non-typical data. It is important to note that the RLS algorithms are also suitable for probing mode estimation. The initialization of the regularized robust RLS method is discussed in [54]. Better numerical behavior of RLS algorithms is accomplished by using QR decomposition to triangularize the input data matrix [55].

The least means squares (LMS) adaptive filtering technique is introduced in [56] [57], while an adaptive step-size LMS is proposed in [58]. The performances of LMS adaptive filtering are improved by using the initial weight vector that is the estimated from an Autoregressive (AR) block processing method [59]. Optimal model order selection using the Bayesian Information Criterion (BIC) for this type of mode estimation is demonstrated in [60], whereas

in [61], the Akaike Information (AIC) and the Final Prediction Error (FPE) criteria are used. In addition, it is showed that FPE asymptotically approaches the AIC when the number of data points increases. Multichannel AR models with Yule-Walker equations are used in [62],[63]. Adaptive tracking RLS algorithms are proposed in [64] and [65] where the Kalman filtering theory is used. The Kalman filtering approach from [64] and [65] makes these methods suitable for the analysis of non-stationary signals. A comparison between the Yule-Walker and subspace methods was provided in [66]. It has to be noted that other signal processing techniques have been tested for mode estimation as well [67],[68].

A more general framework for parameter identification is provided through the so called prediction error theory. In contrast to classical time-series analysis, this theory was developed to incorporate probing excitation in addition to ambient excitation. However, most of the time series methods can be interpreted as a special case of prediction error methods. The first application of prediction error methods in power systems was reported in [69],[70], even though mode estimation was not in the focus of these publications. Instead, the goal was to capture slower dynamics (up to 0.5 Hz). Later, similar methods were applied for mode estimation. Due to the firm mathematical foundation of prediction error methods, they are able to provide straightforward estimate of the uncertainty of the estimated model. This property was used in several publications. In [71], the method for estimating confidence intervals was provided, whereas in [72] a recursive formulation was derived.

Mode estimation algorithms based on Kalman filtering

Kalman filtering is one of the most important estimation techniques in control theory. Naturally, Kalman filtering has been applied to solve different problems in power systems, including mode estimation. The application of Kalman filtering for mode estimation was reported in [73],[74]. Later, the extended Kalman filtering technique, which is able to handle time variant systems, is applied in [75]. In order to increase computational efficiency, a parallelized variant of the extended Kalman filter is developed in [76]. The Kalman filtering has also been applied to detect large disturbances in the system [77]. In this approach, the innovation part was tracked and a sudden change is used as an indicator that something has changed in the system's structure.

Frequency domain methods for mode estimation

Frequency domain methods provide mode estimates by fitting data in the frequency domain. The first application of frequency domain mode estimation was reported in [78], where the signal's spectrum is fitted to a second order

model structure. In [79], frequency domain data are used first to decouple different modes and then to fit such decoupled data to an appropriate model structure. A frequency domain decomposition that uses SVD to extract dominant modes was proposed in [80]. A distributed algorithm for frequency domain decomposition was developed in [81],[82]. The performances of the prediction error and least square frequency domain methods were compared in [83].

Non-parametric methods for mode estimation

Non-parametric methods estimate the power spectrum of a signal or the system's frequency response without fitting it to some predefined model structure. Instead, the spectrum is described with a frequency-by-frequency approach. In the power systems community, non-parametric methods were first applied for coherency identification [84], while the application for mode estimation came later. A non-parametric description of the system eliminates the possibility of errors caused by an inadequate model structure; however the analysis of such models is usually not trivial because there is no simple mathematical representation of the model.

Non-parametric methods offer a comprehensive visualization of the estimated modes as shown in [85]. Also, it is possible to estimate the damping ratios using non-parametric methods as it was demonstrated in [86] and [87]. The usage of orthogonal sliding windows with the aim to reduce the variance of the estimate was proposed in [88]. The application of non-parametric methods in a real-life environment was demonstrated in [89] with four different systems and in the Japanese network [90].

Ringdown mode estimation applied to signals constructed from ambient data

The autocorrelation sequence of measured data implicitly contains information about the generating system's frequency response. This fact can be seen from the following known relationship:

$$y(t) = h(t) * u(t),$$
(1.4)

where $y(t)$ is the output , $h(t)$ is the system impulse response, and $u(t)$ is the input signal, which is assumed to be white noise. This equation can be expressed in terms of correlations, as follows:

$$r_{yy}(k) = h(t) * r_{xy}(k) = h(t) * h(-t) * r_{xx}(k)$$
(1.5)

where $r_{xx}(k)$ and $r_{yy}(t)$ are the autocorrelation sequences of the input and output, respectively, and, $r_{xy}(k)$ is the cross-correlation between the input and output. Because $r_{xx}(k)$ is considered to be a delta impulse, i.e. the identity element for convolution, the autocorrelation of the measured output is actually the natural system response on the previous bounded excitation that is mathematically (but not physically) equal to $h(-t)$. Note that the system is assumed to be causal.

This fact means that the autocorrelation sequence can be used as an input to ringdown mode estimation algorithms such as the Prony or the Eigensystem Realization Algorithm (ERA). Therefore, these algorithms essentially have two steps, where the first step computes the autocorrelation sequence and in the second step well-known ringdown analysis methods are applied. This approach was first applied in [91], where Prony's method is used, whereas [92] employs the ERA method. In [93] the random decrement technique, which is an efficient way to compute the autocorrelation sequences, is used as the first step, while the Wavelet Transform based mode estimation is used in the second step. The random decrement technique was also applied together with Independent Component Analysis in [94].

Methods based on the Hilbert Huang Transform

The dynamic behavior of power systems can be very complex. The methods discussed before assume stationarity of the system, i.e. the system does not change during the mode estimation process. However, this assumption might not be fully satisfied in reality, which is the motivation for treating signals as non-stationary that can contribute to better overall estimation accuracy.

The Hilbert transform is probably the most popular technique for the analysis of non-stationary signals. The main characteristic of the Hilbert transform is that, in contrast to the Fourier transform, it also provides information on how frequency components change over time. Because the application of the Hilbert transform on raw data usually provides a large number of components that are difficult to interpret, empirical mode decomposition is applied with the aim to differentiate a finite number of oscillatory modes (intrinsic mode functions - IMF). IMF is defined as a function that has the same number of extrema as zero crossings, and which satisfies the following condition:

$$\frac{1}{\varepsilon} \int_{t-\frac{\varepsilon}{2}}^{t+\frac{\varepsilon}{2}} IMF(r)\,dr = 0\,, \tag{1.6}$$

where ε is arbitrarily chosen and t a point in time. With these properties IMF signals will have slowly varying amplitudes and phases, what makes them more appealing for the Hilbert spectrum analysis. These two methods combined (Empirical Mode Decomposition and Hilbert Transform) constitute the Hilbert Huang Transform (HHT). The main idea behind this decomposition is that components should represent phenomena that are occurring on different frequency scales. The main disadvantage of EMD is that it is a heuristic method, i.e. there is no formal mathematical proof that it really separates different frequency components. A detailed description of the HHT method can be found in [95].

The first attempts to apply the HHT for the analysis of electromechanical oscillations in power systems was reported in [96] and [97], where the focus was on visualization and result interpretation. In order to improve the performance of the HHT affected by mode mixing, masking techniques were developed and applied in [98]. A method to estimate the critical mode's damping ratio using HHT was proposed in [99]. A more general discussion on how to use HHT techniques for measurements in power system was provided in [100]. In this paper two analytical approaches to examine nonstationarity features are investigated. The first method is based on selective Empirical Mode Decomposition of measured data. The second is based on wavelet shrinkage analysis. In addition, experience with the application of these techniques to quantify and extract nonlinear trends and time-varying behavior is discussed, and the physical interpretation of the proposed algorithms is provided. A discussion on how to separate different frequency components from the measured signals using the HHT is given in [101].

In [102], an improvement of HHT is proposed. First, a local implementation of the EMD is proposed and second, the HT is computed using variable window filters. A modified HHT method with the use of wavelets was proposed in [103]. In [104], the HHT method is used to locate sources of oscillations. This information was used to design local control actions that contribute to improved system damping. A method that ensures the continuity of residuals during sliding estimation was proposed in [105]. This property helps obtaining more stable results because it prevents the time-consecutive IMFs to differ drastically. An improved method that addresses problems related to mode mixing and the "end effect" was proposed in [106]. In this paper, the Symmetrical Extreme Extension (SEE) method was employed to expand the original signal during the processing of EMD and the frequency heterodyne technique was used to overcome the mode-mixing phenomena. In [107], a two level decomposition was used instead of EMD with the aim to solve the mode mixing problem. In addition, the normalized Hilbert Transform was used to address the Gibbs Phenomenon of the traditional Hilbert transform. In [108], empirical orthogonal functions were used to extract dynamic patterns of the system that can be analyzed instead of raw data. Another method based on EMD to remove the trends from the measured

data was proposed in [109]. A comprehensive description of the application of the HHT method in the Japanese grid was reported in [110].

Wavelets methods

The wavelet transform is another popular technique for time-frequency analysis of signals. This technique treats different frequency components differently, resulting a good compromise between time and frequency resolution.

The performance of wavelet-based mode estimation methods has been assessed in [111]. Considerations for wavelet selection were discussed in [112]. A more general discussion on the applicability of the wavelet transform for mode estimation is given in [113]. In [114], the wavelet transform, together with empirical orthogonal decomposition, was used to identify and extract relevant dynamical spatio-temporal patterns in measured signals. Other applications of wavelet transforms have been investigated as well, for instance, coherency identification [115] and mode estimation using ringdown responses [116],[117].

1.2.5   *Mode estimation performances and applications*

In order to find the most suitable among all the methods that have been developed, it is essential to fairly assess the performance of each method. This task is generally very complicated because measured data might have different properties in different systems. For that reason, it is necessary to establish methods for comparing different mode estimation algorithms. The first step in that direction was reported in [118], however further research in this area is needed. Several publications have compared the performance of different mode estimation algorithms with the aim to provide better understanding of the methods [119]-[123]. These comparisons are valuable because the understanding of different properties opens the possibility to combine different methods with the goal to improve overall mode estimation [124].

The theoretical development of methods for mode estimation was followed by practical implementations. The experience gained from these analyses in real-life conditions has provided a new understanding of power system behavior. For instance, the authors in [125] attempt to characterize ambient conditions in power systems in order to better understand its behavior. In addition, analyses in real life conditions have provided understanding of the market value of mode estimation products. Many practical mode estimation implementations have been reported in the literature, and they are discussed in the sequel.

In [126],[127],[128], the experience in the Nordic region is presented where subspace and Kalman based mode estimators were used. A description of the different decision support tools and challenges in implementation of wide area system was discussed in [129]. An attempt to reconstruct a model of the WECC

system using PMU measurements (even though a simplified model) was reported in [130]. The Oscillation Monitoring System (OMS) implemented into the Phasor Data Concentrator at Tennessee Valley Authority was described in [131]. In this system, a frequency domain decomposition is used for ambient data processing, while the event detection is used to trigger Prony analysis of ringdown signals. A system stability monitoring and control developed by Bonneville Power Administration (BPA), Ciber Inc. and Washington State University (WSU) was described in [132].

A detailed description of the Brazilian wide area measurement system was provided in [133]. Data collected with this system were later used for the validation of the model of the Brazilian power system using ambient, rindown and probing signals [134]. A subspace identification method for real time mode estimation in Brazilian system was reported in [135].

An application of parametric (Yule-Walker) and non-parametric methods for mode estimation in the Danish grid was reported in [136]. A similar study has been extended for four different power systems (namely WECC, Eastern US interconnection, Nigerian and Danish system) [89]. A non-parametric FFT-based method was applied in the Singaporean-Malaysian power system [137]. Monitoring of electromechanical oscillations in the European grid using a commercial wide area measurement system was reported in [138]. Oscillation monitoring using the FNET system, which has been developed at Virginia Tech and the University of Tennessee, was reported in [139],[140],[141]. Experience with mode frequency and damping estimation in the Norwegian grid was presented in [142]. Different practical issues in oscillation monitoring were discussed in [143], where a statistical approach for analysis was proposed. Mode estimation in Finland using the random decrement technique and the wavelet transform was described in [93], as well as the Finnish wide area measurement system. A damping controller installed in the Chinese grid that is tuned using the model identified from ambient data was described in [144]. One implementation of a graphical user interface for mode estimation was presented in [145].

1.2.6   Mode shape estimation algorithms

In addition to estimating the critical mode's frequency and damping ratio, it is also helpful to know the dominant path of the oscillation as well as elements (generators) that are involved in the oscillation. This information is contained in the mode shapes.

Generally speaking, in order to estimate mode shapes it is necessary to use multiple measurements to determine how different elements contribute to the oscillation. In [146], mode shapes were estimated using spectral correlation analysis. The communication method and channel matching methods were introduced in [147] and [148]. Mode shape estimation based on estimates of transfer functions was formulated in [149] and a two-variable ARMA model for

eigenvector estimation was presented in [150]. A non-parametric recursive implementation of spectral correlation based mode shape estimation algorithm was developed in [151]. Mode shapes can also be estimated from ringdown signals as demonstrated in [152], where pre-filtering and correlation analysis were used. Mode shape estimation from probing tests using the empirical transfer function estimate (ETFE) technique was proposed in [153]. The difference in this paper compared to other non-parametric based estimators is that the probing signals are available, therefore instead of estimating the spectrum of the signal, the ETFE technique is used. Mode shape estimation using prediction error methods with an ARMAX model was proposed in [154], a similar approach was used in [155] where a SIMO model was estimated using the prediction error method. Application of the wavelet transform for mode shape estimation was introduced in [156]. A comprehensive comparison of mode shape estimation methods was reported in [157].

1.2.7   Probing methods

As stated before, the idea to intentionally excite the system and to use the measured response in order to estimate dynamic properties of the system is relatively old [5],[158]. However, most of these approaches required large disturbances in the system. In [159], an application of system identification methods with low power excitation is introduced with the aim to improve ambient based estimation. The consequence of using this type of excitation is that input-output identification methods are used instead of the output only methods required for ambient based methods. However, it has to be noted that in contrast to ringdown methods, the ambient excitation in this case cannot be neglected.

A method for determining confidence intervals of the estimates from probing tests using the bootstrap method and subspace identification was proposed in [43]. This approach is very similar to the bootstrap method originally proposed for ambient based mode estimation but it was demonstrated that the same approach can be applied for probing tests. The shape (profile) of the time domain probing signals affects the performance of the mode estimator. This property was analyzed in [160],[161] where a probing signal design procedure was proposed. An idea to use several generators for probing was proposed in [162] with the aim of increasing the power of the probing signal, which in case of a single generator can be constrained by the probing equipment. Different subspace methods for probing based mode estimation were tested in [163].

1.2.8   Other research lines

In the previous text, an overview of mode and mode shape estimation methods has been discussed. In addition to these methods, other research directions have contributed to a better understanding of the system dynamics from measured

data. A short overview of the research topics related to mode estimation is given in the sequel.

In [164], as well as in [130],[165]-[168] a full model of the power system was identified using measured data. To this aim, a simplified model structure is used (classical representation). All mode estimation algorithms discussed above are based on open-loop identification algorithms; in [169],[170] a closed-loop identification approach has been investigated. Prior knowledge of the system can be included to improve identification results. For instance in [171], a Bayesian framework is used to estimate a second order model of the system. A very interesting two stage model identification approach was proposed in [172], where the local systems are first estimated and later merged to form a model of the entire system. The importance of locating the sources and causes of electromechanical oscillations was emphasized in [173] where one method for that purpose was proposed.

Even though the damping ratio has been the most widely used small signal stability criterion, some authors proposed other stability indices [174],[175],[176]. For example, the identification of the damping torque instead of the mode's damping ratio estimation was proposed in [177]. The identification of trends in measured data using structural time series models was proposed in [178]. In [179], the complex-singular value decomposition (C-SVD) method is applied on the ensemble matrix (matrix constructed from the measured signals) with the aim to describe both temporal evolution and spatial distribution of the dominant oscillation mode. In [180], an effort has been made to characterize the system state that precedes a large system disturbance. In order to make use of all available measurements, the data fusion approach has been proposed in [181]. An attempt to treat power oscillations as waves that are spreading through the system was proposed in [182]. A method that fits the measured data to an orthogonal polynomial expansion was proposed in [183],[184]. Finally, mode estimation using the Teager-Kaiser energy operator was proposed in [185].

1.3   Challenges in Mode Estimation

The previous subsection provided a general overview of the methods for non-intrusive mode estimation, as well as some challenges that have been successfully addressed to some extent. It can be noticed that a large number of methods have been developed and their characteristics are generally well understood. However, in order to commercialize these tools, it is necessary to address some additional issues that can corrupt the final mode estimation results. These topics are briefly described in the sequel, and some of them are discussed in more details throughout the thesis.

1.3.1   Relevant measured signals

By observing a full order model of the system (Fig. 1.2), it is obvious that every measured signal, i.e. its power spectrum, can be described by a transfer function whose denominator corresponds to the characteristic polynomial of the full order system. However, it can be shown that many measured signals (due to different numerators and zero pole cancelations) do not contain relevant information about the critical mode of interest, which leads to the conclusion that a large amount of data handling can be avoided by using low order system models and relatively few signals from certain locations where the observability of the critical mode is better.

However, the approach of using low order models, despite all benefits, has one major disadvantage. Namely, estimated low order models contain a certain amount of intrinsic bias, which results with biased estimated parameter values (such as damping ratio). In addition, this bias is difficult to assess and has a different value for each signal used in the identification. This means that the estimated critical modes depend on the signals used for the identification, i.e. some critical modes might not be extracted from some signals. Therefore, it is necessary to select appropriate signals for mode estimation in order to obtain accurate results. This can be achieved by characterizing signals according to their properties and purpose. The problem of signal selection is especially difficult in the case of MIMO system identification. It has to be noted that it is not only the location that has to be selected but also the signal type (voltage, current, power etc.). These problems are partially addressed in this thesis.

Properties of different signals for monitoring of events were first discussed in [186]. Signal selection method for mode estimation is explicitly discussed in [187]. In this paper a method for signal selection based on "modal power contribution" as a ranking criterion is proposed. The modal power contribution is defined as the part of the power spectrum that is directly related to the critical mode of interest. The higher value of modal power contribution implies that signal is a better choice for mode estimation. In [188], two new ranking criteria have been proposed. These criteria are also based on the shape of the power spectrum where their geometrical properties were used for the formulation. The basic idea behind these criteria is that signals which have peaks in the power spectrum at the critical mode frequency are good choices for mode estimation. In [189], a classical power system model was used to define Cramer-Rao bounds for different measured signals with the aim to estimate the power system parameters. It has to be noted that some authors focused on selecting the optimal signals that can improve oscillation damping control (such as Power Oscillation Damper), rather than to improve mode estimation for monitoring purposes, for instance in [190].

In the case of probing mode estimation, the optimal signal selection should determine the probing signal as well as measured signals (in contrast to the ambient signal selection where only measured signals are determined), which leaves space for additional performance improvements.

The previously mentioned approaches for the selection of relevant measurements are based on the system's structure; however, other parameters can be taken into consideration, such as measurement noise, reliability and robustness. In addition, it is important to analyze other properties of critical modes, such as their sensitivity to different operational parameters. Finally, a strict requirement for mode estimation methods is to ensure sufficient confidence in the obtained results. The problem of the result confidence is discussed further in the thesis.

1.3.2   Forced oscillations

The forced oscillation phenomena in power systems have sporadically appeared in the literature over the last 40 years [191]. There are different sources of these oscillations. Xuanyin et al. [192] report that the regulation system of steam turbines can cause this kind of oscillatory behavior. Other authors have investigated the impact of cyclic loads in the system [191],[193]. Vournas et al. report, in [194], diesel generators as one of the possible causes for forced low-frequency oscillations. Regardless of the cause, all types of forced oscillations have some common characteristics which can be used for their identification. Considering that a forced oscillation is a permanent vibration with a specific frequency, its spectrum is characterized by a very narrow high amplitude peak. This can be concluded from the fact that an undamped sine signal is represented by a Dirac delta function in the frequency domain. A more detailed discussion on forced oscillations caused by cyclic loads was presented in [195]. A method for identifying causes of forced oscillations that relies on the clustering approach was reported in [173]. A similar problem was addressed in [196] by graph theory. Effects of forced oscillations on mode estimation results and mode shape estimation were analyzed in [87] and [197], respectively. These analyses show that they can severely corrupt mode estimation results and that new mode meter estimators need to be able to provide accurate results even when in the presence of forced oscillations. One approach for tackling negative effects of forced oscillations on mode estimation is proposed in this thesis.

1.3.3   Efficiency of processing large amount of data

With the current trend of deploying a large number of PMUs in power systems, it is obvious that a modern wide area monitoring system has to be capable of receiving, transmitting and processing a large amount of data in a secure, reliable and fast way. Security and reliability of the data storage and transfer is a popular research topic within the ICT research community. One approach to increase computational efficiency and reduce the required data

bandwidth, was addressed using distributed computation as presented in [81],[82],[198]. This approach assumes that mode estimation is should be performed locally at each substation of interest, whereas the global (optimal) results at the central level can be obtained using the local results that are transmitted with significantly reduced bandwidth in comparison with raw measured data. Despite this and similar contributions, more efforts are necessary to develop fast, secure and reliable mode estimation.

1.4   Contributions of This Thesis

The focus of this research was to improve existing mode estimation tools and to address some issues related to the application of these tools. In addition, the aim was to introduce new paradigms and approaches in dealing with mode estimation. The contribution of the thesis can be classified into five domains that also follow the structure of the thesis:

1) Optimal signal selection and optimal PMU placement for mode estimation,
2) Mode estimation considering arbitrary spectral load characteristics,
3) Optimal probing signal design,
4) Optimal model order selection,
5) Practical implementation of a real-time mode estimator for research purposes.

Each of these topics will be covered in a separate chapter and this section will describe briefly the main points made in the thesis.

1.4.1   Optimal signal selection and optimal PMU placement for mode estimation

The common problem that power system operators face in utilizing mode estimation tools is to choose synchrophasor signals that have "sufficient" information about the monitored critical mode. Heuristically, there is a common understanding about some of the properties of good signal candidates, such as peaks in the signals' spectra at the frequency of the mode and location of the signal with respect to the mode's dominant path. However, these means of quantifying the signals' relevance are based on experience and do not provide a mathematically formal description and deeper insight in the signals' properties.

This thesis formulates a numerical criterion that describes the signals' suitability for the mode estimation. This criterion is formulated as the estimation variance of the critical damping ratio. Furthermore, a numerically efficient algorithm to compute the criterion is presented, as well as a fast (approximate) criterion that is used screening signals. These criteria are used to formulate the

optimal signal selection criterion. In addition, the relationship between the defined criteria and the signal spectrum shape is discussed in more detail.

The proposed signal selection method is discussed in Chapter 2, and the method with application examples has been published in a paper in the IEEE Transactions on Power systems [199].

1.4.2 Mode estimation considering arbitrary spectral load characteristics

Ambient based mode estimation exploits the property that the power system is continuously excited by random load changes. It has been hypothesized that it is valid to model these random load changes as white noise. This hypothesis is crucial because it enables the extraction of the power system transfer function from the measured synchrophasor measurements. Unfortunately, by analyzing real-life synchrophasor measurements, it can be noticed that this assumption is not always fully satisfied. This phenomenon is particularly important in the case of the so-called forced oscillations which represent an obvious violation of the white noise assumption.

This thesis proposes a mode estimation algorithm that relaxes the white noise assumption, meaning that good estimation results can be guaranteed regardless of the spectral load characteristics. This is possible if a sufficient number of synchrophasors is available in the system. The proposed procedure is based on the power system separation of the dominant transmission part from the less important distribution part of the system, where emphasis is accordingly given to ensure accurate estimation results of the transmission network modes. Furthermore, if full measurement observability is not available, a method for the reconstruction of the necessary synchrophasor signals is proposed.

The proposed mode estimation method that includes spectral load characteristics is discussed in Chapter 3, and the method with application examples has been published in a paper in the IEEE Transactions on Power systems [200].

1.4.3 Model order selection for mode estimation

Mode estimation methods can be broadly classified as parametric or non-parametric methods. Non-parametric methods generally do not require complex parameter tuning, which makes them easy to use and attractive when obtaining initial mode estimates. In contrast, parametric methods, when the underlying model structure is properly selected, can provide more accurate results as well as deeper insight into the mode estimation process.

Different parametric mode estimation methods have different set of estimation parameters that have to be selected. One of the most important parameters is the

model order of a predefined model structure to which the system response is fitted.

The problem of optimal model order selection has been investigated extensively in the control and signal processing community and these methods are evaluated in this thesis from the perspective of mode estimation in power systems. The methods analyzed in this thesis are: 1) Residual analysis for model order selection, 2) Model order selection-based on singular values, 3) Akaike Information Criterion, 4) Variance-Accounted-For (VAF) as a measure of optimal fitting between measured data and the model's response.

A comparison of different methods for optimal model order selection is provided in Chapter 4. The main results of this comparison have been published in a paper presented at the Power and Energy Conference at Illinois [201].

1.4.4   Optimal probing signal design

Ambient based methods rely on the omnipresent excitation of random load changes. This property makes these methods very attractive because of their simple implementation, i.e. they only require measured signals that are easily available through a WAMS system. However, a disadvantage of this group of methods is their limited accuracy. Namely, accuracy is determined by the intrinsic properties of the power system (level of ambient noise, level of measurement noise, etc.) and the power system operators are generally not able to influence these parameters.

Improved accuracy can be obtained by intentionally introducing a disturbance to the system, where a large disturbance, i.e. large power of the probing signal generally, leads to improved mode estimation results.

The main contribution of this thesis is that it provides a relationship between mode estimation accuracy and the properties of the probing signal. It is shown that the accuracy depends only on the spectrum of the probing signal and not on the time domain signal realization.

This relationship is used to formulate the optimal probing signal design problem, where the power of the probing signal and level of the system disturbance is minimized, whereas the desired mode accuracy is treated as a constraint. The result of this Linear Matrix Inequality (LMI) optimization is the optimal spectrum of the probing signal that can be parameterized as a multisine or continuous spectrum. Further, three different methods have been used for the time domain realization of the probing signal. Emphasis is given to the newly developed method that is able to easily take into account different time domain constraints that can be imposed by probing devices.

It is shown that the proposed method for optimal probing signal design is able to provide the same mode estimation accuracy while requiring less excitation (5-

7 times weaker) in comparison when all frequencies are equally excited. Equivalently, the proposed methodology provides 4-5 times better mode estimation accuracy when the probing signal is optimally shaped in comparison with the white noise probing signal of the same power.

A detailed description of the probing signal design procedure is given in Chapter 5, whereas the most important results are being prepared for publication as a journal paper.

1.4.5   Practical implementation of a real-time mode estimator for research purposes

The focus of this thesis was to contribute with theoretical advancements to enhance the mode estimation process. However, a practical implementation of such algorithms imposes additional challenges that need to be addressed as well. To address such kind of challenges, it is necessary to perform testing integrated mode estimation solutions that include physical Phasor Measurement Units and ICT systems that are fundamental elements of wide area monitoring system (i.e. mode estimation system).

To demonstrate a practical implementation of a mode estimator, the Statnett's Synchrophasor Software Development Kit (SDK) was used as an interpreter of the IEEE C.37.118 protocol, which enabled easy access to the measured synchrophasor data. The mode estimation algorithm itself was implemented in the LabVIEW environment using a state machine software architecture. The developed mode estimation application was tested using synthesized and real synchrophasor measurements.

More details on the practical mode estimator implementation are given in Chapter 6, whereas the main results are published as a conference paper and were presented at Clemson University's Power System Conference [202].

Chapter 2

Optimal Signal Selection and PMU Placement for Mode Estimation

2.1   Introduction

In recent years there has been a trend of increasing the number of PMU installations in power systems, leading to higher degrees of observability in different systems. However, because not all synchrophasor signals contain an equal amount of information about the critical mode of interest, it can be shown that only a limited number of carefully selected signals contain sufficient information for accurate mode estimation. Furthermore, concurrent use of a large number of signals leads to estimation bias as well as higher computational complexity that may not be suitable for online applications. This reasoning poses the research question of optimal signal selection for mode estimation. The first attempts to address this question have been presented in [187] and [188]. In [187], a Modal Power Contribution (MPC) metric is proposed as a signal selection criterion, while in [188], suitable signals are selected based on the geometry of the signals' power spectra. In the more recent papers [82] and [198], two level algorithms for mode estimation have been proposed. In these papers, signals contribute to the final mode estimation according to their weighting factors that represent signals' quality. In [82], the weighting factor is defined as the Fourier Transform magnitude at the critical mode's frequency, whereas in [198], the mode energy is used instead. The means for quantifying the signals'

relevance for mode estimation (either signal selection criteria [187],[188] or weighting factors [82],[198]) have been developed using heuristics that do not offer a formal proof that the selected signals provide the best possible mode estimation results.

The problem of optimal signal selection can be also seen as a problem of optimal PMU placement for mode estimation with the question of where to install the PMUs to obtain the best possible estimation of the critical mode. To the author's best knowledge, this question has not been formulated, even though optimal PMU placement (for other applications such as state estimation and stability assessment) has been investigated in the literature [203],[204]. In the traditional PMU placement problem formulations, the optimization criterion is mainly defined as maximum observability. This observability is defined either in terms of numerical observability or topological observability [204]. However, the methods developed do not provide information about the optimal signals that should be used to obtain accurate mode estimation results.

An estimate of the critical mode's damping ratio can be seen as a realization of a random variable whose variance depends on the signal that is selected as an input to the mode estimator. Therefore, if an unbiased mode estimator is used, *the best signal for mode estimation is the one that provides the smallest variance of the critical mode's damping ratio*. This means that the variance represents the key numerical criterion for ranking the signals according to their quality for mode estimation.

This chapter provides a formal algorithm to compute an estimate of the (asymptotic) variance of the critical parameter estimates for each signal; under the assumption that the signals' power spectra are known in the form of AutoRegressive Moving Average (ARMA) models. The best signals (for mode estimation) are then determined by ranking the signals according to the calculated variances. This algorithm has its foundation in a theorem that gives a formula for the parameter covariance matrix (and consequently the variances of interest) of an arbitrary model parameterization.

The proposed algorithm has the advantage that it uses only parameters of the ARMA models as an input to the algorithm. This makes the variance computation independent of the method used to determine the ARMA models. In the case of off-line PMU placement (for mode estimation), the ARMA models can be obtained from the existing physical power system model (off-line simulation). On the other hand, in the case of selecting the best from the set of available synchrophasor measurements, any identification method can be used (on-line operation).

The proposed algorithm gives a formal approach in determining optimal signals for mode estimation; however, in an on-line setting, it may be computationally expensive to evaluate this algorithm for each signal. For this

reason, a fast pre-selection method (first stage) is formulated in order to
determine a limited number of signals that are possible candidates for the
optimal signal. Later, the formal approach (second stage) is applied only on the
signals selected in the first stage to determine the optimal ranking of the signals.
The proposed methods are applied to synthetic signals from the KTH Nordic 32
test system.

2.2   Power System Model for Describing an Ambient Response

This section describes a general power system model. The presented model
will be used throughout the thesis, whilst this section that treats optimal signal
selection will be using a special case of the presented general power system
model.

Ambient responses, which are of interest here, are mainly driven by small
perturbations in the network, and therefore associated power system dynamic
behavior can be accurately represented by a linear model [205],[206],[207]. The
linear power system model is obtained by linearzing a non-linear model around
some steady state operating point. For this reason, all the variables will describe
deviation from the defined steady state operating point (denoted by Δ).

The inputs of the system are defined as loads variations[1]. The responses
(outputs) of the system are variables measured by PMUs (voltage, current
phasors and other derived quantities) *excluding* measurements at the load buses.
Thus, the power system model can be represented in state-space form assuming
zero initial conditions, as follows:

$$s\Delta\mathbf{X}(s) = \mathbf{A}\Delta\mathbf{X}(s) + \begin{bmatrix}\mathbf{B}_1 & \mathbf{B}_2\end{bmatrix}\begin{bmatrix}\Delta\mathbf{U}_1(s) & \Delta\mathbf{U}_2(s)\end{bmatrix}^T ; \qquad (2.1)$$

$$\Delta\mathbf{Y}(s) = \mathbf{C}\Delta\mathbf{X}(s) + \begin{bmatrix}\mathbf{D}_1 & \mathbf{D}_2\end{bmatrix}\begin{bmatrix}\Delta\mathbf{U}_1(s) & \Delta\mathbf{U}_2(s)\end{bmatrix}^T , \qquad (2.2)$$

where $\Delta\mathbf{U}_1(s)$ and $\Delta\mathbf{U}_2(s)$ are sub-vectors of the input vector $\Delta\mathbf{U}(s)$, denoting
measured and non-measured inputs, respectively. Vector $\Delta\mathbf{X}(s)$ denotes the
state vector and $\Delta\mathbf{Y}(s)$ is a vector of output variables measured by PMUs. Note
that some or all inputs can be measured by PMUs but these signals are not part
of the output vector $\Delta\mathbf{Y}(s)$. Matrices $\mathbf{A}$, $\mathbf{B}$=[$\mathbf{B}_1$ $\mathbf{B}_2$], $\mathbf{C}$ and $\mathbf{D}$=[$\mathbf{D}_1$ $\mathbf{D}_2$] are
system, input, output and control matrices, respectively. Note that the separate
notation for measured and non-measured inputs is introduced and will be used in
Chapter 3, while the simplified form that treats all the inputs equally will be used

---

[1] It is assumed that all control references in the system are held constant, therefore not considered
as controllable inputs in the power systems.

in this chapter.

Using the state space model (1)-(2), the transfer function matrix between loads (at the input) and measured variables (at the output) is computed as follows:

$$\mathbf{H}(s) = \mathbf{C}(s\mathbf{I} - \mathbf{A})^{-1}\mathbf{B} + \mathbf{D} \ . \tag{2.3}$$

The complete model of the system can be written in a developed form as:

$$
\begin{aligned}
H_{11}(s)\Delta u_1(s) + \ldots + H_{1N}(s)\Delta u_N(s) &= \Delta y_1(s), \\
H_{21}(s)\Delta u_1(s) + \ldots + H_{2N}(s)\Delta u_N(s) &= \Delta y_2(s), \\
\vdots \qquad\qquad \vdots \qquad\qquad \vdots & \\
H_{M1}(s)\Delta u_1(s) + \ldots + H_{MN}(s)\Delta u_N(s) &= \Delta y_M(s),
\end{aligned}
\tag{2.4}
$$

where $\Delta u_i(s)$ and $\Delta y_i(s)$ are the i-th elements of the vectors $\begin{bmatrix} \Delta \mathbf{U}_1(s) & \Delta \mathbf{U}_2(s) \end{bmatrix}^T$ and $\Delta \mathbf{Y}(s)$, respectively and H_{ij} is the element of the $\mathbf{H}$ matrix at position (i, j). N denotes the number of inputs (loads) both measured and not measured, i.e. the length of $\mathbf{U}(s)$. M denotes the number of outputs (available PMU measurements and length of $\Delta \mathbf{Y}(s)$). This model can be visually represented as shown in Fig. 2.1.

Fig. 2.1 Model of the power system using loads as inputs and PMU measurements as outputs.

Fig. 2.1. shows that a single output signal can be considered as a sum of *N* components that are driven by only one load (denoted by *x* in Fig. 2.1.). The decomposed signals are used in the formulation of the mode estimation method that is presented in the sequel.

2.3   Approach

As stated before, the power system's ambient response, which can be observed in measured synchrophasor signals, is the result of random fluctuations of loads in the power system [95]. These random load fluctuations at the aggregated level can be represented by white noise [200]. Using linearity of the power system and following the structure of the model from Fig. 2.1, its model can be represented as a set of transfer functions that leads to a mathematical description of the *i*-th measured synchrophasor output y_i (linearization is assumed and deviations (Δ) are omitted to simplify notation):

$$y_i(t) = H_{i1}\hat{e}_1(t) + H_{i2}\hat{e}_2(t) + ... + H_{1N}\hat{e}_N(t), \tag{2.5}$$

where H_{ij} is the transfer function from the *j*-th input to *i*-th output and $\hat{e}_j$ the disturbance associated with the *j*-th input. Because the input is assumed to be white noise of variance $\hat{\sigma}_j^2$, it is denoted by $\hat{e}_j$ instead of the more general designation u_j used in Fig. 2.1.

Consequently using spectral factorization, the corresponding power spectrum of the signal $y_i(t)$ can be written as:

$$\Phi_{yi}(f) = \left|H_{i1}\right|^2 \hat{\sigma}_1^2 + \left|H_{i2}\right|^2 \hat{\sigma}_2^2 + ... + \left|H_{1N}\right|^2 \hat{\sigma}_N^2 = \left|G_{0i}\right|^2 \sigma_i^2 \tag{2.6}$$

As shown in (2.6), this spectrum can also be expressed using one single transfer function G_{0i} that is excited by white noise with variance σ_i^2. The modes of G_{0i} are equal to the modes of the original system (power system). The transfer function G_{0i} can be assumed to be proper, monic and to have a stable inverse.

A parametric (ARMA) model for G_{0i} can be deduced from two sources:

1)   From the measured data. Measured data is used to find the best signals for mode estimation among the set of given measured signals (on-line operation).

2)   From the existing power system model. The existing model is used to determine the best locations for PMUs (off-line simulation). This is usually referred to as an optimal PMU placement problem. One way of deducing ARMA models from the existing simulation model is to apply a frequency domain fitting procedure as presented in [208]. In

this case the frequency domain data are obtained from (2.6) at an arbitrary number of frequency points. An alternative approach is to perform time domain system identification using the data synthetized from the model response. It should be noted that a large identification dataset can be generated and used for this purpose, meaning that the estimated ARMA model can be arbitrary close to G_{0i} [209].

The sequel presents how to obtain the ARMA model from measured data using a prediction error method, assuming that the same procedure can be used for the PMU placement problem formulation i.e. when the ARMA models are computed using the existing power system model[2]. Because the prediction error method can also be used for on-line mode tracking (estimation), a mathematical description of the estimation error is provided as well. This estimation error analysis is used later to define the criterion for optimal signal selection.

Using measured data $y_i(t)$ ($t=1...N$), the estimate of the true system G_{0i} (denoted by $G_i(\hat{\theta})$) is determined within an ARMA model structure $G_i(\theta)$. The identified parameter vector $\hat{\theta}$ is the one that minimizes the prediction error criterion $\frac{1}{N}\sum_{t=1}^{N}\varepsilon^2(t,\theta) = \frac{1}{N}\sum_{t=1}^{N}(G_i^{-1}(\theta)y_i(t))^2$. Suppose that the model structure $G_i(\theta)$ is sufficiently rich to describe the true system G_{0i} (i.e. there is a vector of parameters θ_0 for which $G_i(\theta_0)=G_{0i}$), then the estimate $\hat{\theta}$ is a consistent estimate of that true parameter vector θ_0. Moreover, it can be proven that asymptotically the estimate $\hat{\theta}$ is an unbiased estimate of θ_0 and that the estimate $\hat{\theta}$ is normally distributed around θ_0, i.e. $\sqrt{N}(\hat{\theta}-\theta_0) \sim \mathcal{N}(0, P_\theta)$ with covariance matrix P_θ given by [209]:

$$P_\theta = \sigma_e^2 E\left[\psi(t,\theta_0)\psi(t,\theta_0)^T\right]^{-1},$$
(2.7)

where $\psi(t,\theta_0) = -\dfrac{d\varepsilon(t,\theta)}{d\theta}\bigg|_{\theta=\theta_0}$, and σ_e^2 is the driving noise variance from (2.6).

Since θ_0 is not known, P_θ can be evaluated at $\theta = \hat{\theta}$. In addition, P_θ can be estimated during the identification process as follows[3] [71], [209]:

$$P_\theta = \frac{1}{N}\sum_{t=1}^{N}\varepsilon^2(t,\hat{\theta})\left(\frac{1}{N}\sum_{t=1}^{N}\psi(t,\hat{\theta})\psi(t,\hat{\theta})^T\right)^{-1}.$$
(2.8)

P_θ is a measure of the asymptotic modeling error between $G_i(\hat{\theta})$ and G_{0i} and

---

[2] Other identification methods can be used for estimation of ARMA models as well [29],[81],[45].

[3] Note that P_θ does not depend on the number of data samples N, however, the real variance of the estimate is reduced proportionally when N increases.

therefore, indirectly, of the estimation error of the critical damping ratio that is deduced from $G_i(\bar{\theta})$ [4]. Because P_θ is an indirect measure, it is more useful to deduce the covariance matrix P_ζ of the damping ratio estimates ($\hat{\bar{\zeta}}$). Moreover, the diagonal elements of P_ζ provide a quantitative measure of the accuracy of the damping ratio estimates that can be obtained using a particular signal (diagonal elements of P_ζ represent variances of the damping ratio estimates).

Suppose now that the covariance matrix P_ζ can be estimated, and that it is estimated for all measured signals y_i. The best signal for damping ratio estimation is the one that gives the smallest variance of the critical damping ratio estimate (which is the corresponding element of P_ζ). This reasoning provides the basis to develop a formal algorithm for the selection of the optimal signal for mode estimation applications, which is illustrated in Fig. 2.2.
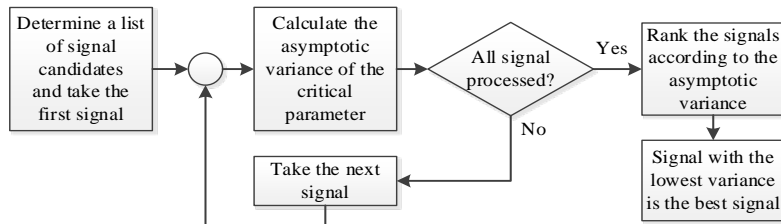
Fig. 2.2 Global algorithm of optimal signal selection for ambient mode estimation.

The sequel provides an algorithm for the computation of P_ζ that uses *only ARMA model parameters* and not the dataset that is used for the identification of the ARMA model. This property makes the signal selection algorithm independent of the identification method used to determine the ARMA model.

2.4   Computation of the Asymptotic Parameter Covariance Matrix

2.4.1   Derivation of a parameterization suitable for the mode estimation application

For the mode estimation application, accurate estimation of the mode damping ratios (ζ) is of essential importance. This means that a new parameterization is required where these parameters (ζ) are in the vector of model parameters ρ. To do this, the identified transfer function is expressed in terms of discrete poles and

---

[4] This damping ratio can be deduced by converting the discrete-time model $G_i(\hat{\theta})$ into a continuous-time model and performing a pole/zero-decomposition of this continuous transfer function.

zeros and then transformed to the continuous domain using the well-known
Tustin approximation. Once, the poles/zeros are expressed as continuous
variables, they can be written in terms of frequencies and damping ratios. The
parameterization obtained contains the parameters of interest (ζ) in the vector of
parameters (ρ). This procedure is demonstrated in the sequel.

The estimated ARMA model in terms of discrete zeros, poles and gain can be
written as follows:

$$H(\theta) = k \frac{\displaystyle\prod_{\substack{i \in Real \\ Zeros}} (1 - q_{ri} \, z^{-1}) \prod_{\substack{i \in Complex \\ Zeros}} (1 - q_{ci} \, z^{-1})(1 - q_{ci}^{*} \, z^{-1})}{\displaystyle\prod_{\substack{i \in Real \\ Poles}} (1 - p_{ri} \, z^{-1}) \prod_{\substack{i \in Complex \\ Poles}} (1 - p_{ci} \, z^{-1})(1 - p_{ci}^{*} \, z^{-1})} \, . \tag{2.9}$$

To express poles/zeros frequencies and damping ratios, the discrete poles and
zeros have to be substituted by continuous domain poles and zeros. This is done
by using Tustin's approximation (2.10) that gives the relationship between
discrete and continuous domains [210]:

$$t_i = \frac{1 + 0.5 c_i T_s}{1 - 0.5 c_i T_s} \, , \tag{2.10}$$

where $t_i \in \{q_{ci}, p_{ci}\}$ and c_i is the i-th continuous domain pole/zero. The real
poles/zeros from (2.9) do not need to be expressed in terms of continuous
domain parameters because there is no frequency and damping ratio associated
to these poles/zeros. In the case of complex poles/zeros, the expression (2.10)
has to be expressed in terms of pole/zero frequency and damping ratio using the
following relationship:

$$c_i = -\xi_i \omega_i \pm \omega_i \sqrt{\zeta_i^2 - 1} \, , \tag{2.11}$$

where ζ_i is the damping ratio of the i-th pole/zero and ω_i its natural frequency.
By substituting (2.11) into (2.10), the following is obtained:

$$t_i = \frac{1 \mp \dfrac{1}{2} \zeta_i \omega_i T_s \pm \dfrac{1}{2} \omega_i T_s \sqrt{\zeta_i^2 - 1}}{1 \pm \dfrac{1}{2} \zeta_i \omega_i T_s \mp \dfrac{1}{2} \omega_i T_s \sqrt{\zeta_i^2 - 1}} \, . \tag{2.12}$$

Expression (2.12) represents the relationship between the desired
parameterization ρ (with continuous domain damping ratios as parameters) and
discrete poles/zeros. Finally, by substituting (2.12) into (2.9), a reparameterized
model is obtained whose derivatives can be easily calculated. One factor of the

reparameterized model is shown in (2.13)-(2.15) (other factors have a similar form):

$$(1 - t_i z^{-1})(1 - t_i^* z^{-1}) = 1 - 2\,\mathrm{Re}\{t_i\}z^{-1} + \left|t_i\right|^2 z^{-2} \tag{2.13}$$

The real part and amplitude of t_i are as follows:

$$\mathrm{Re}\{t_i\} = \frac{1 - 0.25\omega_i^2 T_s^2}{1 + \xi_i \omega_i T_s + 0.25\omega_i^2 T_s^2}\,, \tag{2.14}$$

$$\left|t_i\right|^2 = \frac{\left(1 - 0.25\omega_i^2 T_s^2\right)^2 + (1 - \xi_i^2)\omega_i^2 T_s^2}{\left(1 + \xi_i \omega_i T_s + 0.25\omega_i^2 T_s^2\right)^2}\,. \tag{2.15}$$

2.4.2 Theoretic derivation of the expression for P_ρ as a function of P_θ

As presented in [71] and [209], one way to compute the covariance matrix P_ρ of the model parameter vector $\hat{\rho}$ (one sub-vector of $\hat{\rho}$ is the vector $\hat{\zeta}$, consequently P_ζ can be extracted from P_ρ) is to use a first order Taylor approximation of the mapping between $\hat{\theta}$ and $\hat{\rho}$ (i.e. $\rho = f(\theta)$), and to project the covariance matrix P_θ (estimated using (2.8)), as follows:

$$P_\rho = \left(\frac{d\rho(\theta)}{d\theta}\right) P_\theta \left(\frac{d\rho(\theta)}{d\theta}\right)^T \Bigg|_{\theta = \hat{\theta}}. \tag{2.16}$$

However, a closed-form expression for $\rho = f(\theta)$ does not exist and the matrix $\dfrac{d\rho(\theta)}{d\theta}\bigg|_{\theta = \hat{\theta}}$ must be evaluated numerically as shown in [71]. In addition, this approach assumes that P_θ is known, which means that P_θ has to be computed during the ARMA model identification (usually computed using (2.8)). This can be seen as a disadvantage in the case that the used identification method does not provide matrix P_θ as an output (e.g. subspace identification methods).

This chapter presents an approach that computes P_ρ directly from the estimated model, and at the same time, avoids the numerical evaluation of $\dfrac{d\rho(\theta)}{d\theta}\bigg|_{\theta = \hat{\theta}}$. A block diagram of the proposed approach is illustrated in Fig. 2.3. (thick line), whereas the method from [71] is marked by a dashed line.
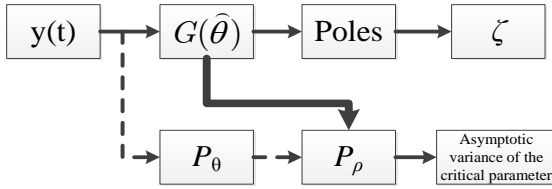
Fig. 2.3 Block diagram of parameter covariance matrix calculation.

In the proposed procedure to compute P_ζ, an estimated ARMA model is treated as an exact representation of reality i.e. $\hat{\theta}=\theta_0$ (even though this introduces a certain error in the calculated P_ζ). The identified ARMA model $G_i(\theta_0)$ is reparameterized with another parameter vector ρ_0 which has the same dimension as θ_0 and whose one sub-vector is ζ_0. This allows deriving an expression for the covariance matrix P_ρ. The variance of the mode of interest is then the corresponding diagonal element of P_ρ. The expression for the calculation of the covariance matrix P_ρ is given in Theorem 1.

Theorem 1: *Let the true SISO system G_0 be proper, monic and to have a stable inverse. Also, assume that G_0 can be described by an ARMA model structure $G(\theta)$ with the parameter set θ, that is, $\exists \theta = \theta_0$ such that $G(\theta_0)=G_0$ and that the estimate of θ_0 (denoted by $\hat{\theta}$) determined by an identification method is an accurate estimate of θ_0, that is, θ_0 can be replaced by $\hat{\theta}$ in the expressions. Also, assume that $G(\theta)$ can be expressed in terms of another set of parameters ρ. Further suppose that the mapping between θ and ρ is such that $\rho(\theta_0)=\rho_0$ and that*

$$\left. \frac{d\rho(\theta)}{d\theta} \right|_{\theta=\theta_0}$$ *is invertible. Then, the approximated expression for the covariance*

matrix of the new parameter vector P_ρ can be computed as follows:

$$P_\rho = E\left[\psi_\rho(t)\psi_\rho(t)^T \right]^{-1}, \tag{2.17}$$

where $\psi_\rho(t)$ is defined as:

$$\psi_p(t) = \left. \left(\frac{dG_i(\rho)}{d\rho} \right)^T \right|_{\rho=\rho_0} G^{-1}(\rho_0)e(t). \tag{2.18}$$

Signal $e(t)$ denotes a white noise process with unity variance.

Proof of Theorem 1:

Without losing generality, it can be assumed in (2.7) that the variance of the driving noise σ_e^2 is equal to one because P_θ does not depend on σ_e^2. Also, note

that the following equation holds:

$$\left.\frac{dG_i(\theta)}{d\theta}\right|_{\theta=\theta_0} = \left.\frac{dG_i(\rho)}{d\rho}\frac{d\rho(\theta)}{d\theta}\right|_{\theta=\theta_0 \wedge \rho=f(\theta_0)=\rho_0} \quad , \text{ (assuming that } \rho \text{ is a function of } \theta,$$

i.e. $\rho = f(\theta)$). Using this expression and the relationship $\psi(t,\theta) = -\dfrac{d\varepsilon(\theta)}{d\theta} = G_{0i}^{-1}\dfrac{dG_i(\theta)}{d\theta}e(t)$, $\psi(t,\theta)$ can be written as:

$$\psi(t,\theta) = \left.\left(G_{0i}^{-1}\frac{dG_i(\rho)}{d\rho}\frac{d\rho(\theta)}{d\theta}\right)^T\right|_{\theta=\theta_0 \wedge \rho=f(\theta_0)=\rho_0} e(t) =$$

$$= \left.\left(\frac{d\rho(\theta)}{d\theta}\right)^T\left(\frac{dG_i(\rho)}{d\rho}\right)^T\right|_{\theta=\theta_0 \wedge \rho=f(\theta_0)=\rho_0} \left(G_{0i}^{-1}\right)^T e(t) = \quad (2.19)$$

$$= \left.\left(\frac{d\rho(\theta)}{d\theta}\right)^T\right|_{\theta=\theta_0} \psi_\rho(t);$$

where the following notation is used:

$$\psi_\rho(t,\rho) = \left.\left(\frac{dG_i(\rho)}{d\rho}\right)^T\right|_{\rho=\rho_0} \left(G_{0i}^{-1}\right)^T e(t) . \quad (2.20)$$

Note that $G_{0i}^{-1} = \left(G_{0i}^{-1}\right)^T$. Substituting (2.19) into (2.7) results with:

$$P_\theta^{-1} = \left.\left(\frac{d\rho(\theta)}{d\theta}\right)^T E\left[\psi_\rho(t)\psi_\rho^T(t)\right]\left(\frac{d\rho(\theta)}{d\theta}\right)\right|_{\theta=\theta_0} ; \quad (2.21)$$

where the fact that $\left.\left(\dfrac{d\rho(\theta)}{d\theta}\right)\right|_{\theta=\theta_0}$ is a deterministic matrix is used. To simplify notation, this can be written as:

$$P_\theta^{-1} = \left.\left(\frac{d\rho(\theta)}{d\theta}\right)^T P_\rho^{-1}\frac{d\rho(\theta)}{d\theta}\right|_{\theta=\theta_0} , \quad (2.22)$$

where $P_\rho^{-1} = E\left[\psi_\rho(t)\psi_\rho^T(t)\right]$ as defined in Theorem 1.

Taking an inversion of the (2.22) and replacing θ_0 by its estimate $\hat{\theta}$, the expression (2.16) is obtained, i.e.:

$$P_\rho = \left(\frac{d\rho(\theta)}{d\theta} \right) P_\theta \left(\frac{d\rho(\theta)}{d\theta} \right)^T \Bigg|_{\theta=\hat{\theta}}. \tag{2.23}$$

This concludes the proof of the theorem.□

It is to be noted that expression (2.18) does not require a closed-form expression of the mapping $\rho=f(\theta)$ between θ and ρ, nor its derivatives. It only requires to be able to obtain an expression of the transfer function $G(\rho)$ and then to obtain the derivative $\dfrac{dG(\rho)}{d\rho}\bigg|_{\rho=\hat{\rho}}$ on this new expression. This step is as easy as for the original parameter vector set (see expression (2.7)). Derivatives of the factors of $H(\rho)$ can be easily computed, i.e. the transfer function $\left(\dfrac{dG(\rho)}{d\rho} \right)^T \bigg|_{\rho=\rho_o} \left(G_0^{-1} \right)^T$ from (2.18) can be determined. It can be noted that only the derivatives of the elementary factors have to be computed because the remaining transfer function does not depend on the parameters of the corresponding elementary factor (other factors are constant).

Even though this theorem is used here to evaluate the variance of the damping ratio, this theorem in fact is general and can be applied to other cases where a change of parameterization is necessary.

At this point it is possible to provide an explanation of why traditional PMU placement algorithms are not able to find the optimal PMU location for mode estimation. It was shown that the variance of the damping ratio depends only on the underlying ARMA model. However, this ARMA model is determined by two factors. The first one is a power system model and the second one is the excitation (noise) that excites the system (see (2.6)). Therefore, PMU placement methods that use only power system models without including characteristics of the ambient excitation (which is the common case) are not able to provide a complete answer about optimal PMU placement for mode estimation applications. The importance of the excitation is also discussed in [187].

In the previous derivation, it is assumed that the order of the ARMA model is appropriately selected. This means, on the one hand, that the model order has to be high enough to describe the dynamics of the system accurately, but on the other hand, it is important to keep the order (and consequently the number of estimated parameters) as low as possible. More information about methods for

optimal model order selection can be found in Chapter 5 of this thesis or in [201].

2.4.3   Numerical algorithm for parameter covariance calculation

This paragraph presents a numerically efficient algorithm for the computation of the asymptotic parameter covariance matrix P_ρ that is defined in Theorem 1. The term $\psi_\rho(t)$, that is given by (2.18), represents an output of a single-input multiple-output system that can be written in a state space form described by A, B, C, D matrices and state vector $x(t)$ as:

$$\begin{aligned} x(t+1) &= Ax(t) + Be(t) \\ \psi_\rho(t) &= Cx(t) + De(t) \end{aligned} . \tag{2.24}$$

Using the property that $e(t)$ and $x(t)$ are uncorrelated ($E[e(t)x(t)]=0$) and the assumption of unity variance of the white noise, the inverse of covariance matrix can be written in terms of the output state space equation:

$$\begin{aligned} E\left[\psi_\rho(t)\psi_\rho^T(t)\right] &= E\left[\left(Cx(t) + De(t)\right)\left(Cx(t) + De(t)\right)^T\right] = \\ &= E\left[Cx(t)x^T(t)C^T\right] + E\left[De(t)e^T(t)D^T\right] = \\ &= CX(t)C^T + DD^T \end{aligned} \tag{2.25}$$

where $X(t)=E[x(t)x^T(t)]$. This term can be computed from the state space equation (2.24):

$$\begin{aligned} X(t+1) &= E\left[\left(Ax(t) + Be(t)\right)\left(Ax(t) + Be(t)\right)^T\right] = \\ &= E\left[Ax(t)x^T(t)A^T\right] + E\left[Be(t)e^T(t)B^T\right] = \\ &= AX(t)A^T + BB^T . \end{aligned} \tag{2.26}$$

In steady state, asymptotically, the following equation holds $X(t+1)=X(t)$, that leads to:

$$X(t) = AX(t)A^T + BB^T , \tag{2.27}$$

which is a Lyapunov equation whose unknown is $X(t)$ and, that can be readily solved using e.g. MATLAB[5]. Substituting the computed $X(t)$ into (2.25), the value $E[\psi_\rho(t)\psi_\rho^T(t)]$ is obtained. Further, by computing the inverse of $E[\psi_\rho(t)\psi_\rho^T(t)]$ the covariance matrix P_ρ is obtained.

The previous results lead to the following algorithm for the computation of the

---

[5] In the MATLAB environment, this matrix equation can be solved efficiently using the function `dlyap`.

parameter covariance matrix:

Step 1:   Find the parameters θ_0 of the underlying ARMA model $G_i(\theta)$ for the selected signal i using a system identification technique.

Step 2:   Express the ARMA model $G_i(\theta)$ in terms of parameters ρ to obtain $G_i(\rho)$, and find the corresponding parameters ρ_0.

Step 3:   Compute the derivatives of $G_i(\rho)$ with respect to the model parameters ρ evaluated at $\rho=\rho_0$.

Step 4:   Compute   the   vector   of   transfer   functions

$$F = \left(\frac{dG_i(\rho)}{d\rho} \right)^T \Bigg|_{\rho=\rho_0} \left(G_i^{-1}(\rho_0) \right)^T.$$

Step 5:   Express the transfer functions F in state space form with one input and a number of outputs that is equal to the number of parameters. Corresponding system matrices are denoted by A,B,C,D.

Step 6:   Solve the Lyapunov equation $A=AXA^T + BB^T$ for X.

Step 7:   Compute $E[\psi_\rho(t)\psi_\rho^T(t)]=CXC^T+BB^T$.

Step 8:   Compute the parameter covariance matrix as: $P_\rho=E[\psi_\rho(t)\psi_\rho^T(t)]^{-1}$.

This procedure provides the asymptotic covariance matrix P_ρ as the final result that contains the asymptotic variances of the estimated damping ratios as diagonal elements. It is important to note that the values of the asymptotic variances do not depend on the number of samples used in the identification. This is not the case for the absolute variance observed that linearly decrease when the longer data set is used for identification i.e. the following holds:

$$Cov(\sqrt{N}\hat{\rho}) \rightarrow P_\rho, \text{ as } N \rightarrow \infty, \text{ and consequently } Cov(\hat{\rho}) \approx \frac{1}{N}P_\rho.$$

2.4.4   Mode estimation in the case of multiple critical modes in the system

The proposed algorithm answers the question of the optimal signal selection for one critical mode of interest. If multiple modes are monitored in the real-time, it is obviously possible to determine a different signal ranking for each of the critical modes (the proposed procedure is performed for each critical mode separately). Based on these results, the recommended practice for real-time mode estimation is to perform estimation separately (as parallel processes) for each critical mode using the corresponding optimal signals.

An alternative to this approach is to use an integral ranking criterion that combines the computed variances of different modes of interest (weighing sum

for instance). The integral criterion provides a unique signal ranking that takes different critical modes into consideration, meaning that there is no need to run parallel mode estimations (as in the previous approach). However, this ranking provides only suboptimal results (each particular mode will be estimated using suboptimal signals).

2.4.5   Remarks on signal selection for mode shape estimation

In the analysis of electromechanical oscillations, it is also useful to obtain information about the mode shapes of the critical modes [28],[149]. The sequel of this subsection provides a short discussion about important considerations for signal selection for mode shape estimation and the relationship between damping ratio and mode shape signal selection.

In contrast to damping ratio estimation, mode shape estimation does not estimate a parameter that is common for all measured signals. Rather, each location has its own true parameter value that needs to be estimated. Furthermore, it can be said that the most relevant signals are those that have the largest influence on the critical mode. Therefore, there are two aspects in signal selection for mode shapes:

1)   Signals that have *the largest participation* in the oscillation.

2)   Signals that provide *the best accuracy* of the mode shape estimate.

The relative mode shape that corresponds to the k-th signal is estimated as [149]:

$$M_k(\lambda_i) \approx \left. \frac{Y_k(s)}{Y_{ref}(s)} \right|_{s=\lambda_i \approx j\omega_i},\tag{2.28}$$

where λ_i is a critical mode, and $Y_k(s)$ and $Y_{ref}(s)$ are the Laplace Transforms of the k-th and reference signals, respectively. If a white noise signal is selected as a reference signal, the mode shape estimation is reduced to an ARMA model estimation. Furthermore, the signals that have a large value of such defined mode shape will also have a large participation in the oscillation, which corresponds to the first aspect of the signal selection for mode shape estimation (large signal participation).

Once the ARMA model (2.28) and its parameter covariance matrix P_θ are estimated, (2.16) can be used to obtain the uncertainty of the frequency response at the mode frequency following the procedure as in Section 2.4.1 (with the difference that the uncertainty of the damping ratio estimate is obtained instead). Further, this uncertainty represents the uncertainty of the mode shape estimate and consequently a measure of the accuracy that can be obtained with a

particular signal (the second aspect of signal selection for mode shape estimation). Note that the new parameterization in (2.16) is required, i.e.

$$\rho(\omega) = M_k(\theta).$$

Based on these results (mode shape values and accuracy of the estimates), it is possible to make a decision on which signals should be used for mode shape estimation.

Mode shape estimation using the considerations above is beyond the scope of this thesis, and subject to on-going research. Therefore, this will not be analyzed in more details in the sequel.

2.5   Signal Selection for On-line Application

This section first discusses the relationship between the estimated damping ratio and its variance computed by (2.17), and further formulates a signal pre-selection method that is beneficial for on-line applications, where computational time can be critical.

2.5.1   Qualitative analysis of the relationship between damping ratio and its variance

To establish a qualitative relationship between the damping ratio and its variance, (2.17) is expressed in the frequency domain by applying Parseval's theorem:

$$P_\rho = \left[\frac{1}{2\pi} \int_{-\pi}^{\pi} \frac{1}{|G_{oi}|^2} \left(\frac{dG(\rho,\omega)}{d\rho} \right)^* \Bigg|_{\rho=\rho_0} \left(\frac{dG(\rho,\omega)}{d\rho} \right) \Bigg|_{\rho=\rho_0} d\omega \right]^{-1}. \qquad (2.29)$$

Using the property of the derived parameterization $G(\rho)$, that it is a product of modes' factors, it is apparent that the value of the term $\frac{1}{G_{oi}} \left(\frac{dG(\rho,\omega)}{d\rho_i} \right) \Bigg|_{\rho=\rho_0}$ in (2.29) depends only on the mode whose parameter is ρ_i (ρ_i is the i-th element of ρ). This is due to cancellations between G_{0i} and $\frac{dG(\rho,\omega)}{d\rho_i}$ for all other modes' factors. Now, it is possible to plot the frequency response of the term $\frac{1}{G_{oi}} \left(\frac{dG(\rho,\omega)}{d\rho_i} \right) \Bigg|_{\rho=\rho_0}$ for different values of ρ_i, where ρ_i represents the damping ratio of the critical mode (ζ_i) while the frequency of the mode ω_i is fixed on the

value ω_{0i}. This plot is shown in Fig. 2.4. Note that fixing the value of ω_i is a justified assumption since it is known that the estimate of ω_i is generally very accurate[6]. This means that the shape of the frequency response plotted in Fig. 2.4. does not change significantly when ω_i is changed.
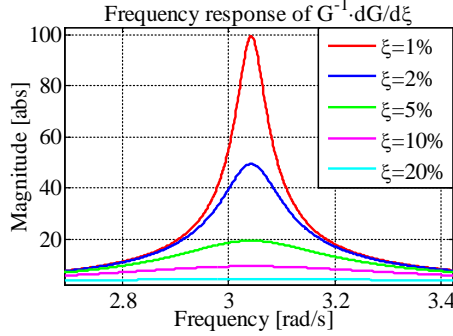

Fig. 2.4 Bode plot of the transfer function $F = \left(dG(\zeta)\,/\,d\zeta \right)\big|_{\zeta=\zeta_0} G_0^{-1}$ *for different values of* ζ.

It can be seen from (2.29) that the diagonal elements of P_ρ^{-1} are equal to the integral of the squared frequency response from Fig. 2.4. Now, assume that the parameter estimates $\hat{\rho}$ are mutually independent. This assumption is equal to the assumption that off-diagonal elements of the matrix P_ρ (i.e. covariances) are equal to zero[7]. Using this assumption, it can be said that the value of integral in (2.29) is a diagonal matrix whose inverse is obtained simply by replacing the elements by their reciprocals. This means that variance of ζ_i is inversely proportional to the area below the corresponding lines in Fig. 2.4, which again inversely depends on ζ_i. Therefore, this directly correlates the value of the critical damping ratio ζ_i and its variance (the smaller damping ratio implies smaller variance).

This conclusion can also be derived from another approach. Let us assume that all parameters in ρ_0 except $\rho_0=\zeta_i$ are known and that only ζ_i has to be estimated. Using the same reasoning from (2.29) and Fig. 2.4, it follows that the larger the damping ratio the larger the estimation variance becomes.

A critical situation in real-life operation is when the damping ratio of the critical mode decreases with time. The previous results show that, in this situation, the accuracy of the estimate will improve, which is a desirable

---

[6] This assumption does not affect the generality of the approach; it only enables simplification of the reasoning and the presentation.
[7] This assumption is not fully satisfied in reality, however it enables a qualitative analysis of the relationship between the values of the parameter estimates and the signal spectrum by simplifying the computation of the matrix inverse in (2.29).

property. On the other hand, when the damping ratio increases, the accuracy of the estimate will decrease. However, since this is not a critical situation for the grid, the smaller accuracy will not affect operation of the system.

2.5.2 Signal pre-selection

Running the formal algorithm for all available synchrophasor signals in real-time can be computationally demanding. Also, this is unnecessary because the majority of the signals will contain little or no information about the mode of interest. This phenomenon might happen due to a zero-pole cancellation effect. For that reason, it is beneficial to develop a fast pre-selection method that will aid in determining if the signal can be considered as a candidate for optimal mode estimation.

This pre-selection algorithm will be formulated in a similar manner as the formal algorithm: A criterion that can be computed efficiently is defined and used for ranking of the signals. Using this ranking, a limited number of the top ranked signals will be selected as candidates for the optimal signal (first stage). In the second stage, the full formal algorithm from Section 2.4 will be applied on the selected signal candidates in order to determine the final ranking.

The proposed pre-selection ranking criterion is defined as the average amplitude of the signal's Fourier transform over a small range around the critical frequency. This procedure finds if there is a peak in the signal's spectrum, which indicates that the critical mode is visible in the analyzed signal. Since the value of the peak is not directly proportional to the accuracy of the obtained estimate, it is necessary to run the formal algorithm and determine the final signals' ranking for optimal mode estimation. This pre-selection criterion can be computed efficiently by using Goertzel's algorithm [211].

If a signal, due to (near) pole-zero cancellation, contains little information about the critical mode, its power spectrum will generally not have a pronounced resonance peak at the frequency of the considered mode i.e. the damping ratio of the estimated mode (if it is observable) will have a large value. Using the results from Section 2.5.1, this implies that the computed ranking criterion will numerically have a large value causing the signal to be discarded. This means that the bias (caused by the lack of information about the critical mode in the signal) will not affect the selection of the top ranked signals.

It is important to note that this section, besides formulating the pre-selection method for signal selection, provides new insight to the commonly accepted premise that signals whose spectrum has a large peak at the mode frequency are likely to be a good choice for mode estimation.

2.6   Application

In order to illustrate the application of the presented methodology for optimal signal selection, the KTH Nordic 32 [212] and the IEEE test systems with 10 generators and 39 buses are used. The KTH Nordic 32 test system has one critical inter-area mode at approximately 0.5 Hz (or 3 rad/s) with damping ratio of 3.52 %, which is closely studied in [212], [213]. The IEEE test system has a critical mode at 0.58 Hz with damping ratio equal to 2.29 %. The simulated synchrophasor measurements are obtained from the simulations where active and reactive powers of all loads are modeled as white noise, which is the only disturbance in the system.

2.6.1   Critical parameter variance computation and validation

The variance of the estimated damping ratio of the critical mode is computed using the methodology presented in Section 2.4. Using the methodology from [201], a model order of 12 is selected as appropriate and used for all the signals. The ranking criterion (variance of the estimate) is computed assuming a first order approximation of the prediction error criterion with respect to the model parameters [209] as well as a Tustin approximation used for mapping between discrete and continuous domains. These approximations inevitably introduce errors in the computed damping ratio variance (it will deviate from the actual variance). To assess the effect of these errors, the computed variance is compared with the sample variance that is obtained using the results of 2000 simulated Monte Carlo mode estimations (for each mode estimation, an independent realization of the excitation is used). This sample variance is multiplied by the number of samples used for the estimation. Modes are estimated using the prediction error method that minimizes the prediction error criterion over the set of ARMA model parameters as shown in Fig. 2.3. In these simulations, 3000 data samples with 5 Hz sampling frequency (10 min data block) are used for each simulation. The variance obtained using Monte Carlo simulations is denoted as "observed" in the sequel.

The results obtained with the KTH Nordic 32 test system are given in Fig. 2.6 and Fig. 2.5, whereas the on-line diagram of the system with the locations of the signal candidates is presented in Fig. 2.7.
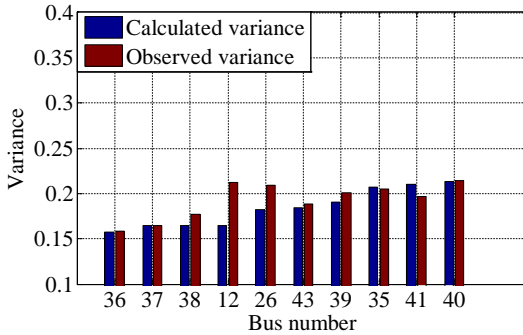
Fig. 2.5 Calculated and observed variance of the estimated damping ratio of the critical mode 0.5 Hz using voltage magnitude synchrophasor signals.
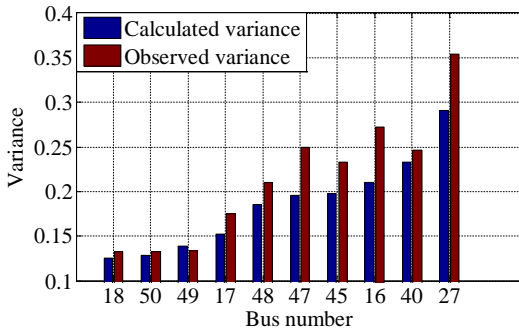
Fig. 2.6 Calculated and observed variance of the estimated damping ratio of the critical mode 0.5 Hz using voltage angles synchrophasor signals.

The results confirm that the variances computed using the approach proposed in this chapter do not significantly differ from the variances obtained using Monte Carlo simulations (the difference is always less than 25 %). Further, the results suggest that the voltage angle signals, if chosen carefully, provide the smallest estimation variance. However, in this particular case, it is possible to choose among a large number of voltage magnitude signals that provide reasonably good accuracy (around 0.2). The locations of the signal candidates provide further insight in the obtained results (Fig. 2.7).

Note that the obtained variances can be interpreted from the perspective of absolute standard deviation of the estimated damping ratio. Namely, the absolute variance when N samples are used for identification is simply obtained by dividing the asymptotic variance (shown in Fig. 2.6 and Fig. 2.7) with N. Further, it is straightforward to express the absolute variance through standard deviation. For instance, if $N=3000$ (as used in the presented test cases), the

asymptotic variance of 0.15 will represent an absolute variance of $5 \cdot 10^{-5}$. Further, the corresponding standard deviation of the damping ratio estimate will be 0.707% (computed as $\sqrt{5 \cdot 10^{-5}} \cdot 100\%$), whereas it is known that the true system's damping ratio is 3.52%. This damping ratio estimation accuracy of 0.707% is maximal accuracy that can be accomplished using only ambient data. A further accuracy improvement can be accomplished using probing methods as presented in Chapter 5 of this thesis. As it will be shown, the absolute variance of $5 \cdot 10^{-7}$ (which corresponds to 10 times lower standard deviation, i.e. 0.070%) can be accomplished with a reasonable low-power excitation.
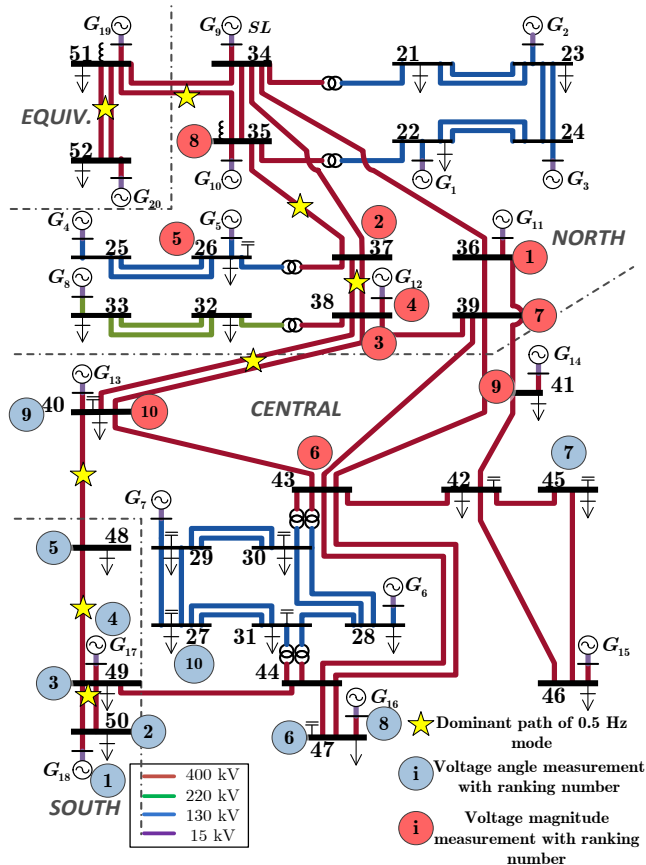

Fig. 2.7 Single-line diagram of the KTH Nordic 32 Test System with the locations of the candidate signals for ambient mode estimation.

Based on the results of modal analysis it is known that the critical 0.5 Hz

mode causes an oscillation of the area represented by generators 17 and 18 against the Northern part of the system. It can be noticed that the best voltage angle signals are in the vicinity of these generators. On the other hand, voltage magnitude signals that are in the vicinity of buses 36-37 provide the smallest variance of the damping ratio. The results conclusively show that the optimal locations are very different when different signal types are used. This can be explained by the fact that the voltage angles deviations will be largest in the proximity of the dominant oscillating generators, whereas voltage magnitude oscillations at these buses can be significantly suppressed by the reaction of automatic voltage regulators. More details on this phenomenon can be found in [213].

The proposed signal selection algorithm has been derived under the assumption that the prediction error estimator is unbiased as commonly assumed in mode estimation algorithms. However, due to the zero pole cancelation and the reduced model order that is used to describe the full system dynamics, a certain amount of bias is an inevitable consequence. This bias is a complex phenomenon for which an analytical expression does not exist. In the sequel, the bias obtained with different signals is analyzed using Monte Carlo simulations. For each signal, 2000 Monte Carlo mode simulations are run and the mean value of the mode damping ratio estimates is used for the bias calculation (the bias is the difference between this value and the true value which is equal to 3.52%).

Fig. 2.8 and Fig. 2.9 show damping ratio estimates obtained as the mean of the 2000 estimates from Monte Carlo simulations, as well as the absolute value of the bias (the red line shows the absolute value of the difference between the solid blue line and the true damping ratio value denoted by the blue dashed-dotted line). Fig. 2.8 shows results for 15 the top-ranked voltage magnitude signals, whereas Fig. 2.9 shows results for the 15 top-ranked voltage angle signals.
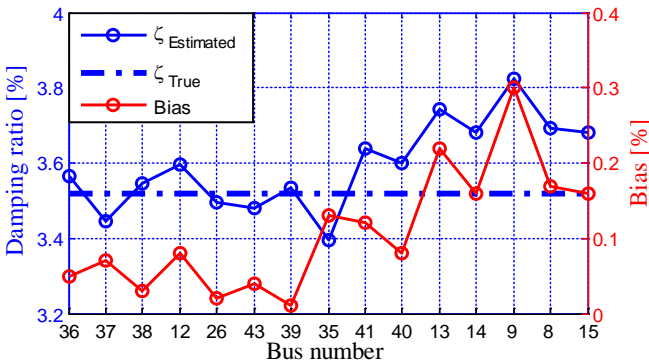
Fig. 2.8 Bias analysis of the top ranked voltage magnitude signals from the KTH Nordic 32 test system.
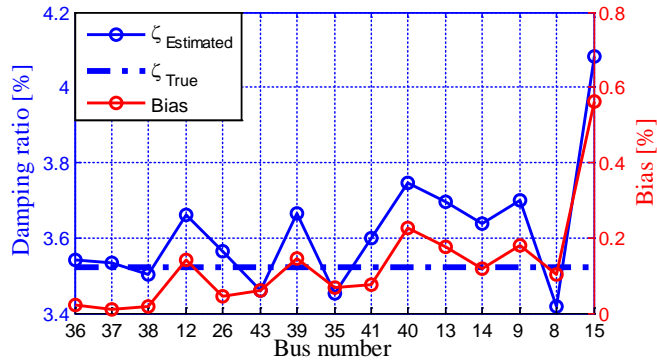
Fig. 2.9 Bias analysis of the top ranked voltage angle signals from the KTH Nordic 32 test system.

The results suggest that the top ranked signals with the proposed methods tend to provide a smaller value of the bias (the red lines in Fig. 2.8 and Fig. 2.9 are almost monotonically increasing).

2.6.2   Signal pre-selection

As it was concluded before, the power spectra of the measured signals can be used for optimal signal pre-selection. In other words, the optimal signals for damping ratio estimation will have large peaks in their spectra at the critical mode frequency. The validity of this assumption is analyzed by comparing the power spectra of the voltage magnitude signals. The results are presented in Fig. 2.10 and Fig. 2.11.
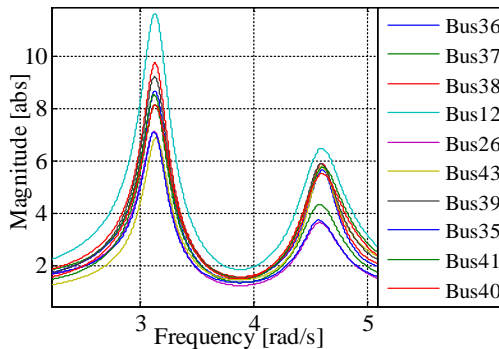
Fig. 2.10 Power spectra of the best 10 voltage magnitude signals ranked based on the methodology from Section 2.4.
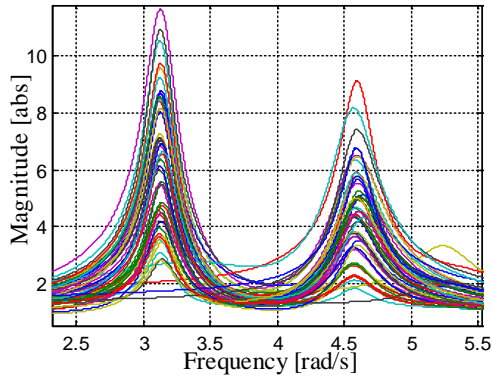
Fig. 2.11 Power spectra of all voltage magnitude signals.

Fig. 2.10 and Fig. 2.11 show that the 10 best signals for the 0.5 Hz mode have in general large peaks (according to Fig. 2.10) compared to all signals whose power spectra are given in Fig. 2.11.

Numerical comparisons between the pre-selection and formal algorithm for voltage magnitude signals are given in Table 2.1.

It can be seen that among the first 10 signals that are determined by the pre-selection algorithm, the 4 best signals computed by the formal algorithm are present. Also, the best 10 signals determined by the formal algorithm (highlighted) are contained in the 22 first signals computed by the pre-selection algorithm. Further, it can be noticed that the pre-selection tends to favor the signals measured directly at the middle voltage generator buses (buses denoted by numbers 1-20) even though these signals do not ensure the optimal mode estimation (according to the formal algorithm).

Table 2.1 Comparison of the pre-selection and formal algorithm in the case of voltage magnitude signals.

	Pre-selection		Proposed method	
	Bus No.	Criterion Value	Bus No.	Criterion Value
1	12	11.61	36	0.160
2	14	10.88	37	0.164
3	11	10.46	38	0.164
4	38	9.73	12	0.164
5	13	9.54	26	0.182
6	39	9.20	43	0.184
7	15	8.75	39	0.191
8	36	8.66	35	0.201
9	5	8.63	41	0.210
10	37	8.48	40	0.213
11	9	8.47	13	0.221
12	32	8.46	14	0.228
13	10	8.32	9	0.231
14	40	8.16	8	0.239
15	41	8.14	15	0.242
16	8	7.98	11	0.251
17	34	7.21	1	0.253
18	26	7.09	22	0.261
19	35	7.06	34	0.262
20	1	7.04	24	0.271
21	42	7.02	45	0.285
22	43	6.90	25	0.298

A similar analysis has been conducted for voltage angle signals, and the results are reported in Table 2.2.

Table 2.2 Comparison of the pre-selection and formal algorithm in the case of voltage angle signals.

	Pre-selection		Proposed method	
	Bus No.	Criterion Value	Bus No.	Criterion Value
1	**16**	21.66	**18**	0.125
2	**18**	21.43	**50**	0.129
3	**50**	20.35	**49**	0.139
4	**49**	19.74	**17**	0.153
5	**48**	19.01	**48**	0.185
6	**47**	15.83	**47**	0.196
7	**17**	12.90	**45**	0.198
8	**45**	12.63	**16**	0.210
9	7	10.79	**40**	0.233
10	46	10.62	**27**	0.291
11	29	7.19	46	0.316
12	**27**	7.15	13	0.324
13	31	7.10	43	0.349
14	41	6.81	16	0.354
15	**40**	6.62	29	0.372

Table 2.2 shows even better matching between the pre-selection and formal algorithm in case of voltage angle signals, compared to the voltage magnitude signals. The first 15 pre-selected signals contain the 10 best signals determined by the formal algorithm (highlighted).

2.6.3 Comparison of signal selection methods

This section provides a comparison among different signal selection methods, namely the proposed method is compared with the methods proposed in [188] (denoted by CF1) and in [187] (denoted by MPC). In addition, the variance of the damping ratio estimate obtained using Monte Carlo simulations is reported (observed variance), even though this method is not applicable for on-line signal selection.

Firstly, voltage magnitude and angle signals synthetized using the KTH Nordic 32 test system were used to obtain rankings with different criteria. The values of different computed criteria and corresponding rankings (top ten signals for each criterion) are shown in Table 2.3 and Table 2.4.

Table 2.3 Comparison of different signal selection algorithms using voltage magnitude signals from the KTH Nordic 32 test system.

Observed variance (Bus/Value)		Proposed method (Bus/Value)		CF1[188] (Bus/Value)		MPC[187] (Bus/Value)	
36	0.159	36	0.16	42	0.453	40	27.98
37	0.165	37	0.164	37	0.150	47	26.82
38	0.177	38	0.164	39	0.143	42	4.16
43	0.189	12	0.164	14	0.113	38	3.73
41	0.197	18	0.182	15	0.104	51	2.75
39	0.201	43	0.184	51	0.098	14	2.29
35	0.205	39	0.191	31	0.090	31	1.64
26	0.209	35	0.201	34	0.081	25	1.53
12	0.212	41	0.21	36	0.079	16	1.51
40	0.214	40	0.213	6	0.079	52	1.47

Table 2.4 Comparison of different signal selection algorithms using voltage angles signals from the KTH Nordic 32 test system.

Observed variance (Bus /Value)		Proposed method (Bus / Value)		CF1[188] (Bus / Value)		MPC[187] (Bus / Value)	
50	0.132	18	0.125	18	0.169	6	2.76
18	0.133	50	0.129	7	0.161	17	1.81
49	0.134	49	0.139	29	0.146	7	1.66
44	0.152	17	0.153	16	0.129	13	1.13
17	0.175	48	0.185	31	0.129	18	0.82
28	0.198	47	0.196	17	0.126	40	0.74
48	0.211	45	0.198	6	0.115	16	0.65
45	0.233	16	0.210	51	0.092	47	0.49
40	0.246	40	0.233	40	0.088	31	0.46
47	0.249	27	0.291	50	0.076	44	0.421

The results show that the final ranking results obtained with different algorithms differ significantly, however it can still be noticed from Fig. 2.7 that buses selected with different methods are relatively close to each other with some exceptions.

Fig. 2.12 and Fig. 2.13 show the performance of the three signal selection methods in terms of the obtained bias that is calculated using 2000 Monte Carlo simulations. The results are shown for the top 10 ranked signals (as in Table 2.3

and Table 2.4) separately for voltage magnitude (Fig. 2.12) and voltage angle (Fig. 2.13) signals.
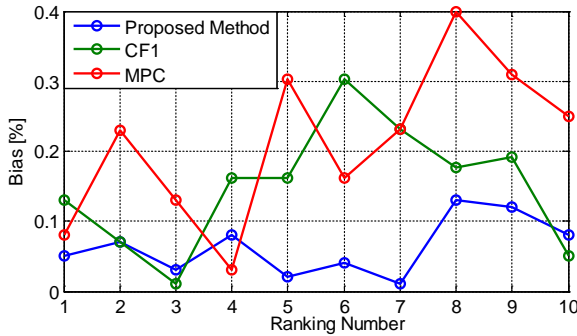
Fig. 2.12 Comparison of biases obtained with the top-ranked voltage magnitude signals from the KTH Nordic 32 test system using different signal selection methods.
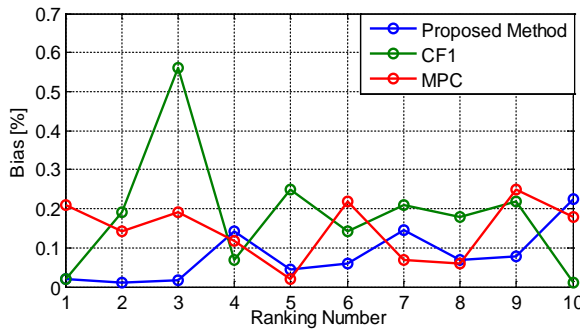
Fig. 2.13 Comparison of biases obtained with the top-ranked voltage angle signals from the KTH Nordic 32 test system using different signal selection methods.

The presented results show that the top ranked signals with the proposed method provide smaller values of bias (with a few exceptions). This can be seen from the fact that the blue line is placed below the other lines for most signals.

Further, this comparison is performed using the IEEE Test system with 39 buses and 10 generators. A characteristic of this system is that it has one critical mode at 0.58 Hz and a damping ratio of 2.29%, where generator 1 has a very large inertia, which makes other generators oscillate against generator 1. A single line diagram of the test system with the optimal locations determined by the proposed method is shown in Fig. 2.14.
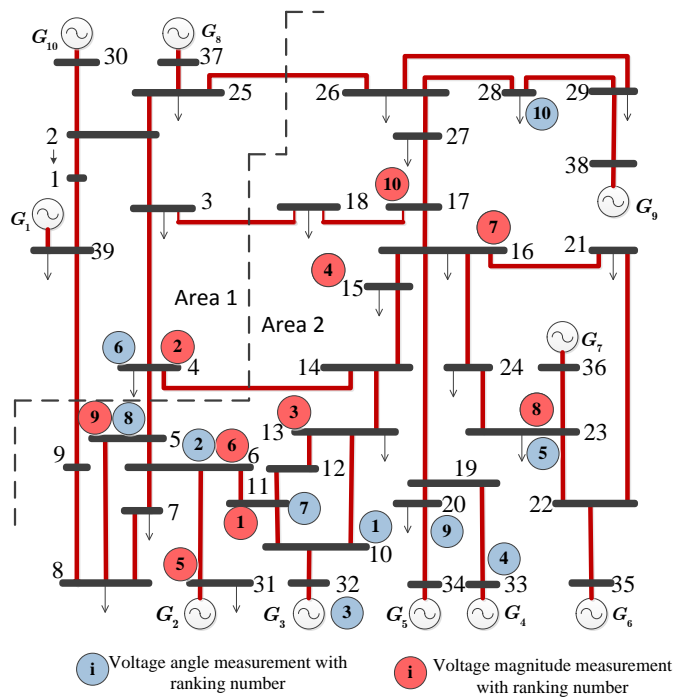
Fig. 2.14. Single-line diagram of the KTH Nordic 32 Test System with the locations of the candidate signals for ambient mode estimation.

Numerical results obtained by the different signal selection methods are presented in Table 2.5 and Table 2.4. These results suggest that the optimal locations for voltage angle signals are closer to the generators than the voltage magnitude signals. A difficulty with this system is that there is no single dominant mode path, rather, there are multiple paths that transfer oscillations from generator 1 to other oscillating generators. This explains the relatively dispersed optimal locations.

The results obtained using the other two methods ([187] and [188]) show that the 10 top optimal locations overlap to some extent with the results from the proposed method. Due to multiple mode paths this system in general shows that several locations can provide sufficiently good mode estimation results.

*Table 2.5 Comparison of different signal selection algorithms using voltage
magnitude signals from the IEEE 39 bus test system.*

Observed variance (Bus/Value)		Proposed method (Bus /Value)		CF1[188] (Bus/Value)		MPC[187] (Bus/Value)	
13	0.160	11	0.122	16	0.156	28	1.228
11	0.175	4	0.122	11	0.123	31	0.792
12	0.183	13	0.124	33	0.101	34	0.783
31	0.158	15	0.141	25	0.099	15	0.740
32	0.188	31	0.152	12	0.083	32	0.739
15	0.189	6	0.161	31	0.081	29	0.693
27	0.201	16	0.162	13	0.069	10	0.690
10	0.207	23	0.175	23	0.068	8	0.635
14	0.216	5	0.181	5	0.064	33	0.623
6	0.218	17	0.193	27	0.062	16	0.622

*Table 2.6 Comparison of different signal selection algorithms using voltage
angles signals from the IEEE 39 bus test system.*

Observed variance (Bus/Value)		Proposed method (Bus /Value)		CF1[188] (Bus/Value)		MPC[187] (Bus/Value)	
11	0.052	10	0.049	16	0.156	33	1.14
4	0.053	6	0.049	11	0.123	32	1.11
23	0.055	32	0.050	33	0.101	31	0.75
6	0.056	33	0.050	29	0.091	20	0.51
28	0.057	23	0.051	12	0.083	23	0.43
12	0.058	4	0.053	26	0.072	26	0.35
26	0.061	11	0.053	10	0.071	15	0.30
5	0.070	5	0.054	23	0.068	6	0.29
10	0.071	20	0.056	6	0.063	10	0.28
20	0.072	28	0.056	28	0.057	5	0.27

Similarly to Fig. 2.12 and Fig. 2.13, a bias analysis is performed for the IEEE
39 bus system. The results are shown in Fig. 2.15 and Fig. 2.16 where a similar
conclusion can be drawn, which is that the proposed method generally selects
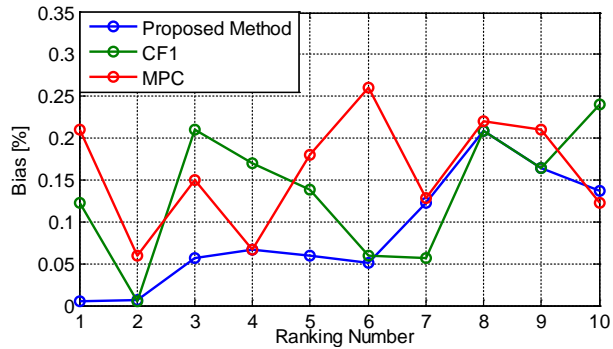signals that also provide smaller bias.

Fig. 2.15 Comparison of biases obtained with the top-ranked voltage magnitude signals from the IEEE 39 bus test system using different signal selection methods.
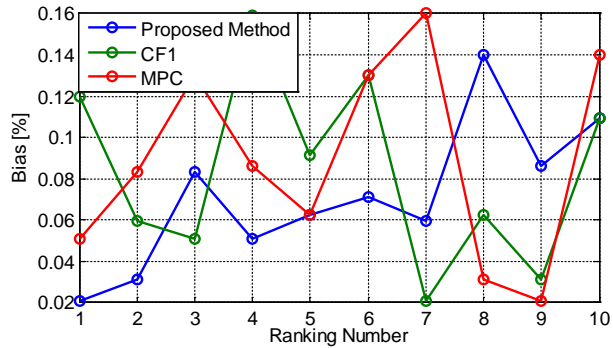
Fig. 2.16 Comparison of biases obtained with the top-ranked voltage angles signals from the IEEE 39 bus test system using different signal selection methods.

2.6.4   Effect of measurement noise and selected model order on the calculated ranking criterion

The presence of measurement noise alters the spectrum of the measured signals and, consequently, the mode estimation results and estimated variance of the damping ratio. The effects of measurement noise on mode estimation are analyzed in [200],[214], whereas the effect on the estimated damping variance (ranking criterion) is analyzed in the sequel. This is done by analyzing signals that are synthetized by adding different levels of white Gaussian noise (described by Noise to Signal Power ratio-NSR) to the voltage magnitude signal of bus 38 (the KTH Nordic 32 test system). The synthetized signals are used for ARMA

model estimation with settings described in the previous section. Finally, the obtained ARMA models are used as an input to the proposed method to obtain the variance of the critical damping ratio. The results of the performed analyses (Fig. 2.17) show how the estimated critical damping ratio and its variance change with different level of noise.
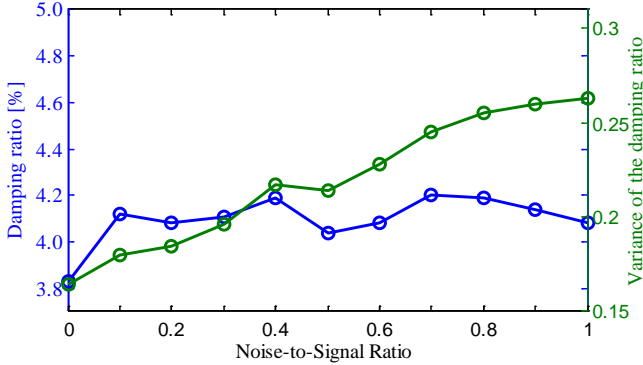
Fig. 2.17 Effect of measurement noise on computed ranking criterion.

The results show that the measurement noise increases the estimated variance. The final ranking of the signals will obviously depend on the level of the noise on each measurement, however a positive thing is that signals with more noise will be negatively penalized (the computed variance increases with noise).

In the previous studies, the order of the ARMA model was selected to be equal to 12 (determined using methodologies from [201]). However, it is necessary to assess how the results of the proposed methodology change when a sub-optimal model order is selected. To do that, the KTH Nordic 32 test system is used to simulate one realization of synchrophasor signals. These signals are used as an input to the proposed method where different values of the selected ARMA model orders are used. The calculated damping ratio variances (criterion values) for different signals are shown in Table 2.7 (the selected model order 12 is highlighted).

Table 2.7 Effects of the selected model order on the estimated variance of the
critical mode's damping ratio.

Model order	Voltage magnitude		Voltage angles	
	Bus 38	Bus 36	Bus 18	Bus 49
10	0.232	0.178	0.126	0.112
11	0.155	0.152	0.125	0.133
12	**0.161**	**0.153**	**0.124**	**0.134**
13	0.165	0.168	0.134	0.125
14	0.153	0.161	0.121	0.144
15	0.154	0.158	0.129	0.136
16	0.160	0.168	0.120	0.152

Table 2.7 shows that the computed variance does not change significantly when the model order is non-optimal, but even this small deviation can cause changes in the final signal ranking. However, it has to be noted that as long as the model order is high enough to describe the dynamics of the system and if a real-time mode estimator uses the same model order, the obtained ranking will be correct even in the case when a non-optimal order is used (the mode estimation will not be optimal but because the estimated variance is correct, the ranking will be adequate).

2.6.5 Computational performance of the proposed method

Following the description of the proposed algorithm in Section 2.4, it is possible to assess its computational performance. The first step of the proposed algorithm is pre-selection. A typical required time for the pre-selection ranking criterion (FFT analysis) computation using a MATLAB implementation and an off-the-shelf personal computer (Intel i7, 2.7 GHz CPU, 8 GB of RAM) is around 0.4 ms per signal.

The result of the pre-selection method is a list of a relatively small number of signals (less than 50 regardless of the system size) for which the final ranking criterion has to be computed. The final ranking criterion for one signal is computed as follows:

1) ARMA model computation (Step 1 in Section 2.4.3). Formally, this is not part of the ranking criterion computation. ARMA models can be obtained from different sources. For instance, following the two level architecture from [82],[198], ARMA models can be computed at the substation level.

2) Model manipulation (Steps 2-5 from Section 2.4.3).

3) Variance calculation (Steps 6-8 from Section 2.4.3).

Typical computational times required for the above procedures using a

MATLAB implementation a personal computer are given in Table 2.8.

Table 2.8 Computational performances of the proposed signal selection method.

Model order	ARMA computation	Model manipulation	Variance calculation
10	1.441 s	0.175 s	0.018 s
12	1.841 s	0.258 s	0.023 s
14	1.916 s	0.341 s	0.027 s
16	2.049 s	0.465 s	0.031 s

The results show that the total computational time, even for the largest systems can be held below 60 s (30 pre-selected signals, 2 s each), whereas the criterion computation time itself can be held below 10 s. By applying the decentralized approach proposed in [82],[198] or using a compiled programming language with better performance (C for example), the computational time can be significantly reduced. Regardless of this, the obtained time delay is acceptable, especially taking into account that long data blocks (10 minutes in the presented case studies) are used as an input, which makes a 60 s delay relatively small.

2.7 Summary

This chapter proposed a criterion and an algorithm that ranks synchrophasor signals according to their ability to estimate parameters of the critical mode (frequencies and damping ratios) with lowest variance. The value of the ranking criterion is computed directly from the model that describes the spectrum of the measured synchrophasor signal. These models can be obtained in two ways depending on the application: 1) from the physical model of the power system in the case of off-line PMU placement problem with the objective of optimal mode estimation, or 2) from on-line measurements in the case of on-line optimal signal selection problem which is used for mode estimation.

This chapter emphasizes the fact that mode estimation, as one of the most important synchrophasor applications, requires special attention, even in the planning stage when PMU locations are decided. Traditionally, this was not the case because PMU locations are mainly determined based on state estimation application requirements. Also, during the operation it is advisable to periodically check if the used signals provide the best possible results because operational changes in the power system can cause a change in the critical modes as well as the signals that contain most information about these modes.

Chapter 3

Ambient Mode Estimation Considering Spectral Load Properties

3.1   Introduction

It is reasonable to assume that aggregated loads changes at the low voltage level can be represented by a Gaussian white noise as shown in [91] [8]. However, considering only the transmission network (which is common practice for transmission system operators), aggregated loads at the high voltage level have a spectrum whose distribution is determined by dynamic characteristics of the local distribution and surrounding transmission systems. Further, intrinsic oscillatory behavior of loads (load oscillations) [87], [195], makes spectral load properties even more complex. These considerations highlight that aggregated load spectra might not be accurately described by a simple function such as white noise.

Even though the properties of input signals have been included in probing mode estimation, the existing mode estimation algorithms that use ambient responses assume that the spectral distributions of the loads are known in advance and constant, i.e. loads are represented by Gaussian white noise [215], [215]. As explained above, this assumption is very strict and may not be satisfied in real-world power systems [87].

---

[8] Load changes are assumed to be white noise, however load signal itself is represented by an integral of white noise. The use of integral of white noise as a load model instead of pure white noise introduces one additional pole at the complex plane origin which is visible in the measured signals. The locations of other modes are not changed.

This chapter proposes a mode meter algorithm which relaxes this assumption, i.e. the method does not assume any underlying load spectral distribution. This refinement makes mode estimates more accurate and independent of spectral load characteristics. The method assumes that load active and reactive powers are available from PMUs placed directly at the load buses. This assumption, even though not satisfied in present-day power systems, is expected to be fulfilled in the near future [215]. However, if some signals are not measured directly, they can be reconstructed using the inverse of the existing power system model, providing estimates of the load spectrums and information about the correlation between loads and measured system outputs. The method adopts an Autoregressive Moving Average (ARMA) model as an underlying model of the system. Using the estimated correlations and definition of the ARMA model, the problem of mode estimation is formulated as an unconstrained linear least-squares problem which can be solved using well known optimization techniques. The algorithm concurrently uses all available synchrophasor signals from the network providing a robust estimate of critical system modes.

The performances of the proposed algorithm are evaluated in the presence and absence of forced oscillations which are result of the load oscillations. The results are compared with two mode estimators: the Yule-Walker algorithm which is widely accepted as a method with good overall performances [215], and the N4SID method as a representative of the group of subspace identification methods [40].

3.2   Methodology

From the system identification and mode estimation viewpoint, it is neither necessary nor feasible to track all changes in the distribution system due to the large number of components and continuous changes in the operating conditions. Further, distribution systems are usually radially connected to the transmission system. This makes the identification of oscillatory events originating at the distribution level relatively straightforward (due to their local nature).Taking into account the aforementioned considerations, the power system model used in this chapter describes dynamics of the transmission system with the distribution system represented by active and reactive power injections at all load buses, i.e. distribution system dynamics are not represented explicitly.

The model of the power system that takes into account the aforementioned consideration is described in a mathematically equivalent form to one described in Section 2.2 where loads aggregated at the transmission/distribution border points are considered as the inputs (without assuming white noise properties).

The block diagram of the proposed method is depicted in Fig. 3.1. The method assumes that all inputs (loads) are measured, whereas outputs are arbitrarily

chosen in accordance with the available PMUs in the system. In the case that some inputs are not measured, these signals are reconstructed using the existing model of the system. The rest of the section describes each step in detail.
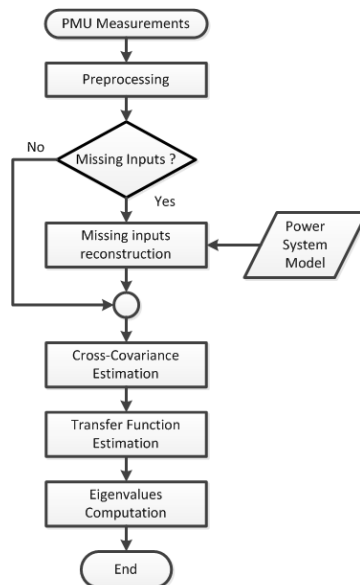

Fig. 3.1 Global block diagram of the proposed method.

3.2.1   Data preprocessing

As the first step in the method, preprocessing aims to remove erroneous data and the mean of the measured signal. Further, the signal is downsampled to 5 Hz in order to improve computational efficiency of the algorithm. More details about preprocessing steps can be found in [87], [216].

3.2.2   Reconstruction of unavailable signals and cross-correlation estimation

The second step reconstructs the signals of active and reactive load powers which are not available from the PMUs. The approach consists in using available information about the system (the existing power system model in this case) in order to obtain an estimate of the required inputs (loads). This procedure avoids the use of predefined signals (such as Gaussian white noise) for representing the loads.

To reconstruct unavailable input signals from the measured outputs, it is necessary to find the inverse system of (2.1)-(2.2). An inverse system of the linear dynamical system is defined as a system which, when fed by the output of the original system, at the output it gives the inputs (excitation) of the original

system [217]. It is assumed that the original system is defined by (2.1)(2.2) and that there is no noise at the output. By using (2.2), the unknown inputs ($\Delta \mathbf{U}_2(s)$) can be expressed as:

$$\Delta \mathbf{U}_2(s) = -\mathbf{D}_2^{-1}\mathbf{C}\Delta \mathbf{X}(s) - \mathbf{D}_2^{-1}\mathbf{D}_1 \Delta \mathbf{U}_1(s) + \mathbf{D}_2^{-1}\Delta \mathbf{Y}(s) , \qquad (3.1)$$

what represents the output equation of the inverse system. By substituting $\Delta \mathbf{U}_2(s)$ from (3.1) into (2.2) , the state space equations of the inverse system are obtained:

$$s\Delta \mathbf{X}(s) = \left[\mathbf{A} - \mathbf{B}_2\mathbf{D}_2^{-1}\mathbf{C}\right]\Delta \mathbf{X}(s) + \\ + \left[\mathbf{B}_1 - \mathbf{B}_2\mathbf{D}_2^{-1}\mathbf{D}_1\right]\Delta \mathbf{U}_1(s) + \left[\mathbf{B}_2\mathbf{D}_2^{-1}\right]\Delta \mathbf{Y}(s) \qquad (3.2)$$

By introducing the following notation,

$$\mathbf{A}' = \mathbf{A} - \mathbf{B}_2\mathbf{D}_2^{-1}\mathbf{C}, \qquad (3.3)$$

$$\mathbf{B}_1' = \mathbf{B}_1 - \mathbf{B}_2\mathbf{D}_2^{-1}\mathbf{D}_1, \qquad (3.4)$$

$$\mathbf{B}_2' = \mathbf{B}_2\mathbf{D}_2^{-1}, \qquad (3.5)$$

$$\mathbf{C}' = -\mathbf{D}_2^{-1}\mathbf{C}, \qquad (3.6)$$

$$\mathbf{D}_1' = -\mathbf{D}_2^{-1}\mathbf{D}_1, \qquad (3.7)$$

$$\mathbf{D}_2' = \mathbf{D}_2^{-1}, \qquad (3.8)$$

a standard state space formulation of the inverse system can be written as:

$$s\Delta \mathbf{X}(s) = \mathbf{A}'\Delta \mathbf{X}(s) + \mathbf{B}_1'\Delta \mathbf{U}_1(s) + \mathbf{B}_2'\Delta \mathbf{Y}(s) , \qquad (3.9)$$

$$\Delta \mathbf{U}_2(s) = \mathbf{C}'\Delta \mathbf{X}(s) + \mathbf{D}_1'\Delta \mathbf{U}_1(s) + \mathbf{D}_2'\Delta \mathbf{Y}(s) . \qquad (3.10)$$

The number of rows in matrix $\mathbf{D}_2$ has to be greater or equal to the number of columns, and the rank of $\mathbf{D}_2$ must be equal to the number rows (number of unknown input signals). If $\mathbf{D}_2$ is not a square matrix, pseudo-inversion is used, which is defined by:

$$\mathbf{D}_2^{-1} = \left(\mathbf{D}_2^T\mathbf{D}_2\right)^{-1}\mathbf{D}_2^T . \qquad (3.11)$$

Vectors $\Delta \mathbf{X}(s)$, $\Delta \mathbf{U}_1(s)$, $\Delta \mathbf{U}_2(s)$ and $\Delta \mathbf{Y}(s)$ maintain the definitions given in Chapter 2. Once the inverse system is determined, unknown input signals are computed by time-domain simulation of the linear system (3.9)-(3.10).

At the beginning of this section it was assumed that all input signals are measured or reconstructed. However cross-correlations between inputs and

outputs carry all necessary information for mode estimation[9], as time domain input signals are not directly used in the proposed mode estimation method. A k-th element in the cross-correlation sequence between two signals ($x_i(n)$ and $x_s(n)$) is estimated as follows:

$$r_{is}(k) = \frac{1}{N} \sum_{n=0}^{N-k-1} x_i(n+k)x_s(n).$$ (3.12)

In the process of signal reconstruction, a known model of the system is used. This represents a well-known "chicken and egg" problem, because a good signal reconstruction is obtained only if the system that we aim to identify is already known, i.e. the system can be identified accurately only if it is already known. There are many approaches to tackle this problem but the main idea behind is usually to use a rough initial model that is improved through an identification process. Iteratively, the solution converges to the true system. This approach will not be discussed further in this thesis, instead, only an initial model will be used to obtain final mode estimation.

3.2.3 Transfer function estimation

As described above, one output signal (measurement) is determined by all inputs (loads) in the system. Using the ARMA model formulation, the equations associated with the i-th output can be written as [218]:

$$
\begin{aligned}
x_{i,1}(n) + \sum_{l=1}^{p} a_p(l)x_{i,1}(n-l) &= \sum_{l=0}^{q} b_{i,1}(l)u_1(n-l) \, ; \\
x_{i,2}(n) + \sum_{l=1}^{p} a_p(l)x_{i,2}(n-l) &= \sum_{l=0}^{q} b_{i,2}(l)u_2(n-l) \, ; \\
\vdots \qquad\qquad \vdots \qquad\qquad &\quad\; \vdots \\
x_{i,N}(n) + \sum_{l=1}^{p} a_p(l)x_{i,N}(n-l) &= \sum_{l=0}^{q} b_{i,N}(l)u_N(n-l),
\end{aligned}
$$ (3.13)

where $x_{i,j}(n)$ is the contribution of the j-th input to the i-th output at the sample n, whereas p and q are the autoregressive and moving average model orders, respectively, with corresponding coefficients $a_p(l)$ and $b_{i,j}(l)$.

In equations (3.13), it is assumed that all denominator coefficients ($a_p(l)$) for each transfer function are the same (considering the unique characteristic polynomial of the system).

The sum of all equations associated with the i-th output (3.13) leads to:

---

[9] Autocorrelation is a special case of cross-correlation where both signals are identical.

$$x_i(n) + \sum_{l=1}^{p}\left(\overbrace{\sum_{s=1}^{N} a_p(l) x_{i,s}(n-l)}^{= x_i(n-l)} \right) = \sum_{l=0}^{q}\sum_{s=1}^{N} b_{i,s}(l) u_s(n-l) , \qquad (3.14)$$

and further:

$$x_i(n) + \sum_{l=1}^{p}\left(a_p(l) \sum_{s=1}^{N} x_{i,s}(n-l) \right) = \sum_{l=0}^{q}\sum_{s=1}^{N} b_{i,s}(l) u_s(n-l) . \qquad (3.15)$$

By multiplying both sides with $x_i(n\text{-}k)$ and taking expected values denoted by $E\{\cdot\}$, the following expression is obtained:

$$E\{x_i(n)x_i(n-k)\} + \sum_{l=1}^{p} a_p(l) E\{x_i(n-l)x_i(n-k)\} =$$

$$= \sum_{l=0}^{q}\sum_{s=1}^{N} b_{i,s}(l) E\{u_s(n-l)x_i(n-k)\}. \qquad (3.16)$$

Using the definition of the autocorrelation and cross-correlation sequences and assuming that inputs are wide-sense stationary [218], (3.16) can be written in compact form as:

$$r_{ii}(k) + \sum_{l=1}^{p} a_p(l) r_{ii}(k-l) = \sum_{l=0}^{q}\sum_{s=1}^{N} b_{i,s}(l) r_{is}(k-l) , \qquad (3.17)$$

or in equivalent form:

$$\sum_{l=1}^{p} r_{ii}(k-l) a_p(l) - \sum_{l=0}^{q}\sum_{s=1}^{N} r_{is}(k-l) b_{i,s}(l) = -r_{ii}(k) , \qquad (3.18)$$

where $r_{ii}(k)$ is the autocorrelation sequence of the i-th output signal and $r_{is}(k)$ is the cross-correlation between i-th output signal and s-th input (load) signal. These correlation sequences are estimated using (3.12). Note that all signals have zero mean due to the assumption of an underlying linear model and the performed preprocessing steps. This ensures that covariances and correlations can be used interchangeably.

The same set of equations can be written for all available output signals ($i= 1,\ldots, M$). Further, an arbitrary number of correlation coefficients can be used ($k=1,\ldots, K$), forming a set of linear $M{\cdot}K$ equations. By using a sufficient number of autocorrelation and cross-correlation elements, it is possible to form an over-determined system of equations given by (3.18). The resulting system is linear in the unknown ARMA model parameters. ARMA parameters are computed from (3.18) using least squares or any other linear programming solver [219]. Note

that this is an unconstrained linear least-square problem.

3.2.4 Computation of system eigenvalues

The computed ARMA model parameters define the characteristic polynomial of the system. The roots of the characteristic polynomial are the system poles (eigenvalues) in the z-domain which can be transformed to the s-domain using the well-known transform [205]:

$$\mathbf{s} = \mathbf{\sigma} + j\mathbf{\omega} = \frac{1}{T_s}\ln(\mathbf{z}), \qquad (3.19)$$

where T_s is the signal's sampling period and $\mathbf{z}$ is the vector of the computed poles in the z-domain. $\mathbf{\sigma}$ and $\mathbf{\omega}$ are the real and imaginary components of the modes in the s-domain ($\mathbf{s}$), respectively. Once the s-domain modes of the system are calculated, the damping ratio of the i-th pole (ζ) can be easily computed from:

$$\zeta_i = \frac{-\sigma_i}{\sqrt{\sigma_i^2 + \omega_i^2}}, \qquad (3.20)$$

in order to perform a small signal stability assessment of the system.

3.3   Study Cases

The proposed method is demonstrated using the KTH Nordic 32 test system [212]. The system has 44 inputs (22 load buses) and a total of 52 buses where the voltage magnitudes are measured. In addition to the 0.5 Hz that was analyzed in the previous section, the analyses in this section will also focus on the second electromechanical mode present in the system (0.73 Hz). The modes' properties obtained from the classical small signal stability analysis are given in Table 3.1. Also, study cases are carried out to assess the performance of the proposed method and to compare it to other methods (the Yule-Walker and N4SID methods, later referred to as conventional methods).

Table 3.1 Dominant modes of the KTH Nordic 32 test system.

Mode 1		Mode 2	
Frequency(f) [Hz]	Damping ratio (ζ) [%]	Frequency (f) [Hz]	Damping ratio (ζ) [%]
0.4987	3.5223	0.7322	3.1801

In all studies, a 13 minutes data window is used for mode estimation (3900 samples are obtained after the preprocessing procedure where the signal is downsampled to 5 Hz).

The Autoregressive model order of the estimated model is chosen to be 25, whereas the moving average order is equal to 2. For the proposed method, 125 elements of the correlation sequences are used (K=125) which corresponds to a 25 second interval with 5 Hz sampling rate. Considering that the system has 52 outputs (M=52), the total number of equations in the unconstrained linear least-square problem is equal to 6500. The statistical properties of the three estimators are evaluated with 1000 independent Monte-Carlo simulations.

3.3.1   Mode estimation in the presence of a forced oscillation

The main advantage of the proposed method is that it takes into account the properties of the input spectrum. For the sake of simplicity, the most comprehensive non-white signals, i.e. white noise with only one permanent oscillation, are used to model load variations. This type of load behavior (sometimes referred to as cyclic load) has been identified in the power system literature [191]. It can be caused by some specific industrial processes [193] or intrinsic element properties, such as diesel generators [194]. This topic has gained more interest in recent time with the deployment of a large number of wind turbines which show oscillatory behavior due to the mechanical properties of the turbine [220].
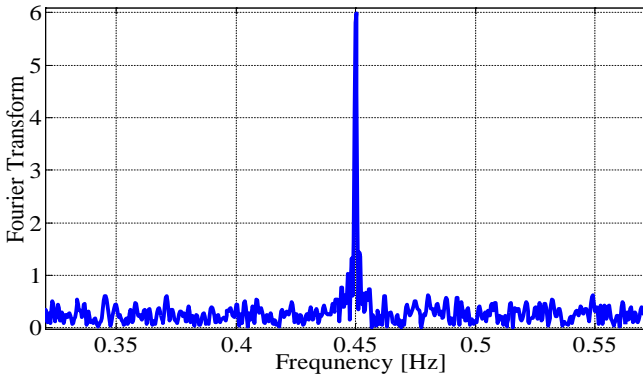
Fig. 3.2 Fourier transform of the active power signal with a load oscillation at 0.45 Hz.

In this study, all load signals (active and reactive powers) are modeled by a load oscillation at 0.45 Hz, which is added to a Gaussian white noise with signal-to-noise ratio of 17 dB (the squared amplitude of the sinusoidal signal component is 25 times smaller than the noise variance). The Fourier transform of the generated load signal is shown in Fig. 3.2. Measurement errors are neglected in the simulation studies.

The results of the performed simulations are shown in Fig. 3.3-Fig. 3.5, while

numerical results are given in Table 3.2. The obtained results show that both estimators which do not take into account the shape of the load spectrum (Yule-Walker and N4SID) wrongly estimate 0.45 Hz as the most critical electromechanical mode, making the true system mode at 0.5 Hz unobservable (invisible). Also, damping of this artificial mode is estimated with very small variance (around 0.001) because the forced oscillation is clearly visible in the spectrum of the measured signals. On the other side, the proposed algorithm correctly discerns the forced oscillation from the *true* system modes in the mode estimation process (mode at 0.45 Hz is not present in Fig. 3.5). This is possible because information about the load oscillation is extracted from the measured input signal and the corresponding correlation sequences.
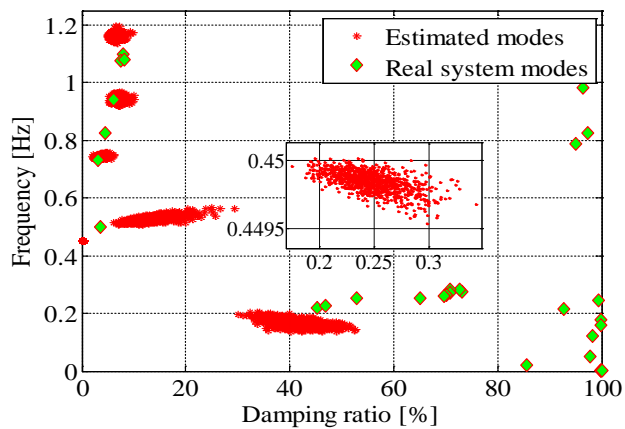
Fig. 3.3 ARMA 25/2 mode estimation using the Yule-Walker method in the presence of forced oscillations at 0.45 Hz.
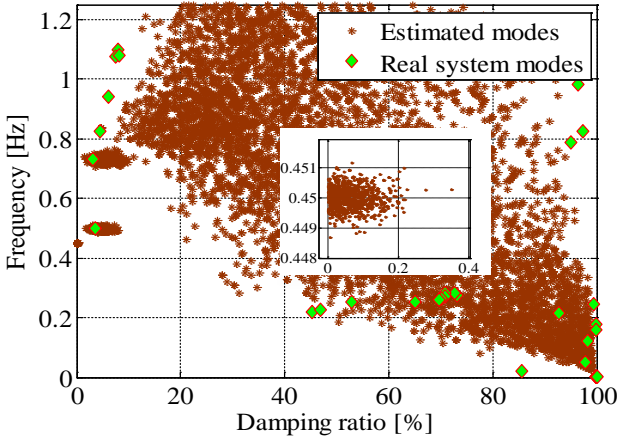
Fig. 3.4 ARMA 25/2 mode estimation using the N4SID method in the presence of forced oscillation at 0.45 Hz.
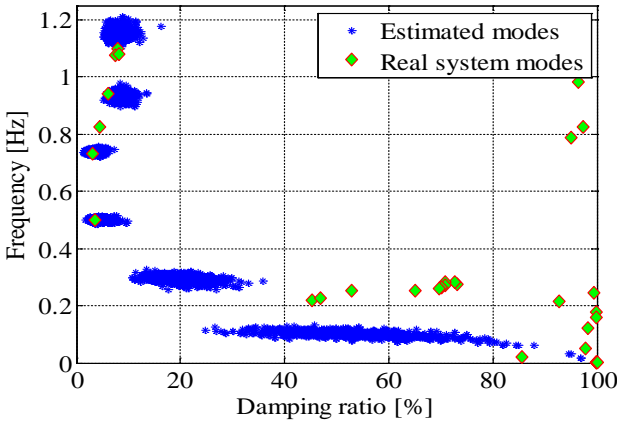
Fig. 3.5 ARMA 25/2 mode estimation using the proposed method in the presence of forced oscillation at 0.45 Hz.

These results show that the "white noise load" assumption used in the Yule-Walker and N4SID methods is essential for accurate mode estimation. However, as illustrated in Fig. 3.3-Fig. 3.5, this assumption might not hold and consequently it will affect the results of the mode estimation. On the other hand, the proposed method is not sensitive to the input load spectrum, i.e. it discerns from the main network modes and neglects specific load dynamics.

Table 3.2 Stochastic properties of the estimation results in the case where a forced oscillation is present in the load signals.

Method / Parameters		Yule-Walker	N4SID	Proposed Method
Mode 1	Mean {f} [Hz]	0.4498	0.4500	0.5009
	Mean {ζ} [%]	0.2470	0.0621	4.8334
	Var {f}	5.745e-9	1.253e-7	2.709e-5
	Var {ζ}	6.798e-4	0.0024	1.4035
Mode 2	Mean {f} [Hz]	0.7445	0.7308	0.7393
	Mean {ζ} [%]	3.7522	4.8403	3.5531
	Var {f}	1.7872e-5	5.154e-5	3.173e-5
	Var{ζ}	0.3640	1.6854	0.6730

Another important observation is that when a forced oscillation appears close to one of the true system modes, it deteriorates the accuracy of the Yule-Walker's method for that *true* system mode. In this case Mode 1 at 0.4987 Hz is estimated with significantly increased damping and large variance (Fig. 3.3). In contrast to that, the N4SID method accurately estimates Mode 1 with a variance which is in accordance to general N4SID performance (Fig. 3.4). Finally, these results show that Yule-Walker shows inferior performance in the presence of the forced oscillation compared to N4SID method, even though both methods show the drawback of estimating the artificial mode at 0.45 Hz.

In order to determine the distribution of the obtained estimates by the proposed method, a larger number (10 000) of Monte Carlo simulations with randomly generated load variations is performed. It is found that the estimates obey a normal Gaussian distribution function which is shown in Fig. 3.6.
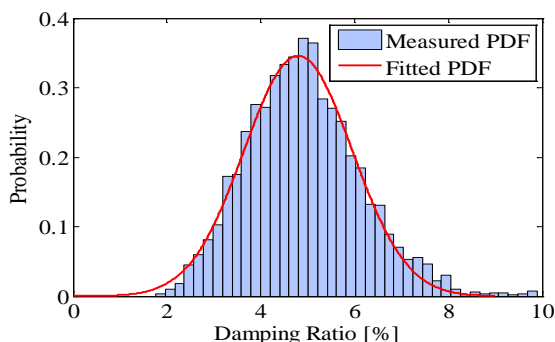

Fig. 3.6 Probability distribution function (PDF) of the estimates.

3.3.2   Mode estimation with loads modeled as pure Gaussian white noise

The three mode estimators are compared in the case where input load changes are driven by white noise. This analysis shows that the proposed method provides results with similar accuracy as the conventional methods when their "white noise assumption" is fully satisfied. The results of the three estimators are given in Fig. 3.7-Fig. 3.9, whereas numerical results are summarized in Table 3.3.

It can be noticed that in this case study Yule-Walker's method provides slightly better results in terms of variance. This is because the "white noise load" assumption (which is incorporated into the Yule-Walker and N4SID methods) is fully satisfied.
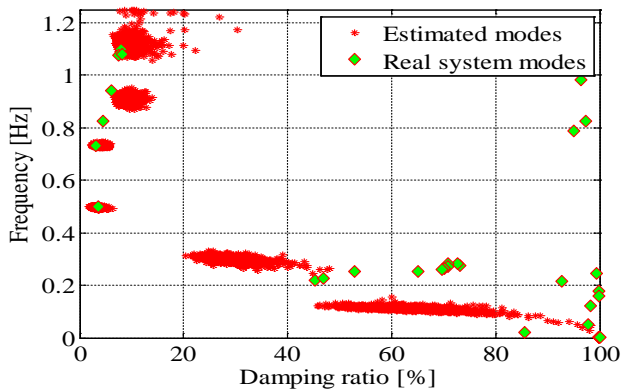
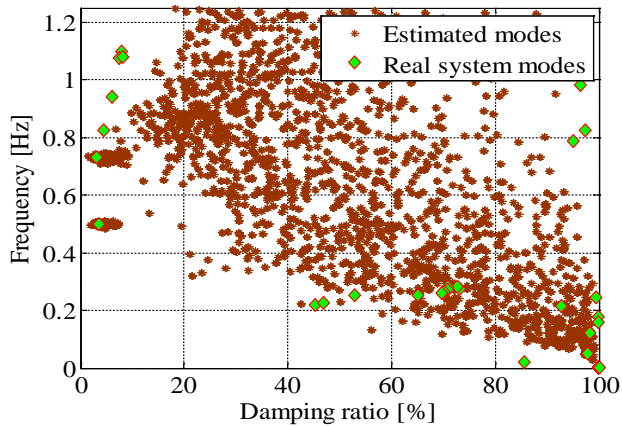*Fig. 3.7 ARMA 25/2 mode estimation using the Yule-Walker method with white noise at all inputs.*

Fig. 3.8 ARMA 25/2 mode estimation using the N4SID method with white noise at all inputs.

On the other hand, the proposed method estimates the input specta based on measurements leading to higher variance of the estimate. N4SID generally shows inferior performances, both in terms of variance and mean value of the estimate.
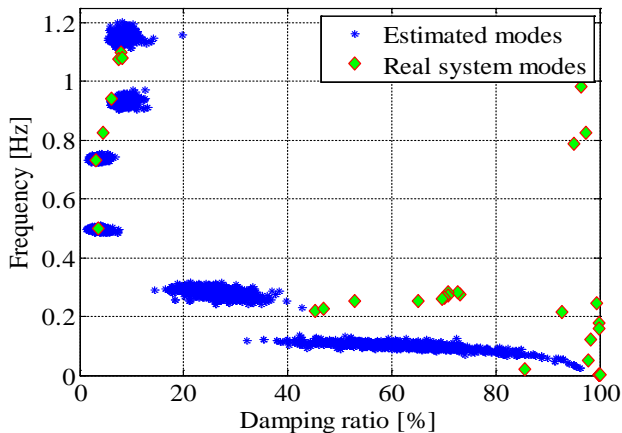

Fig. 3.9 ARMA 25/2 mode estimation using the proposed method with white noise at all inputs.

In addition, the N4SID method shows very poor results when the modes are well damped. Even though these modes are not of interest for mode estimation, the results show that the N4SID algorithm is not suitable for application when more information about well damped modes is required. Fig. 3.7 - Fig. 3.9 show one general deficiency of the mode estimation algorithms: closely located modes significantly affect the accuracy of the mode estimates (e.g. modes with

frequencies from 0.7 to 1.2 Hz and damping ratio below 15 %).

This analysis shows the importance of the "white noise load" assumption for conventional methods, whereas the proposed method obtains accurate results regardless of the load spectrum.

Table 3.3 Stochastic properties of the estimation results in the base case (loads are modeled as a white noise).

	Method Parameters	Yule-Walker	N4SID	Proposed Method
Mode 1	Mean {f} [Hz]	0.4972	0.4978	0.4966
	Mean {ζ} [%]	3.3081	4.1213	3.8104
	Var {f}	8.8670e-6	1.6260e-5	1.6592e-5
	Var {ζ}	0.2728	0.7942	0.8561
Mode 2	Mean {f} [Hz]	0.7334	0.7309	0.7386
	Mean {ζ} [%]	3.8184	4.7095	3.5497
	Var {f}(10e-5)	1.4072e-5	6.2711e-5	2.3151e-5
	Var{ζ}	0.3563	1.7925	0.5965

3.3.3 Mode estimation using the different types of synchrophasor signals

In the previous sections, voltage magnitude synchrophasor measurements are used with the aim to assess the performance of the proposed method. However, the mode estimation method has been derived without assuming any particular output signal type, therefore different signals (such as active and reactive powers, currents and voltage angles) can also be used for the mode estimation. Table 3.4 shows the results of the estimation of the two critical electromechanical modes with measurement signals of different type.

Table 3.4 Stochastic properties of the estimation results with measured signals of different type.

	Signals Paramaters	P	Q	P and Q	Currents	Voltage Angles
Mode 1	Mean {f} [Hz]	0.4984	0.4947	0.4957	0.4972	0.4876
	Mean {ζ} [%]	3.4598	4.8100	4.1088	3.687	3.6147
	Var {f}(10e-5)	2.1430	0.9188	2.9195	2.5516	8.6658
	Var {ζ}	1.0031	0.8956	0.3995	1.0146	0.7794
Mode 2	Mean {f} [Hz]	0.7510	0.7396	0.7471	0.7424	0.7364
	Mean {ζ} [%]	4.2281	3.4986	3.9582	4.2144	3.6546
	Var {f}(10e-5)	7.0669	1.0833	4.9610	3.0993	26.605
	Var{ζ}	2.0461	0.6622	0.5883	1.0455	0.7605

From the results in Table 3.4, it can be concluded that any type of signal can be successfully used for mode estimation, but the combination of active and reactive power signals provides estimates with slightly lower variance. One reason for this is that number of analyzed signals in this case is larger compared to other analyzed cases. Voltage angle signals provide high observability of the modes (because of their relatively low variance compared to the number of used signals), whereas the use of current signals provides less encouraging results.

3.3.4   Effects of measurement noise on estimation accuracy

In order to assess the robustness of the proposed method in the presence of measurement noise, different noise levels are simulated and the estimation results are compared with the case where no measurement noise is present. The noise is modeled by adding Gaussian white noise to the measured signals. The noise-to-signal ratio (NSR) used is defined as a ratio between the variance of the measurement noise and the variance of the ambient data analyzed. Fig. 3.10 shows howthe   mean values and variances of the estimates (frequency and damping ratio) change with the different levels of measurement noise. The colored range in Fig. 3.10 represents ± 0.5 standard deviation of the estimation.
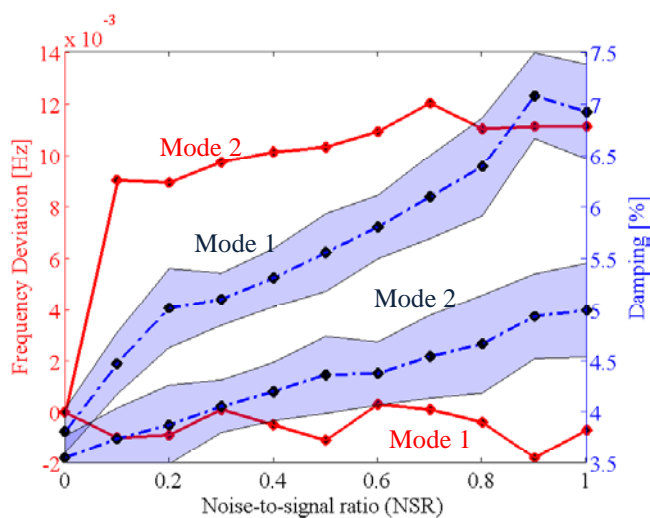

Fig. 3.10 Effects of measurement noise on frequency and damping estimation.

In the case of frequency estimation, the standard deviation is of order 10^{-5}, therefore, this range appears as a thin line in Fig. 3.10. An important conclusion is that a large amount of noise does not significantly affect the frequency estimation. On the other hand, the estimated damping ratio increases with the increase of the noise level whereas the variance is not significantly increased.

3.3.5 Effects of load sensitivity on mode estimation

As stated before, the proposed method neglects the behavior of the load, meaning that the method always estimates modes which are associated only with the transmission part of the system (transfer function between load buses and measured signals). Biases introduced by the load behavior can be analyzed using the load model from [206]:

$$P_L = P_0 \left(\frac{V}{V_0} \right)^{\alpha} (1 + K_{pf} \Delta f) , \tag{3.21}$$

$$Q_L = Q_0 \left(\frac{V}{V_0} \right)^{\beta} (1 + K_{qf} \Delta f) , \tag{3.22}$$

where*:*

-   P_0 and Q_0 are the initial active and reactive loads;

-   V_0 is a voltage magnitude at the initial operating condition;

-   The α and β coefficients describe load active and reactive power dependence on voltage variation;

-   K_{pf} and K_{qf} describe load active and reactive power dependence on frequency deviation. In these studies, typical ranges for the load coefficients are adopted from [206].

The dependence of the location of the first critical mode at 0.5 Hz on different load sensitivity coefficients is shown in Fig. 3.11 and Fig. 3.12.
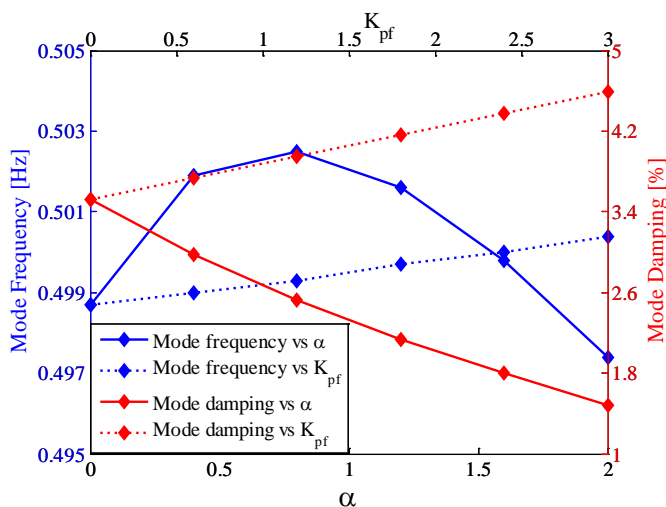
Fig. 3.11 Sensitivity of the mode location to load active power change caused by variations in voltage and frequency.
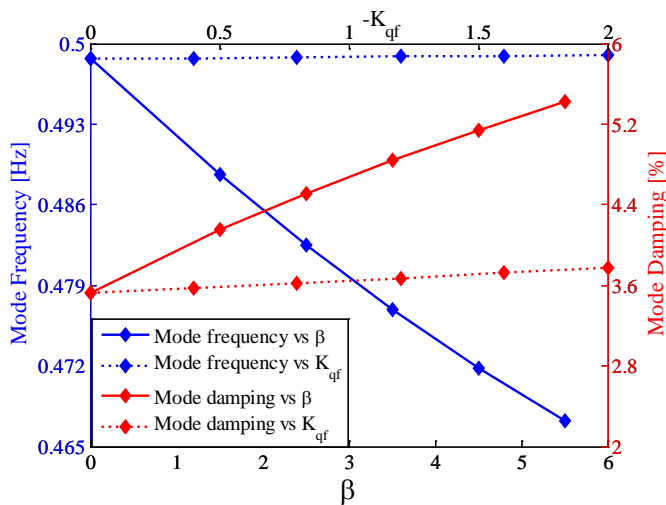

Fig. 3.12 Sensitivity of the mode location to load reactive power change caused by variations in voltage and frequency.

It can be concluded that the mode frequency is not significantly affected by load sensitivities, except in the case of reactive power sensitivity to voltage deviation.

System mode damping is more sensitive to load characteristic changes (see

Fig. 3.11 and Fig. 3.12). Based on the presented results, the modes of the whole system can be computed from the estimated modes by knowing the model of the loads and using (3.21) and (3.22). As can be seen in Fig. 3.11 and Fig. 3.12, the uncertainty in the load parameters does not introduce significant error in the mode estimation.

3.3.6   Mode estimation in the case of reconstructed signals

Even though it is envisioned that all buses in the transmission network will be equipped with PMUs in the future, it is necessary to consider a situation where some load buses are not equipped with PMUs or some PMU measurements are not available due to device or communication malfunction. In this regard, the proposed methodology is employed to reconstruct missing measurements at load buses. It is reasonable to expect that a large number of missing load signals and the existing model uncertainty negatively affect the accuracy of the reconstruction procedure. However, even in the case where none of the loads are measured, the procedure provides better estimation of the input-output cross-correlations compared to those of any other predefined spectral distribution.

To analyze the method's dependency on model inaccuracy, the generator's inertias and exciters' gains are intentionally changed to model this uncertainty. These model parameters are chosen under the assumption that they have a large influence on electromechanical oscillations [205], [207]. In addition, to analyze the dependency on measurement unavailability, none of the input (load) signals are measured and therefore they are all reconstructed using the methodology previously presented.

Three test cases are analyzed where the generators' inertias and exciters' gains are changed by 10 %, 20 % and 50 % from their original values, respectively. This is done in such way that half of the generators have their original values increased, while the other half have these values decreased. The dominant modes of these modified (uncertain) models are given in Table 3.5. For each level of model inaccuracy 100 independent random load variations are simulated and the modes are estimated for each one of them. The results from the proposed mode estimation method are presented in Fig. 3.13-Fig. 3.15.
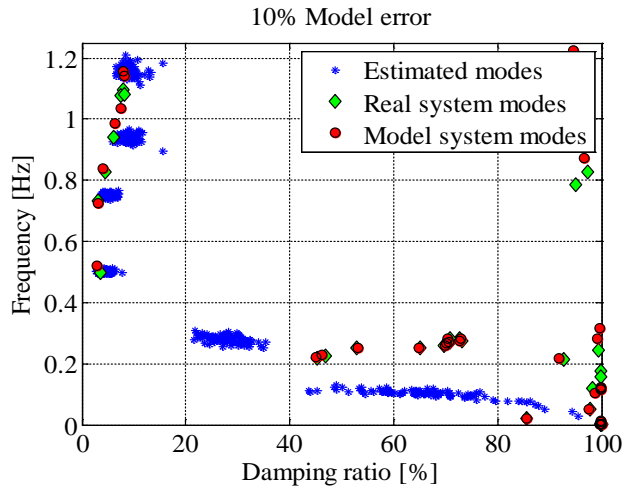
Fig. 3.13 Mode estimation results using the proposed algorithm with no measured inputs and assumed model with 10 % error.
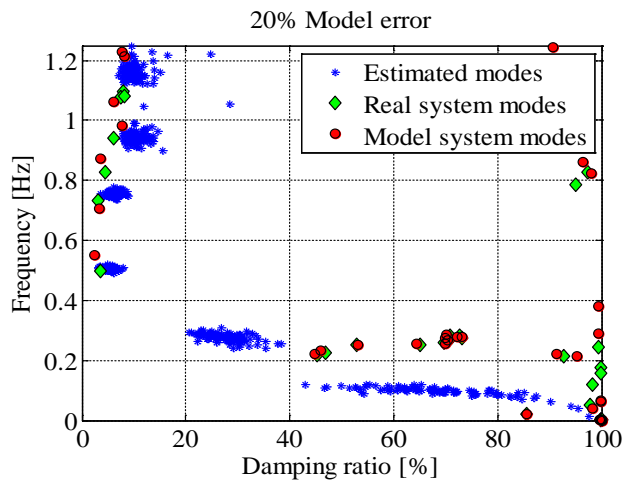

Fig. 3.14 Mode estimation results using the proposed algorithm with no measured inputs and assumed model with 20 % error.
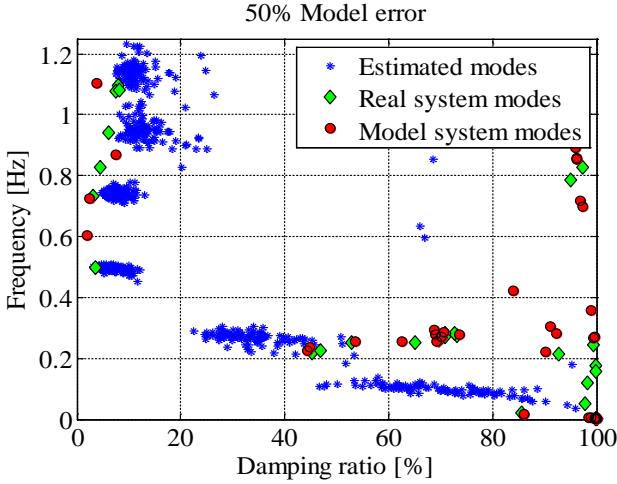
*Fig. 3.15 Mode estimation results using the proposed algorithm with no
measured inputs and assumed model with 50 % error.*

Table 3.5 Dominant system modes for different model uncertainty levels.

Model	Mode 1		Mode 2	
	Frequency (f) [Hz]	Damping (ζ) [%]	Frequency(f) [Hz]	Damping (ζ) [%]
0%	0.4987	3.5223	0.7322	3.1801
10 %	0.5225	2.9569	0.7251	3.1857
20 %	0.5494	2.3961	0.7075	3.3520
50 %	0.6060	1.9014	0.7237	2.3556

Since an inaccurate model is used in the algorithm, the correlation sequences
obtained will be imprecise, leading to less reliable but still satisfactory mode
estimates which can be seen in Table 3.6. However, the most important property
of the estimator, its ability to discern and neglect forced oscillations, is still kept
due to the fact that forced oscillations are detected from the input data even with
erroneous model parameters such as the ones used in these study cases.

Table 3.6 Stochastic properties of the estimation results in the case without measured input signals and different model uncertainty.

		10% Model Variation	20% Model Variation	50% Model Variation
Mode 1	Mean $\{f\}$ [Hz]	0.5022	0.5064	0.4966
	Mean $\{\zeta\}$ [%]	4.5042	5.2139	6.8878
	Var $\{f\}$	1.967e-5	2.508e-5	5.197e-5
	Var $\{\zeta\}$	0.8344	1.0106	2.3343
Mode 2	Mean $\{f\}$ [Hz]	0.7522	0.7547	0.7427
	Mean $\{\zeta\}$ [%]	4.9322	6.2311	7.4958
	Var $\{f\}$	3.318e-5	6.470e-5	1.623e-4
	Var$\{\zeta\}$	0.6412	0.9853	1.6479

The results in Table 3.6 show that, regardless of the model uncertainty, the forced oscillation is not identified as a true system mode. However, model uncertainty has an effect on the accuracy of the estimation process; this can be seen in the mean value and variance of the estimate (larger uncertainty leads to larger bias and variance). Fig. 3.13-Fig. 3.15 also show that the uncertain model does not create bias in the estimated mode frequency but slightly increases the value of the estimated damping ratio.

The use of an inaccurate model to distinguish between a forced oscillation and a real system mode imposes a possible problem in the case where the model contains no information about the dominant mode. In that case, the real system mode can be interpreted as a forced oscillation and therefore it might not be reported to the operator.

3.3.7 Effects of measurement noise on input signal reconstruction

Measurement noise in the output signals (which are used for the reconstruction of the unavailable input signals) corrupts the quality of the estimated input signals. In the studies performed, a fully accurate model is assumed, meaning that the measurement noise is the only cause of errors for input signal reconstruction.

Different measurement noise levels (up to 1.1 NSR) are simulated and six different sets of output signals are used in the reconstruction process. The selected output signal sets used in the reconstruction process are:

- *Set 1* - Voltage magnitudes in all buses and 60 both active and reactive power flow measurements[10].

---

[10] There are 80 lines in the system, and PMUs can be installed at both ends.

- *Set 2* - Voltage angles in all buses and 60 both active and reactive power flow measurements.

- *Set 3* - Voltage magnitudes and angles in all buses and 80 both active and reactive power flow measurements.

- *Set 4* - Voltage magnitudes and angles in all buses and 80 both active and reactive power flow measurements, as well as 80 current magnitude measurements.

- *Set 5* - Voltage magnitudes and angles in all buses and active and reactive power flow measurements at both ends of all lines in the system.

- *Set 6* - Voltage magnitudes and angles in all buses and active and reactive power flow measurements as well as current magnitude measurements at both ends of all lines in the system.

The computed dependence between noise level in the measured output and the resulting noise in the reconstructed input is given in Fig. 3.16. Two cases are analyzed, the noise level produced at the active power inputs and the noise level at the reactive power inputs.

From Fig. 3.16, it can be concluded that the first set of measurements provides satisfactory accurate input estimation. This is due to the fact that the NSR of the estimated input signal is around 2 for active power and less than 1.5 for reactive power in the case of 1.1 NSR in the output measurements. This proportion approximately holds for all noise levels. A larger number of measured signals reduces the effect of the output noise. In addition, with the larger number of measured signals, the noise produced at the input has a lower NSR compared to the NSR of the original (output) measurements.
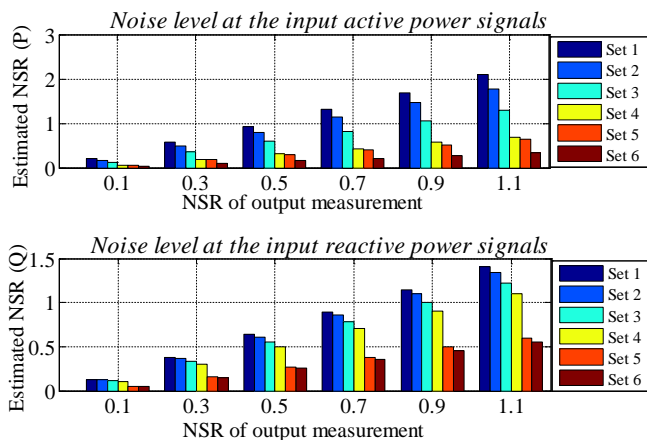
Fig. 3.16 Errors in load signal estimation by using the inverse power system model caused by output measurement noise.

3.4   Discussion

3.4.1   Topology change

Topology changes may lead to a significant displacement of the modes. Because the time window used for the estimation is in range of 10-15 minutes, the estimator may not be able to instantaneously calculate new (correct) results after a significant topology change. Instead, the estimated modes have a smooth transition to the correct results.

The ambient system response is present in the measured signals all the time, whereas topology changes may introduce additional transient responses. The transient response can be used for mode estimation (employing methods that use transient responses) in order to crosscheck the results obtained using an ambient mode estimator.

If the model is used for input signal reconstruction, it is necessary to update the model after a topology change to reflect the current state of the system. The effects of using an inaccurate model of the system are analyzed in the previous section.

3.4.2   Computational complexity

The computational complexity of the proposed method is mainly determined by two steps in the algorithm, namely:

- *Unconstrained linear least-squares problem*. The least-squares problem is solved in every estimation cycle. The computation time depends on the

number of unknown model parameters which is equal to $N \cdot M \cdot q + p$. In the analyzed problem (6500 equations), the required solution time is around 50 s using a MATLAB implementation and a personal computer[11]. The number of unknown parameters is especially sensitive to the order of the numerator (q) in the estimated ARMA model. A high order of the numerator leads to high order of the least-squares problem, which significantly reduces the computational performance of the method.

- *Pseudoinversion* as a part of the input signal reconstruction. This step can take significant computational time in the case where a large number of input measurements is missing (up to 7 minutes for the reconstruction of 5000 input signals using a MATLAB implementation and a personal computer). This step is performed only once after the model of the system is updated, therefore, the computational performance is less critical in this case.

All other steps of the methodology (such as the correlation coefficient computation) require negligible computational time and do not affect the overall computation performance.

3.5   Summary

This chapter proposes a method for mode estimation using ambient synchrophasor data which relaxes the widely accepted assumption that the loads are accurately described by white noise. The proposed method is founded on the hypothesis that a large number of PMUs is deployed in the system. Despite the fact that this is not the case in present-day power systems, we believe that a sufficient number of PMUs will be deployed in the near future.

The results obtained confirmed that the method correctly exploits information about spectral load properties, enabling the estimator to deal only with *true* system modes. These results indicate that the proposed method will provide more accurate mode estimates in real-life operating conditions where loads can have unpredictable spectral characteristics.

The results obtained suggest that unavailable input signals can be extracted with satisfactory accuracy even with a relatively inaccurate model of the power system. The performed analyses also show that the proposed method provides comparatively accurate results even in the case where the "white noise" load assumption is satisfied, meaning that the proposed method, compared to conventional methods, does not compromise accuracy by any means.

The proposed method correctly estimates the modes of the transmission part of the system. If necessary, the modes of the overall system (including loads) can

---

[11] Intel i7, 2.7Ghz CPU and 8 GB of RAM.

be estimated using existing load models to compensate for the bias introduced by the loads.

The analyses show that the level of measurement noise affects the estimation accuracy, particularly the damping ratio estimation accuracy. The computational performance predominantly depends on the selected order of the numerator in the estimated ARMA model. A high order can result in unacceptable high dimensions of the least-squares problem.

The proposed methodology gives a new perspective in the mode estimation problem. Still, forced oscillations and their effects on mode estimation algorithms in general need to be investigated more thoroughly in real-life conditions. Preassembly, the best results in practice can be obtained by confronting results from different approaches in an integrated manner; this is a topic for future research. It is also important to investigate new methods for obtaining faster response of the mode estimator in order to make estimation more accurate during transients.

Chapter 4

Least Costly Probing Signal Design

4.1   Introduction

Probing based methods for mode estimation represent a compromise between ambient and ringdown mode estimation methods. These methods use a low magnitude probing signal as an excitation to the system [221]. These methods are non-intrusive but, due to the known excitation, are able to provide more accurate mode estimation results compared to ambient data-based methods. A low magnitude excitation (probing) can be generated by modulating the following signals:

1) Reference signals of automatic voltage regulators,
2) Reference signals in the control systems of FACTS devices (active and reactive power, voltage control, etc),
3) Reference signals of turbine governors.

Assuming a given location and the reference signal used for the probing, there is a question on how this signal should look like in order to obtain the best possible mode estimate. This issue was first addressed in [222], where different design considerations have been discussed. However, a formal mathematical formulation of the probing signal design procedure has not been provided.

In the control theory community, the problem of optimal experiment (probing) design for system identification has been analyzed thoroughly [223],[224],[225]. The traditional approach in experiment design is to determine an input signal that ensures a high system performance from the control perspective [225]. More

recently, the least costly experiment paradigm was proposed [226],[227]. In this approach, the experiment is designed with respect to the allowed uncertainty of the estimated model.

In this chapter, the least costly paradigm is adopted for the design of the probing signal. The probing signal is designed in such a way that the uncertainties of the critical modes' damping ratio estimates are lower than a predefined threshold. The design procedure is formulated as a Linear Matrix Inequality (LMI) optimization problem with the power spectrum of the probing signal as a decision variable. The decision variable is parameterized (described) by:

1)   The signal's autocorrelation function (ACF), or
2)   The amplitudes of the sine waves in a multisine signal.

The objective function is defined as a weighted sum of two components: 1) the variance of the injected probing signal, and 2) the mean square of the output signal deviation that represents the level of the system disturbance. The constraints in the LMI formulation are the maximal tolerable variances of the estimates of the critical damping ratios.

The optimal probing power spectrum that is determined can be realized with different time-domain signals. Three time-domain signal realization methods are presented in the sequel. Two of them are proposed here and used for realizing the probing signals whose power spectrum is described by an autocorrelation sequence, whereas the third method is used to generate a multisine signal, as proposed in [222].

The contributions of this chapter are summarized as follows:

1)   The expression that relates accuracy of mode estimation and spectrum of the probing signal is derived.
2)   Reactive power injection is proposed for probing.
3)   The least costly experiment design approach is adopted, modified and applied for design of probing signal. The modification introduces the mode estimation accuracy as a constraint. Two spectrum parameterizations are used (multisine and continuous spectrum).
4)   A signal realization method that considers time domain constrains has been developed.
5)   Two additional signal realization methods have been applied (FIR filter and multisine).
6)   The case studies demonstrate significant accuracy improvements when the probing signal is optimally shaped (4-5 times better accuracy of the mode estimation for the same input power).

4.2   Background

As described in the thesis introduction, an ambient system response measured by Phasor Measurement Units (PMUs) can be described by a single transfer function $H(z)$ excited by white noise $e(t)$, where the white noise represents random load changes at an aggregated level. This ambient response is also present during probing tests when the system is intentionally excited. Assuming system linearity and using the principle of superposition, the measured synchrophasor signal $y(t)$ can be decomposed into two components: One as a result of ambient excitation ($H(z)e(t)$) and another as a result of probing ($G(z)u(t)$), as shown in Fig. 4.1 and previously described in Fig. 1.5. Signal $u(t)$ is the probing signal that can be designed and $G(z)$ represents a transfer function between the probing signal and the measured output signal $y(t)$.
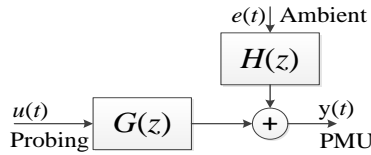

Fig. 4.1 Power system model during probing tests.

Since both transfer functions in Fig. 4.1 ($G(z)$ and $H(z)$) can be derived from the same state space model of a power system, it is reasonable to assume that both transfer functions have the same denominators. This defines an ARMAX (AutoRegressive Moving Average with eXogenous inputs) model structure of the system [154]:

$$y(t) = \frac{B(z,\theta)}{A(z,\theta)} u(t) + \frac{C(z,\theta)}{A(z,\theta)} e(t) , \qquad\qquad (4.1)$$

where z is the time shift operator and θ is a vector of model parameters. $A(z,\theta)$, $B(z,\theta)$ and $C(z,\theta)$ are polynomial functions in z. This model can be expressed in terms of another parameter vector $\rho = f(\theta)$, of which one subvector is the vector ζ that represents the damping ratios of all system modes. This reparameterization consists of the conversion of the discrete poles and zeros of (4.1) into the continuous domain and expressing them as a function of ρ, i.e. poles/zeros' frequencies and damping ratios, as shown in Chapter 2 and [199]. The resulting model is:

$$y(t) = \frac{B(z,\rho)}{A(z,\rho)} u(t) + \frac{C(z,\rho)}{A(z,\rho)} e(t) . \qquad\qquad (4.2)$$

This model, and consequently its modes, can be identified from the measured data using a prediction error method [209]. If it is assumed that: 1) the model structure used in the identification has sufficiently high order to describe the true

system, 2) $G(\rho)$ is strictly proper, and that 3) $H(\rho)$ is proper, monic and has a stable inverse, the estimate obtained with a prediction error method is an asymptotically unbiased estimate of the true system parameters ρ_0 [12]. Furthermore, the covariance matrix of the parameter estimates P_ρ is given by [209]:

$$
\begin{aligned}
P_\rho^{-1} = &\left(\frac{N}{\sigma^2} \frac{1}{2\pi} \int_{-\pi}^{\pi} F_u(\omega, \rho_0) F_u^*(\omega, \rho_0) \Phi_u(\omega) d\omega \right) + \\
&+ \left(\frac{N}{2\pi} \int_{-\pi}^{\pi} F_e(\omega, \rho_0) F_e^*(\omega, \rho_0) d\omega \right),
\end{aligned}
\tag{4.3}
$$

where:

- N is the number of data points used for identification,
- ρ_0 represents the true system parameter vector,
- $\Phi_u(\omega)$ is the power spectrum of the probing signal,
- σ^2 is the variance of the ambient (driving) noise, and
- the functions $F_u(\omega, \rho_0)$ and $F_e(\omega, \rho_0)$ are defined as follows:

$$
F_u = H^{-1}(\omega, \rho) \frac{\partial G(\omega, \rho)}{\partial \rho} \text{; and } F_e = H^{-1}(\omega, \rho) \frac{\partial H(\omega, \rho)}{\partial \rho}.
$$

Equation (4.3) provides the relationship between the power spectrum of the probing signal $\Phi_u(\omega)$ and the accuracy of the estimation that is described by P_ρ. It should be noted that (4.3) assumes that the true system parameters ρ_0 are known. Because the true value of ρ_0 is not known, an initial estimate of ρ_0 will be used for the purpose of optimal probing design. The initial estimate of ρ_0 can be obtained from an existing physical model of the system or with initial system identification.

4.3   Optimal Power Spectrum of the Probing Signal

The general block diagram of the proposed probing signal design procedure is given in Fig. 4.2. The input to the algorithm is a user defined maximal tolerable variance of the critical modes' damping ratio estimates. An LMI optimization procedure provides the optimal spectrum of the probing signal. This procedure is described in this section, whereas the methods for the realization of the time-domain probing signal are described in the following section.

---

[12] An estimate of ρ_0 can also be obtained by first estimating the ARMAX model (4.1), and then by using the mapping $\rho=f(\theta)$.
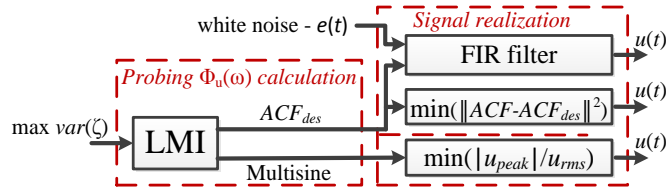
Fig. 4.2 Block diagram of the proposed probing signal design methods.

4.3.1   Objective function of the LMI optimization problem

The objective of the optimization procedure is to find the power spectrum that minimizes the system disturbance induced by the probing signal, as well as the control effort of the probing device. This objective function can be formalized as:

$$\min_{\Phi_u(\omega)} J = \left(\frac{k_1}{2\pi} \int_{-\pi}^{\pi} \Phi_u(\omega) d\omega \right) + \left(\frac{k_2}{2\pi} \int_{-\pi}^{\pi} |G|^2 \Phi_u(\omega) d\omega \right), \qquad (4.4)$$

where $\Phi_u(\omega)$ is the power spectrum of the input (probing) signal. k_1 and k_2 are weighting factors. The selected output signal should reflect the level of the disturbance caused by the probing experiment.

4.3.2   Power spectrum parameterization

The power spectra of the probing and output signal in (4.4) have infinite dimensions which are impossible to handle by digital computers. Therefore, it is necessary to adopt a finite dimensional approximation (parameterization) of the spectra. Two parameterizations are used here: 1) signal autocorrelation sequence, and 2) multisine. In the sequel, (4.3) and (4.4) are expressed in terms of these two parameterizations.

Spectrum parameterization using a signal's autocorrelation sequence

Using the parameterization based on the autocorrelation sequence, the power spectrum of the probing signal is defined as:

$$\Phi_u(\omega) = \sum_{r=-M}^{M} c_r e^{j\omega r} > 0 \text{ , with } c_r = c_{-r}, \qquad (4.5)$$

where M is the order of approximation and c_r $(r=0,\dots,M)$ is the signal's autocorrelation sequence (decision variable).

Now, the objective function (4.4) can be expressed in terms of the defined parameterization (by substituting (4.5) into (4.4)):

$$
\min_{c_r (r=0...M)} J = \left(\frac{k_1}{2\pi} \int_{-\pi}^{\pi} \sum_{r=-M}^{M} c_r e^{j\omega r} d\omega \right) +
$$
$$
+ \left(\frac{k_2}{2\pi} \int_{-\pi}^{\pi} G(\omega,\rho_0)G^*(\omega,\rho_0) \sum_{r=-M}^{M} c_r e^{j\omega r} d\omega \right).
\tag{4.6}
$$

In the same manner, (4.3) can be formulated as:

$$
P_\rho^{-1} = \left(\frac{N}{\sigma^2} \frac{1}{2\pi} \int_{-\pi}^{\pi} F_u(\omega,\rho_0)F_u^*(\omega,\rho_0) \sum_{r=-M}^{M} c_r e^{j\omega r} d\omega \right) +
$$
$$
+ \left(\frac{N}{2\pi} \int_{-\pi}^{\pi} F_e(\omega,\rho_0)F_e^*(\omega,\rho_0)d\omega \right).
\tag{4.7}
$$

The expressions (4.6) and (4.7) can be further manipulated to obtain a form suitable for the definition of an LMI problem. It can be noticed that both, (4.6) and (4.7), are comprised of summands that have a general form as follows[13]:

$$
\frac{1}{2\pi} \int_{-\pi}^{\pi} T(\omega)T^*(\omega) \sum_{r=-M}^{M} c_r e^{j\omega r} d\omega ,
\tag{4.8}
$$

where $T(\omega)$ is a vector of known transfer functions and c_r is a real number. In the sequel, it will be shown how to express (4.8) in the form $\sum_{r=0}^{M} R_r c_r$ which is later used in the LMI problem formulation.

Because $T(\omega)$ is not a function of r, (4.8) can be rewritten as:

$$
\sum_{r=-M}^{M} c_r \frac{1}{2\pi} \int_{-\pi}^{\pi} T(\omega)T^*(\omega)e^{j\omega r} d\omega .
\tag{4.9}
$$

Using Parseval's theorem and the fact that $e^{j\omega}$ is the transfer function of the forward shift operator, the following holds:

$$
\sum_{r=-M}^{M} c_r \frac{1}{2\pi} \int_{-\pi}^{\pi} T(\omega)T^*(\omega)e^{j\omega r} d\omega = \sum_{r=-M}^{M} c_r \frac{1}{2\pi} \int_{-\pi}^{\pi} \Phi_{\bar{y}(t),\bar{y}(t-r)}(\omega)d\omega =
$$
$$
= \sum_{r=-M}^{M} c_r E[\bar{y}(t)\bar{y}^T(t-r)].
\tag{4.10}
$$

---

[13] Note that some summands do not have all elements of the general form. The first summand in (4.6) is obtained by choosing $T(\omega)=1$, and the second summand in (4.8) is obtained for $M=0$.

In (4.10), E denotes the expected value of a random process, $\overline{y}(t) = T(z)\overline{e}(t)$ with $\overline{e}(t)$ white noise of unit variance and $\Phi_{\overline{y}(t),\overline{y}(t-r)}$ is the cross-spectrum between $\overline{y}(t)$ and $\overline{y}(t-r)$. Due to symmetry ($c_r = c_{-r}$), (4.10) can be written as:

$$\sum_{r=-M}^{M} c_r E[\overline{y}(t)\overline{y}^T(t-r)] = c_0 R_0 + \sum_{r=1}^{M} c_r (R_{r+} + R_{r+}^T) ,\qquad (4.11)$$

where $R_{r+} = E[\overline{y}(t)\overline{y}^T(t-r)]$ for $r > 1$, and $R_0 = E[\overline{y}(t)\overline{y}^T(t)]$. Note that with R_{r+} and R_0 calculated, it is trivial to express (4.8) in the desired form (

$\sum_{r=0}^{M} R_r c_r$), i.e. it can be written as $R_r = R_{r+} + R_{r+}^T$ for $r>0$, and $R_r = R_0$ for $r=0$. Consequently, this also provides an algorithm for expressing (4.6) and (4.7) in the desired form. Therefore, the following paragraphs will provide the algorithm for the calculation of R_{r+} and R_0.

To compute R_{r+} and R_0, the transfer function vector $T(z)$ first needs to be expressed in single-input multiple-output (SIMO) state space form, as follows:

$$\begin{aligned} \overline{x}(t+1) &= A\overline{x}(t) + B\overline{e}(t) \\ \overline{y}(t) &= C\overline{x}(t) + D\overline{e}(t). \end{aligned}\qquad (4.12)$$

Now, the matrix R_{r+} can be written as follows:

$$\begin{aligned} R_{r+} &= E\left[\overline{y}(t)\overline{y}^T(t-r)\right] = \\ &= CE\left[\overline{x}(t)\overline{x}^T(t-r)\right]C^T + CE\left[\overline{x}(t)\overline{e}^T(t-r)\right]D^T = \\ &= CX_r C^T + CX_{er} D^T . \end{aligned}\qquad (4.13)$$

To obtain (4.13), it was used that $\overline{e}(t)$ is white noise and that $E\left[\overline{e}(t)\overline{x}(t-r)\right] = 0$ for all $r \geq 0$. From the control system theory it is known that the following holds for all values of r:

$$\overline{x}(t) = A^r \overline{x}(t-r) + \sum_{i=1}^{r} A^{i-1} B\overline{e}(t-i) ,\qquad (4.14)$$

therefore, the expression for X_{er} from (4.13) can be written as:

$$X_{er} = E\left[\left(A^r\bar{x}(t-r) + \sum_{i=1}^{r} A^{i-1}B\bar{e}(t-i)\right)\bar{e}^T(t-r)\right] =$$

$$= E\left[\left(A^r\bar{x}(t-r) + A^{r-1}B\bar{e}(t-r)\right)\bar{e}^T(t-r)\right] = \qquad (4.15)$$

$$= A^{r-1}BE\left[\bar{e}(t-r)\bar{e}^T(t-r)\right] = A^{r-1}B.$$

In a similar way, the expression for X_r can be written as:

$$X_r = E\left[\left(A^r\bar{x}(t-r) + \sum_{i=1}^{r} A^{i-1}B\bar{e}(t-i)\right)\bar{x}^T(t-r)\right] =$$

$$= E\left[A^r\bar{x}(t-r)\bar{x}^T(t-r)\right] = A^r E\left[\bar{x}(t)\bar{x}^T(t)\right] = A^r X, \qquad (4.16)$$

where X can be written as:

$$X = E\left[\left(A\bar{x}(t-1) + B\bar{e}(t-1)\right)\left(A\bar{x}(t-1) + B\bar{e}(t-1)\right)^T\right] =$$

$$= AXA^T + BB^T. \qquad (4.17)$$

Equation (4.17) constitutes the Lyapunov equation $X = AXA^T + BB^T$ that can be solved for X, which provides a solution for X_r.

Now, using the obtained expressions for X_r and X_{er} and the value of the computed X, (4.13) can be written as:

$$R_{r+} = CX_r C^T + CX_{er}D^T = CA^r XC^T + CA^{r-1}BD^T. \qquad (4.18)$$

At this point only R_0 needs to be determined. Following the same approach as in the case of R_{r+}, the following holds:

$$R_0 = E\left[\bar{y}(t)\bar{y}^T(t)\right] = E\left[\left(C\bar{x}(t) + D\bar{e}(t)\right)\left(C\bar{x}(t) + D\bar{e}(t)\right)^T\right] =$$

$$E\left(C\bar{x}(t)\bar{x}^T(t)C^T\right) + E\left(D\bar{e}(t)\bar{e}^T(t)D^T\right) = CXC^T + DD^T. \qquad (4.19)$$

Now, using the general expressions (4.8)-(4.11), (4.18) and (4.19) the objection function defined by (4.6) can be written in a linear form with respect to the coefficients c_r ($r=0,\dots,M$), i.e using the derived form ($\sum_{r=0}^{M} R_r c_r$):

$$\min_{c_r (r=0\dots M)} J = k_1 c_0 + k_2 \sum_{r=0}^{M} Q_r c_r, \qquad (4.20)$$

where Q_r ($r=1,\dots,M$) are constant matrices.

Further, following the same procedure, (4.7) can be written as:

$$P_\rho^{-1} = \frac{N}{\sigma^2} \sum_{r=0}^{M} R_r c_r + NS ,$$

(4.21)

where R_r $(r=0,\ldots,M)$ and S are constant matrices.

Multisine power spectrum parameterization

A multisine signal is defined by the following expression:

$$u(t) = \sum_{r=1}^{M} A_r \cos(\omega_r t + \varphi_r) ,$$

(4.22)

where A_r, ω_r and φ_r are the amplitude, frequency and phase of the r-th sine component. Consequently, the power spectrum of a multisine signal is equal to:

$$\Phi_u(\omega) = \frac{\pi}{2} \sum_{r=1}^{M} A_r^2 \delta(\omega - \omega_r) + A_r^2 \delta(\omega + \omega_r) .$$

(4.23)

Following a similar procedure as in the previous subsection, the objective function (4.4) is expressed in terms of the multisine parameterization by substituting (4.23) into (4.4):

$$\min_{A_r^2(r=1\ldots M)} J = \left(\frac{k_1}{2} \sum_{r=1}^{M} A_r^2 \right) + \left(\frac{k_2}{2} \sum_{r=1}^{M} |G_0(\omega_r, \rho_0)|^2 A_r^2 \right),$$

(4.24)

where $A_r^2 (r = 1,\ldots,M)$ is the decision variable.

Further, the relationship between the probing signal's power spectrum and the estimation covariance matrix (defined by (4.3)) can be expressed in terms of the multisine parameterization (by substituting (4.23) into (4.3)):

$$P_\rho^{-1} = \frac{N}{2\sigma^2} \sum_{r=1}^{M} \mathrm{Re}\left\{ F_u(\omega_r, \rho_0) F_u^*(\omega_r, \rho_0) \right\} A_r^2 +$$
$$+ \frac{N}{2\pi} \int_{-\pi}^{\pi} F_e(\omega, \rho_0) F_e^*(\omega, \rho_0) d\omega.$$

(4.25)

Note that this expression can be simplified as:

$$P_\rho^{-1} = \frac{N}{\sigma^2} \sum_{r=1}^{M} R_r c_r + NS \; , \tag{4.26}$$

where R_r is derived trivially from (4.25), and the procedure for the derivation of S given in the previous subsection.

4.3.3 Constraints used in the LMI optimization problem

The accuracy of the mode estimation is determined by the estimation variances of the critical modes' damping ratios (ζ_i.). These variances are the diagonal elements of P_ρ (see (4.3)). Therefore, sufficiently accurate mode estimation is obtained if the variance of each critical damping ratio ζ_j is constrained to be smaller than some user-defined value. This is written as:

$$\mathrm{var}(\zeta_j) = P_\rho(i,i) = e_i^T P_\rho e_i < r \; , \text{i.e.} \; r - e_i^T P_\rho e_i > 0 \tag{4.27}$$

where r is the user-defined constraint (maximal allowed value of the critical variance), i is the index of a critical mode's damping ratio in the parameter vector ρ_0, and e_i is a unity vector whose i-th element is equal to one. When several modes need to be accurately estimated, a constraint defined by (4.27) is added for each critical mode.

As it can be seen from (4.3), the relationship between P_ρ (or $e_i^T P_\rho e_i$) and the decision variable (power spectrum of the probing signal) is non-linear due to the inversion operation. In order to formulate an LMI form of the constraint (4.27), this relationship has to be convexified. This can be done by exploiting the Schur complement property that a matrix is positive definite if and only if its Schur complement is positive definite [228]. Since (4.27) can be represented in the form of Schur complement, an equivalent constraint would be a constraint on the positive-definiteness of the matrix whose Schur complement is equal to $r - e_i^T P_\rho e_i$. Therefore, the constraint (4.27) can be written as:

$$\begin{bmatrix} r & e_i^T \\ e_i & P_\rho^{-1} \end{bmatrix} > 0 \; . \tag{4.28}$$

The constraint defined by (4.28) has a form of an LMI. This can be seen when P_ρ^{-1} in (4.28) is replaced by (4.26) or (4.21) (depending on the parameterization adopted).

Another constraint that has to be taken into account is that the obtained power spectrum must be positive for all frequencies (physical constraint). When the power spectrum is parameterized using an autocorrelation sequence, the spectrum's positivity can be guaranteed by the existence of a symmetric matrix Z that satisfies the following LMI constraint [226],[227]:

$$\begin{bmatrix} Z - A^T Z A & C^T - A^T Z B \\ C - B^T Z A & D + D^T - B^T Z B \end{bmatrix} > 0, \tag{4.29}$$

where A, B, C and D matrices are defined as follows:

$$A = \begin{bmatrix} 0 & 0 \\ I_{m-1} & 0 \end{bmatrix}_{M \times M} ; \quad B = \begin{bmatrix} 1 & 0 & ... & 0 \end{bmatrix}_{1 \times M} ;$$

$$C = \begin{bmatrix} c_1 & c_2 & ... & c_M \end{bmatrix}_{1 \times M} ; \quad D = c_0 / 2 .$$

When the multisine parameterization is used, this problem is solved by imposing non-negativity of the decision variable:

$$A_r^2 \geq 0; \quad \text{for} \quad r = 1, 2, ..., M . \tag{4.30}$$

4.3.4   LMI optimization problem formulation

The previous subsections describe two types of LMI optimization problems (that differ only by the power spectrum parameterization adopted) whose solutions provide the optimal spectrum of the probing signal. The optimization problem that uses the autocorrelation-based parameterization is defined by the objective function (4.20) subject to (4.28) and (4.29), considering relationship (4.21). On the other hand, the optimization problem that uses the multisine parameterization is defined by the objective function (4.24) subject to (4.28) and (4.30), considering relationship (4.26). For the sake of simplicity, the defined optimization problems will be rewritten here:

LMI   optimization   formulation   using   autocorrelation parameterization

$$\min_{c_r (r=0...M)} J = k_1 c_0 + k_2 \sum_{r=0}^{M} Q_r c_r , \tag{4.31}$$

subject to:

$$\begin{bmatrix} r & e_i \\ e_i^T & \dfrac{N}{\sigma^2} \sum_{r=0}^{M} R_r c_r + NS \end{bmatrix} > 0 , \tag{4.32}$$

$$\begin{bmatrix} Z - A^T Z A & C^T - A^T Z B \\ C - B^T Z A & D + D^T - B^T Z B \end{bmatrix} > 0 , \tag{4.33}$$

where all variables are defined before.

LMI   optimization   using   multisine   spectrum parameterization

$$\min_{A_r^2 \, (r=1...M)} J = \left(\frac{k_1}{2} \sum_{r=1}^{M} A_r^2 \right) + \left(\frac{k_2}{2} \sum_{r=1}^{M} \left| G_0(\omega_r, \rho_0) \right|^2 A_r^2 \right), \quad (4.34)$$

subject to:

$$\begin{bmatrix} r & e_i \\ e_i^T & \dfrac{N}{\sigma^2} \sum_{r=1}^{M} R_r c_r + NS \end{bmatrix} > 0, \quad (4.35)$$

$$A_r^2 \geq 0; \quad \text{for } r = 1, 2, ..., M, \quad (4.36)$$

where all variables are defined before.

4.4   Probing Signal Realization

Section 4.3 provides an optimal power spectrum of the probing signal. However, a spectrum can be realized with different time-domain signals, which leaves additional opportunity for optimization. One property of the signal that can be considered in the optimization is the signal's magnitude (because probing equipment might have a physical limitation regarding the signal magnitude that can be obtained). Another important property of the signal that can be optimized is its *crest factor* [222], defined as:

$$Cr\{u(t)\} = \frac{max\{|u(t)|\}}{rms\{u(t)\}} = \frac{max\{|u(t)|\}}{\sqrt{\dfrac{1}{2\pi} \int_{-\pi}^{\pi} \Phi_u \, d\omega}} = \frac{max\{|u(t)|\}}{\sqrt{var\{u(t)\}}}. \quad (4.37)$$

The crest factor describes the signal's magnitude relative to the variance which is obtained from the LMI optimization ($var\{u(t)\}$ is a result of the optimization). Smaller values of the signal's crest factor are beneficial because they impose smaller strain on the probing equipment [222].

In the sequel of this chapter, three methods for the realization of time-domain signals with specified power spectra are presented. Two methods are used for the realization of probing signals whose spectrum is described by an autocorrelation sequence, whereas the third method realizes multisine signals.

4.4.1   Signal realization with constrained signal's magnitude

The sequel describes a method for obtaining a time-domain signal with a given power spectrum and constrained magnitude. This method can be seen as a special case of the method proposed in [229], [230].

The desired spectrum is described by the autocorrelation sequence ACF_{des}, which is defined as $ACF_{des}(r) = c_r$ for $r=0,\ldots,M$, (see (4.5)), and $ACF_{des}(r) = 0$ for, $r=M+1,\ldots,M+K$, where K is an arbitrary positive integer constant. The main idea of the method is to minimize the discrepancy between ACF_{des} and the sample autocorrelation sequence of the probing signal $u(i)$.

The signal's sample autocorrelation of lag τ, computed using k data points, is given by:

$$ACF_k(\tau) = \frac{1}{k} \sum_{i=\tau+1}^{k} u(i)u(i-\tau) = \frac{k-1}{k} ACF_{k-1}(\tau) + \frac{1}{k} u(k)u(k-\tau), \quad (4.38)$$

The optimal signal can be found iteratively. In the iteration m, a signal window of size L is determined ($u(k)$ for $k=(m-1)L+1,..,mL$). The defined signal window is computed by minimizing the following objective function:

$$\min_{u(k)} \sum_{\tau=0}^{M+K} \left(ACF_{mL}(\tau) - ACF_{des}(\tau) \right)^2 , \qquad (4.39)$$

subject to:

$$u_{min} < u(k) < u_{max}, \qquad k=(m-1)L+1,.., mL, \qquad (4.40)$$

where u_{min} and u_{max} are lower and upper bound, respectively.

The optimization problem defined by (4.39)-(4.40) is a nonlinear optimization problem which can be solved in the MATLAB environment by the command "`fmincon`". The full length signal $u(k)$ with N elements is therefore determined in $ceil(N/L)$ iterations. Note that the complete signal can be determined in only one iteration if $L=N$. However, if N is large, the optimization problem can be impractical to solve due to the large dimension of the decision variable (dimension is equal to L). In other words, a fixed value of L makes this type of signal realization scalable.

It is important to note that the methodology presented above can be easily modified to include other types of time-domain constraints that would need to be considered depending on the specific characteristics of the probing equipment. This makes the described method very appealing for practical application.

4.4.2   Signal realization using an FIR filter

A signal with the desired spectrum can be realized by passing a white noise signal through an appropriate filter. In this case, the squared frequency response of the filter has to be equal to the desired signal's power spectrum. Therefore, the problem of signal realization is equivalent to finding the parameters of the filter. If it is assumed that the filter has an FIR structure, its parameters can be obtained using a spectral factorization technique [231]. To this end, the application of the method described in [231] is straightforward because the input to the method is a signal's autocorrelation sequence, and the outputs are the parameters of the FIR filter.

It should be noted that this procedure is not suitable for multisine spectrum parameterization. This can be concluded from the fact that a multisine autocorrelation sequence is indefinitely long; therefore, it is not possible to approximate it using an FIR filter. A more physical explanation is that generating a sine signal from the white noise requires a very narrow banded filter, which results in a filter of impractically large order.

This type of signal realization has the advantage that is easy to implement. Once the filter's parameters are determined, an arbitrarily long signal is generated simply by filtering white noise. On the other hand, a disadvantage is that the magnitude of the signal is not explicitly constrained, which can result in a relatively large crest factor.

4.4.3   Multisine realization with minimization of crest factor

The multisine signal spectrum that is determined as a result of the LMI optimization provides the amplitudes of the sine waves that compose the signal. However, the phases of the sine waves are not determined (they do not affect the spectrum). By exploiting this freedom to choose sine phases, it is possible to obtain signals with minimal crest factors. A method to minimize the crest factor of a multisine signal is presented in [222] and used here without modifications.

4.5   Case Studies

The theory and techniques presented in Section 4.3 and Section 4.4 are validated through simulations using the KTH Nordic 32 test system [212]. It is assumed that a FACTS device with the capability of injecting reactive power is installed at bus 48. This reactive power injection is selected as the input used for probing. As an output, the voltage magnitude of bus number 38 is selected and used for mode estimation. The disturbance is evaluated using the same output signal, i.e. the deviation of the voltage magnitude is selected as a measure of the disturbance caused by the probing experiment. The KTH Nordic 32 test system

has two critical modes at 0.5 Hz and 0.76 Hz. The probing signal will be designed to accurately estimate the damping ratios of these two modes.

It was mentioned that an initial estimate of ρ_0 is required to perform optimal probing signal design. This initial estimate is obtained through an identification procedure. The data for this identification are generated with the linearized high-order power system model. The ambient excitation (active and reactive power injections) is modeled by unity variance white noise in all load buses, whereas the input signal is chosen to be white noise with a variance of 10 000. The order of the identified models ($G(z)$ and $H(z)$) are chosen to be equal to 12. This initial estimate has a limited accuracy that will be improved by using the optimal probing. The duration of the optimal probing signals, which is determined in the sequel, is chosen to be 10 minutes, i.e. 3000 data samples (the sampling frequency is equal to 5 Hz).

4.5.1   Minimization of the probing signal variance

In the first case study, the power spectrum of the probing signal is obtained by minimizing its variance ($k_1=1$ and $k_2=0$ in (4.4)) with the constraint that the variance of the damping ratios' estimates is smaller than 10^{-5} (for both modes). In these studies, three types of probing power spectra are designed: 1) white noise ($M=0$), 2) a signal whose power spectrum is described by an autocorrelation sequence ($M\neq0$), and 3) a multisine. The variance of the white noise probing signal is obtained directly from (4.3) by replacing $\Phi_u(\omega)$ with a constant function. The multisine signal is designed with a frequency resolution of 0.01 Hz. In the case of a continuous spectrum signal representation, the spectrum is described by 21 coefficients ($M=20$).

The obtained probing spectra are shown in Fig. 4.3 and Fig. 4.4 with the corresponding signals' variances shown in Table 4.1.
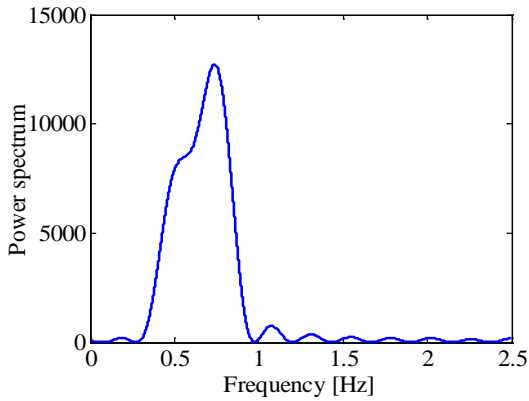
Fig. 4.3 Spectrum of the optimal input signal with continuous spectrum parameterization when the input variance is minimized.
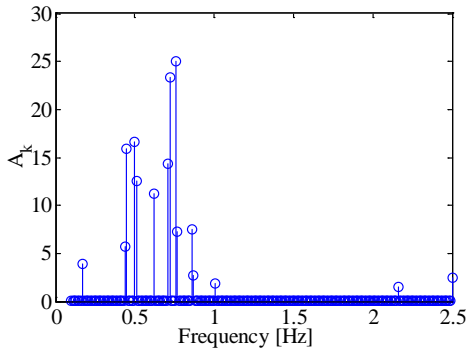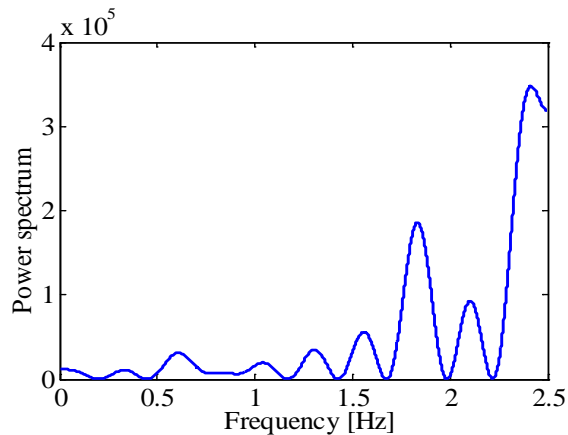

Fig. 4.4. Spectrum of the optimal multisine input signal when the input variance is minimized.

Table 4.1 Introduced system disturbance when the variance of the probing signal is minimized.

	White noise	Multi-sine	FIR filter
$var(u(t))$	10410.0	1179.8	1901.4
$var(y(t))$	1.6761	2.0915	1.5994

It can be noticed that the white noise excitation has a much larger (required) input and output variance (disturbance) compared to the optimal multisine and the FIR realization. These results mean that *the same accuracy* of mode estimation can be obtained with *5-7 times weaker excitation*. Also, it can be shown that when *the same input power* is used, the proposed methodology

provides 4-5 times better accuracy of the mode estimation. These results present the main benefit of the proposed method for optimal probing signal design.

Also, the signal's energy is mostly allocated around the critical modes' frequencies (0.5 Hz and 0.76 Hz). This is understandable because the easiest way to excite the mode is to introduce an excitation exactly at the frequency of the mode.

The signals are generated assuming that the ambient excitation has unity variance in all load buses of the power system. Thus, the obtained probing signal variance from Table 4.1 represents a ratio between the probing signal variance and the variance of the ambient excitation (the adopted relative value is equal to one).

4.5.2   Minimization of the output signal variance

The goal in this case study is to minimize the response of the system introduced by the probing signal ($k_1=0$ and $k_2=1$ in (4.4)). Therefore, in this case the variance of the output signal (measured voltage magnitude) is minimized. The variances of the damping ratio estimates are constrained to be smaller than 10^{-5} (for both critical modes). The obtained probing spectra are shown in Fig. 4.5 and Fig. 4.6 with the values of the signals' variances shown in Table 4.2.

Fig. 4.5 Spectrum of the optimal probing signal with continuous spectrum parameterization when the output variance is minimized.
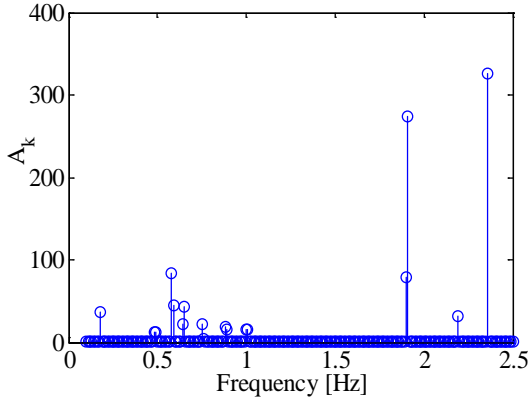
Fig. 4.6 Spectrum of the optimal multisine probing signal when the output variance is minimized.

Table 4.2 Introduced system disturbance when variance of the output signal is minimized.

	White noise	Multi-sine	FIR
$var(u(t))$	10410.0	101850	50558
$var(y(t))$	1.6761	1.2424	1.3928

The variance of the probing signal is very large (Table 4.2) as compared to the case when the probing signal's variance was minimized (Table 4.1). It is interesting to note that the high frequency components carry most of the signal's power. This is due to the low system gain at these frequencies; thus, a probing signal with such components does not disturb the system significantly. In addition, the minimization of the output variance does not reduce this variance to a large extent. This can be explained by the fact that certain level of disturbance is required in order to obtain accurate mode estimation results.

4.5.3   Minimization of the weighed sum of probing signal and output variances

In order to minimize both probing (input) and output variance, a weighted sum is taken as a criterion (denoted by $var\{uy(t)\}$). The weighting factors are chosen to be $k_1=0.5$ and $k_2=1000$ because the output variance has a numerical value that is roughly 2000 times smaller. The obtained probing spectra are shown in Fig. 4.7 and Fig. 4.8, with the signals' variances shown in Table 4.3.
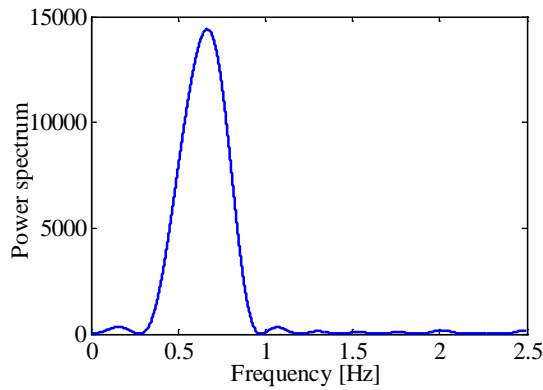
Fig. 4.7 Spectrum of the optimal probing signal with continuous spectrum parameterization when both, probing and output variances are minimized.
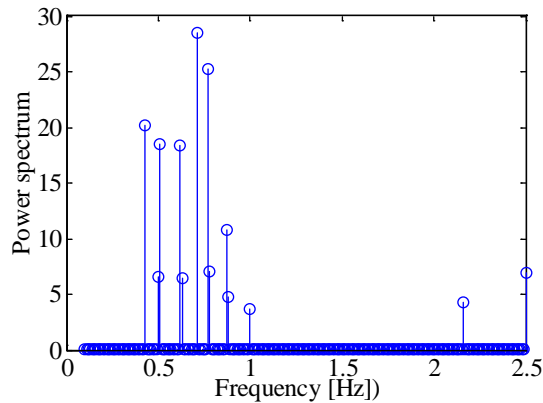

Fig. 4.8 Spectrum of the optimal multisine probing signal when both, probing and output variances are minimized.

Table 4.3 Introduced system disturbance when the variance of the input and output signals is minimized.

	White noise	Multi-sine	FIR filter
$var\{u(t)\}$	10410.0	1441.6	1933.6
$var\{y(t)\}$	1.6761	1.598	1.5515
$var\{uy(t)\}$	6881.1	2318.8	2518.2

This type of criterion represents a compromise between the two previously presented criteria. However, it can be noted that high frequencies do not contribute significantly to the mode estimation accuracy, and thus, these components are suppressed (compared to the case when only the output variance

is minimized). The result is that the power spectrum shape is similar to the case when only probing signal's variance is minimized (see Table 4.1).

4.5.4 Validation of the damping ratio variance constraint

The procedure presented in Section 4.3 is derived using several assumptions. One of them is infinite data length (the obtained expressions describe asymptotic behavior). Also, different approximations are used in the derivation such as the Tustin approximation for expression of continuous domain parameters (mode frequency and damping ratio), the first order approximation of the expression for P_ρ, etc. (see [209] for more details). Therefore, it is necessary to assess if the actual estimation variance (obtained using Monte Carlo simulations) corresponds to the design values.

Four different values of the constraint for damping ratio variances are applied and optimal probing signals are obtained. Using the designed probing signals as an input, the modes are estimated using the prediction error method in 1000 Monte Carlo simulations. The results are then used to compute the "actual" variance of the estimation process. The system is identified using an ARMAX model structure, while the modes are calculated afterwards from the identified model. The signals are realized using FIR filter and multisine parameterization. The results for the 0.5 Hz mode are presented in Table 4.4.

Table 4.4 Variances of the damping ratio estimates observed using Monte Carlo simulations.

Signal	Objective function	Applied Constraint Value			
		10^{-5}	$5 \cdot 10^{-6}$	10^{-6}	$5 \cdot 10^{-7}$
FIR filter	$var\{u(t)\}$	$1.29 \cdot 10^{-5}$	$5.89 \cdot 10^{-6}$	$9.17 \cdot 10^{-7}$	$5.01 \cdot 10^{-7}$
	$var\{y(t)\}$	$1.33 \cdot 10^{-5}$	$5.99 \cdot 10^{-6}$	$1.02 \cdot 10^{-6}$	$4.83 \cdot 10^{-7}$
	$var\{uy(t)\}$	$1.18 \cdot 10^{-5}$	$6.18 \cdot 10^{-6}$	$9.71 \cdot 10^{-7}$	$4.91 \cdot 10^{-7}$
Multi-sine	$var\{u(t)\}$	$1.11 \cdot 10^{-5}$	$6.11 \cdot 10^{-6}$	$1.34 \cdot 10^{-6}$	$6.02 \cdot 10^{-7}$
	$var\{y(t)\}$	$1.26 \cdot 10^{-5}$	$6.31 \cdot 10^{-6}$	$9.98 \cdot 10^{-7}$	$4.71 \cdot 10^{-7}$
	$var\{uy(t)\}$	$1.23 \cdot 10^{-5}$	$6.44 \cdot 10^{-6}$	$1.26 \cdot 10^{-6}$	$5.83 \cdot 10^{-7}$

The results in Table 4.4 show a certain deviation of the estimation variance from the design values, but this difference is always less than 35%. Regardless, applying the probing methods will always lead to a better estimation variance as compared to the ambient data-based method (the obtained accuracy with the ambient data-based method for the same setup and zero input signal is $1.65 \cdot 10^{-5}$).

4.5.5 Comparison of different signal realization methods

In Section 4.4 three methods for signal realization are presented and their performances are compared here. The power spectrum obtained by minimizing probing signal's variance with required accuracy of 10^{-5} (Table 4.1) is used for the realization of time-domain signals.

Signal realization with constrained magnitude

In the case of signal realization using constrained magnitude, the crest factor can be defined by an analyst. However, an excessive reduction of the crest factor can compromise the shape of the obtained power spectrum (the signal might not have the power spectrum/autocorrelation that was designed). To evaluate the fit between the desired and obtained spectrum, the criterion defined by (4.39) is used. First, it is analyzed how this criterion changes with different values of the signal limits (and consequently the crest factor). The value of L is chosen to be equal to 2. The results are shown in Fig. 4.9.
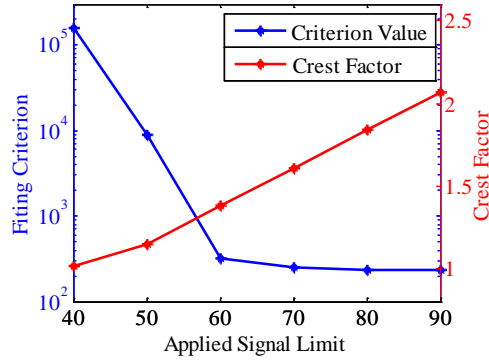
Fig. 4.9 Fitting criterion and crest factor as a function of the applied signal magnitude limit.

Fig. 4.10 shows the obtained sample autocorrelation sequence for different values of the applied magnitude constraint. It can be noticed that when the accuracy is constraint to 10^{-5}, a sufficiently good fit is obtained for magnitudes larger than 50 which corresponds to a fitting criterion smaller than 1000.
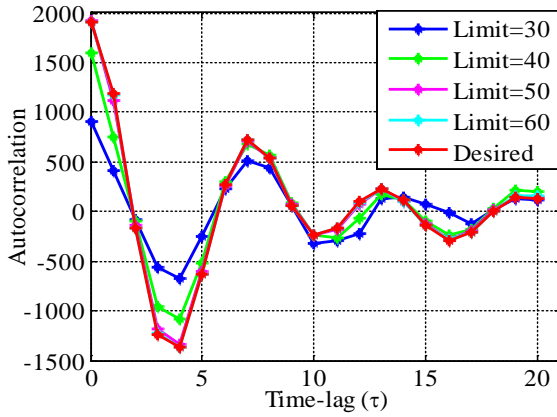
Fig. 4.10 Obtained sample autocorrelation sequence as a function of the applied signal limit.
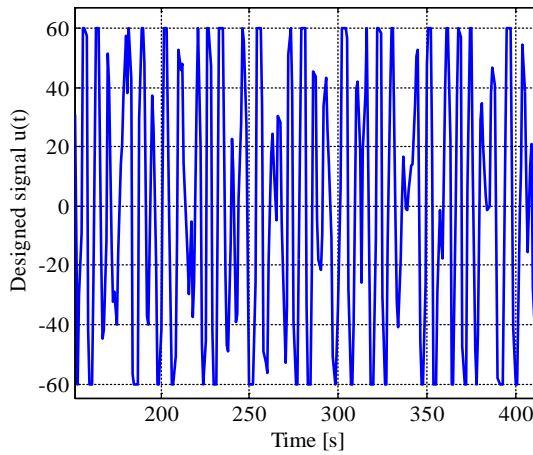

Fig. 4.11 Part of the designed probing signal with the magnitude constrained to 60.

The time-domain realization of the designed signal with the magnitude constrained to 60 is shown in Fig. 4.11.

Signal realization using an FIR filter

The method to realize the probing signal using an FIR filter does not allow control over the crest factor value. Therefore, the obtained crest factors for

different optimization criteria and estimation accuracy levels are only reported in Table 4.5.

Table 4.5 Crest factor for signals obtained using FIR filters.

Objective function	Applied Constraint Value			
	10^{-5}	$5 \cdot 10^{-6}$	10^{-6}	$5 \cdot 10^{-7}$
var$\{u(t)\}$	3.7193	3.6738	3.6463	3.6472
var$\{y(t)\}$	3.6962	3.6924	3.6274	3.6614
var$\{uy(t)\}$	3.6509	3.7130	3.6394	3.6726

The obtained crest factors are in the range from 3.62 to 3.72 for all realizations. Note that the signals' magnitudes can be obtained using (4.37) and values in Table 4.1 and Table 4.5.

Multisine realization with minimization of crest factor

As presented previously, the goal is to find the vector of sine waves' phases that minimize the crest factor [222]. The procedure is initialized by choosing random phases. Table 4.6 presents values of crest factors for signals whose spectra were determined before.

Table 4.6 Crest factors of the designed multisine signals.

Objective function	Method	Applied Constraint Value			
		10^{-5}	$5 \cdot 10^{-6}$	10^{-6}	$5 \cdot 10^{-7}$
var$\{u(t)\}$	Random phases	4.034	4.143	3.980	4.418
	Optimal phases	3.272	3.354	2.981	3.469
var$\{y(t)\}$	Random phases	2.863	3.323	3.639	4.137
	Optimal phases	2.618	2.941	3.012	3.221
var$\{uy(t)\}$	Random phases	3.579	4.182	4.236	3.901
	Optimal phases	2.754	3.338	3.693	3.472

It can be noticed that the obtained crest factor is reduced significantly compared to the case with random phases. However, observe that these values depend on the spectrum and phases used for initialization. The obtained crest factors are in the range from 2.6 to 3.7, what makes this type of signal realization comparable to the method which uses an FIR filter.

The presented results show characteristics of the different signal realization methods such as the crest factor and signal magnitude (related by (4.37)). However, the final decision on whether the obtained probing signal is suitable or not will depend on the characteristics of probing equipment and the operators' judgment of the acceptable disturbance level introduced by the probing experiment.

4.6   Summary

This chapter proposed a methodology for probing signal design used for power system mode estimation. Probing experiments in power systems are costly processes that have to be planned carefully. One of the important design considerations in the planning stage is the shape of the probing signal. This chapter solved this problem by taking into consideration the desired mode estimation accuracy and limitations imposed by probing equipment. It was shown that only the power spectrum of the signal (not the time-domain signal realization) determines the accuracy of the mode estimation process. This property enables a two stage approach where the probing power spectrum is determined in the first stage, and in the second stage, a time-domain probing signal is generated aiming to satisfy the constraints imposed by the probing equipment. Even though these constraints are commonly related to the probing signal's crest factor, this chapter proposed a more general framework for time-domain signal realization that can be adapted to incorporate more complex constraints imposed by real-life probing equipment.

Even though the proposed methodology treats estimation accuracy as a hard constraint, the actual (observed) estimation accuracy differs because of the assumptions and approximations used in the derivation of the methodology. Therefore, it is recommended to apply a reasonable margin when the desired estimation accuracy is defined. In addition, it must be noted that the quality of the design process depends on the accuracy of the power system models used for design. These models may originate either from: (a) a physical modelling, or (b) an estimation processes. The accuracy of such models will thus depend on different sources of errors, either modeling assumptions in (a) or estimation accuracy in (b). The impact of such errors was not the subject of analysis here, and is open for further investigation.

Chapter 5

Model Order Selection

5.1   Introduction

Mode estimation methods may have different sets of estimation parameters that have to be chosen carefully in order to obtain accurate estimation results. However, the model order used for fitting the measured system responses is a common parameter for most parametric methods. Generally speaking, the choice of model order defines the richness of the selected model structure. The richer the model structure is, the more accurate model can be obtained if sufficient amount of data is used. However, a richer model structure also means larger number of parameters that need to be estimated. Consequently, it is more difficult to find the "true" parameter values with a fixed data parcel length, which results in higher variance of the estimated parameters. Therefore, there is a trade-off between model structure richness (model order) and estimated parameter variances. This trade-off does not have a unique solution and generally, the optimal model depends on the particular application and different approaches can be used to compute it.

The problem of optimal model order selection has been investigated extensively in the control and signal processing community [39],[232],[233]. However, a comparison of these methods has not been analyzed explicitly from the perspective of mode estimation in power systems.

This chapter gives an overview and a discussion of four methods that can be used as an aid in determining optimal model orders. These methods are: 1) Residual analysis for model order selection [209], 2) Model order selection based

on singular values [39], 3) Akaike Information Criterion [61], 4) Variance-Accounted-For (VAF) as a measure of optimal fitting between the measured data and the model response [39].

The main difference between probing based methods and ambient/ringdown based methods is the existence of a known input to the system. This difference affects the selection of the model order, however, similar procedures can be used when either ambient or ringdown mode estimation methods are applied.

The model order selection algorithms are assessed using simulation outputs from the KTH Nordic 32 test system and the IEEE test system with 50 generators and 145 buses. The optimal model order is determined for selected input and output signals. Comparisons of the obtained results are used to draw general conclusions about recommended model order values for mode estimation applications.

5.2   Model Order Selection Algorithms

5.2.1   Residual analysis based model order selection

As described previously, an ambient system response measured by a Phasor Measurement Unit (PMU) can be described by a single transfer function $H(z)$ excited by white noise $e(t)$, where the white noise represents random load changes at an aggregated level. This ambient response is also present during probing tests when the system is intentionally excited. Assuming the system linearity and using the principle of superposition, the measured synchrophasor signal $y(t)$ can be decomposed into two components: one as a result of ambient excitation ($H(z)e(t)$), and another as a result of probing ($G(z)u(t)$) as shown in Fig. 4.1 and Fig. 5.1. Signal $u(t)$ is the known probing signal and $G(z)$ represents a transfer function between the probing signal $u(t)$ and the measured output signal $y(t)$. It is assumed that $G(z)$ and $H(z)$ have the same denominators which means that an ARMAX model accurately describes the system [154]. This implies that the modes of $G(z)$ or $H(z)$ represent the poles/modes of the system that needs to be determined.
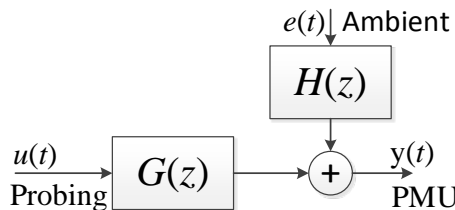

Fig. 5.1 Power system model during probing tests.

By minimizing the prediction error criterion over a set of model parameters, the unknown transfer functions are determined. The prediction error criterion is defined as:

$$I(\theta) = \frac{1}{N}\sum_{t=1}^{N}\varepsilon^2(t,\theta),\qquad\qquad(5.1)$$

where $\varepsilon(t) = H^{-1}(z)\big[y(t) - G(z)u(t)\big]$.

In the case of perfect model estimation, it can be shown that $\varepsilon(t)$ is white noise and that any deviation from the true model parameters causes an increased value of the prediction error criterion. In addition, it is obvious that $\varepsilon(t)$ should not be correlated with past inputs $u(t)$. These two facts constitute two criteria for model validation and consequently model order selection [209]. These criteria are evaluated by plotting the autocorrelation sequence of $\varepsilon(t)$ and the cross-correlation between $u(t)$ and $\varepsilon(t)$. If the model order is sufficiently rich to describe the system, the obtained autocorrelation should have the autocorrelation of white noise (a peak at 0 and close to zero for other values). In turn, the cross-correlation should be close to zero for all values. Then the optimal model order is the smallest one for which the defined requirements are satisfied. The cross-correlation test gives better insight if $G(z)$ is of the right order (assuming that $G(z)$ and $H(z)$ are not related as in ARMAX structure), while the autocorrelation test gives overall information about $G(z)$ and $H(z)$. This approach essentially relies on the analyst's judgement on when the defined criteria are satisfied. Further, this imposes difficulties when the model order needs to be determined in an automatized fashion. However, an important property of this approach is that it provides additional insight about the system's behavior and not just the value of the optimal model order.

5.2.2 Model order selection using singular values

Subspace identification methods are known for being able to provide numerically efficient and robust results even for complex systems [39]. Another benefit of subspace identification methods is that they provide straightforward ways for model order selection. Subspace algorithms aim to extract the column space of the system observability matrix $O_{obs} = [C\ CA\ CA^2 ... CA^n]^T$ from measured data. Without going into details about different subspace methods, it can be said that the observability matrix column space is determined by performing a singular value decomposition (SVD) on an appropriate matrix obtained from measurement data matrices (matrices whose elements are known input data or measured outputs). Determining the dimension of the column spaces is equivalent to selecting the model order. This can be achieved by calculating the singular values obtained during the computation of the

observability matrix column space. If the measured signal contains a relatively small amount of process or measurement noise, the number of singular values whose magnitude is relatively large will be exactly equal to the model order. Even if it is not possible to clearly distinguish the true model order, this approach allows to see how and to what extent additional parameters (added by increasing the model order) can influence the fit between measured and modeled outputs. Essentially, the optimal model order will be selected when the additional singular value (singular value that corresponds to additional model order) is not significantly lower from the previous singular value or when its value approach the singular values that are the result of the noise in the system. In this thesis, the MOESP subspace identificaiton method is used to demonstrate the applicability of singular values for optimal model order selection.

5.2.3 Akaike Information Criterion for model order selection

Any information criteria can be viewed as a cost function of two parts: a loss function and a model complexity penalty. In this context, the Akaike Information Criterion is not an exception. One of its versions can be written in the following way:

$$AIC(\rho) = N \ln(I(\theta)) + \rho n, \tag{5.2}$$

where,

N - number of data samples,

n - number of system parameters (characterizing the order of the system), and

ρ - regularization coefficient, which is usually equal to 2.

The idea behind such formulation is that AIC puts a penalty on the use of models with orders higher than necessary. It should be noted that this penalization factor can also be used in combination with singular value based model order selection. An advantage of the AIC is that minimization can be performed with respect to different model structures. More details about AIC and general identification theory can be found in [61].

5.2.4 Variance Accounted For criterion for model order selection

A comprehensive way of evaluating the goodness of fit between measured data and the data obtained by the estimated model is the so-called Variance-Accounted-For (VAF) performance index. This index is defined as:

$$VAF = \max\left\{0, \left[1 - \frac{\frac{1}{N}\sum_{k=1}^{N}(y(k) - \widehat{y}(k\,|\,k-1))^2}{\frac{1}{N}\sum_{k=1}^{N}(y(k))^2}\right] \cdot 100\%\right\}, \qquad (5.3)$$

where $\widehat{y}(k\,|\,k-1)$ is the one step ahead predictor defined as:

$$\widehat{y}(k\,|\,k-1) = H^{-1}(z)G(z)u(t) + \left[1 - H^{-1}(z)\right]y(k).$$

As described in [209], the prediction error method is derived under the assumption that $H^{-1}(z)$ is a proper and monic transfer function with a stable inverse. This means that $\left[1 - H^{-1}(z)\right]y(k)$ depends only on past values of $y(k)$ and not on $y(k)$ itself.

Instead of using the one-step ahead predictor $\widehat{y}(k\,|\,k-1)$ in (3), it is also possible to use the signal $\widehat{y}(k)$ simulated with the model over the period of interest. The difference between these two approaches (one step ahead predictor vs fully simulated signal) is that in the latter case, previous measurements are not used to improve the prediction as it was done for $\widehat{y}(k\,|\,k-1)$. In other words, if previous measurements are not used for prediction, the VAF indicates how the model output matches the measured signals over a longer period of time, whereas the one step ahead predictor better explains the matching of short term system dynamics.

Here, it is also important to make a distinction between the data used for model identification and the data used for validation. The criterion (5.3) can be obtained in both cases, but if the identification set is used, the criterion can show misleading high values indicating a good fit which are caused by overfitting. Therefore the recommended practice is to use half of the data for identification and half for validation. Once the model order is decided, the identification can be carried out one more time using the whole data set in order to increase the accuracy of the identified model.

5.3   Case Studies

5.3.1   Study using the KTH Nordic 32 Test System

This section shows results obtained using the KTH Nordic 32 test system. All simulations have been performed using 3000 data samples which correspond to 10 minutes of measurements at 5 Hz sampling frequency (downsampled and pre-processed original PMU stream). In this example, it is assumed that reactive

power injection in bus 41 is the input signal, whereas the measured voltage magnitude at bus 48 is considered as the output.

Fig. 5.2-Fig. 5.5 show the autocorrelation sequences of the identification residuals (upper part of the figures) and the cross-correlations between the residuals and input signals (lower parts of the figures). The autocorrelation and cross-correlation sequences are plotted with the time lag (number of samples) as an independent variable.
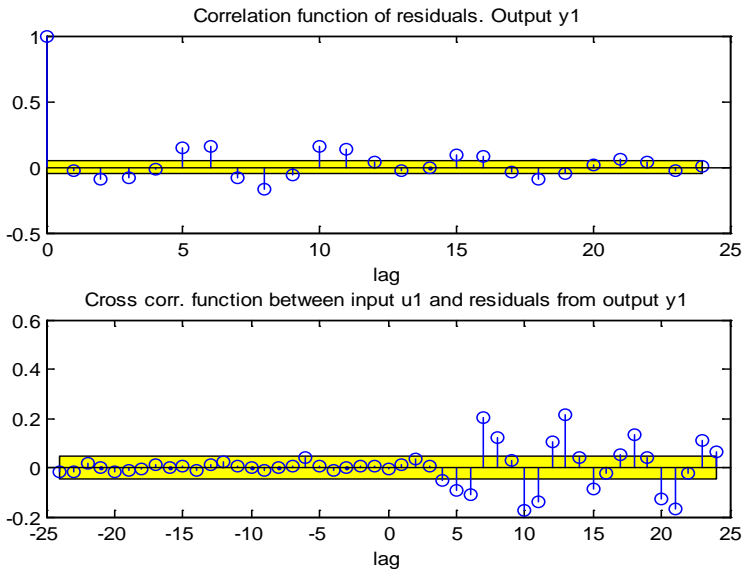

Fig. 5.2 Autocorrelation of $\varepsilon(t)$ and cross-correlation between $\varepsilon(t)$ and $u(t)$ for model order 6.

Good identification results correspond to very small values in the auto and cross-correlation sequences except at the zero-lag element in the autocorrelation sequence (the residual is supposed to be white noise). An adopted threshold for which the value can be considered small corresponds to 99 % confidence interval (corresponds to the range of residual values with a specific probability of being statistically insignificant for the system). The numerical value of the threshold is around 0.05 and it is marked with a yellow strip in Fig. 5.2. Fig. 5.3 shows that this criterion is satisfied for model order 12.
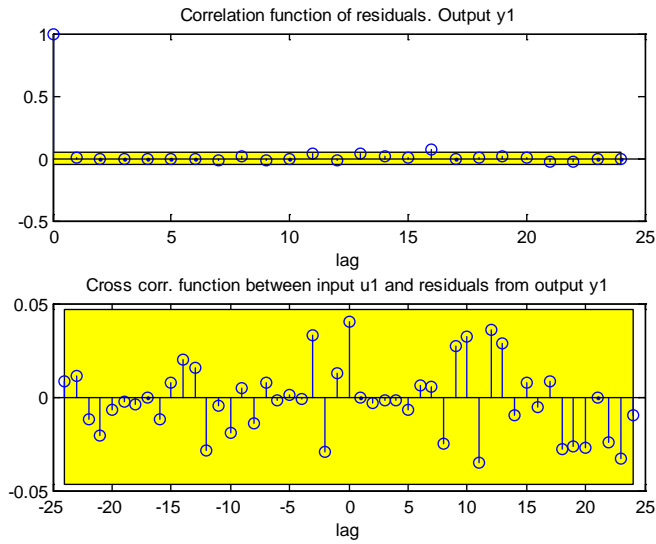
Fig. 5.3 Autocorrelation of $\varepsilon(t)$ and cross-correlation between $\varepsilon(t)$ and $u(t)$ for model order 12.
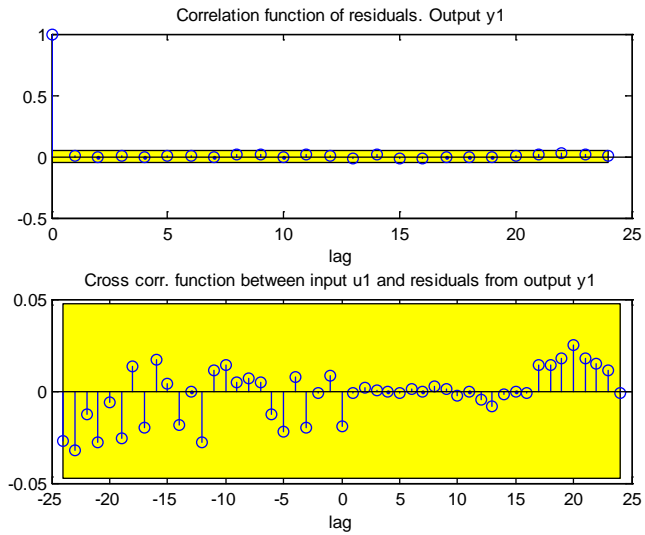

Fig. 5.4 Autocorrelation of $\varepsilon(t)$ and cross-correlation between $\varepsilon(t)$ and $u(t)$ for model order 18.
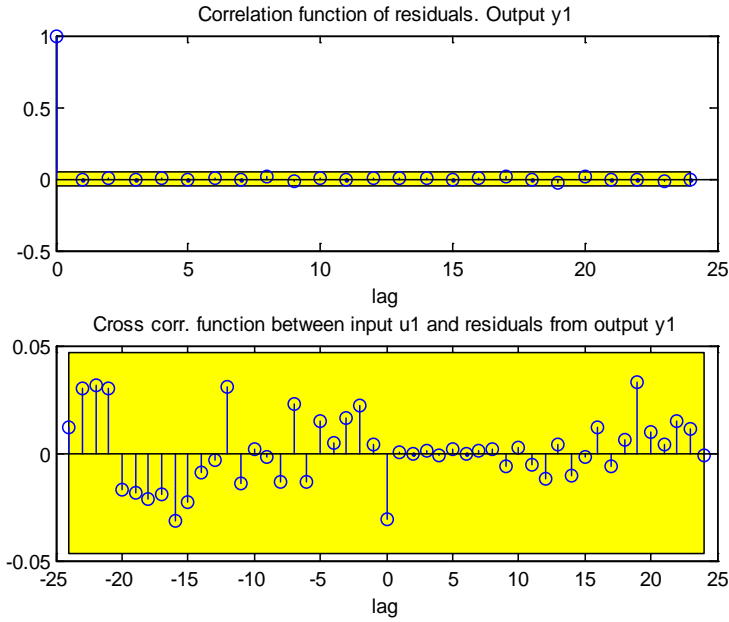
*Fig. 5.5 Autocorrelation of $\varepsilon(t)$ and cross-correlation between $\varepsilon(t)$ and $u(t)$
for model order 22.*

The singular values, obtained using the MOESP subspace identification algorithm, are presented in Fig. 5.6. This figure shows how an increase in model order contributes to a better data fit. In other words, a smaller last singular value (with corresponding model order) implies a better fit between the model and the underlying process). However, the model orders higher than 18 do not lead to any visible improvement, while the computational burden is increased.
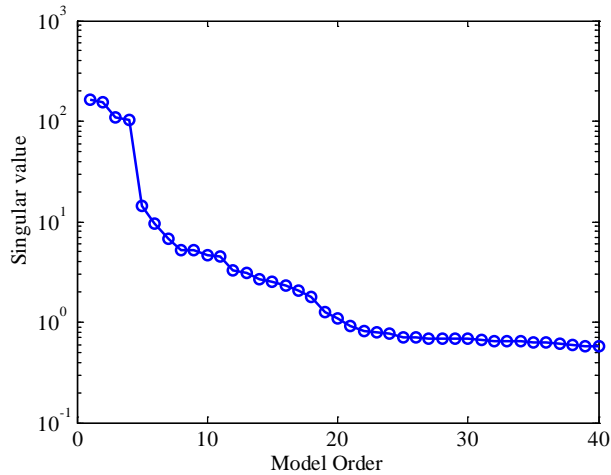
Fig. 5.6 Singular values obtained from the MOESP subspace identification algorithm (KTH Nordic 32 test system).

A similar approach can be used in analyzing the Akaike Information Criterion (AIC). Fig. 5.7 also shows calculated AIC for different model orders. In addition it shows the effect of the penalizing factor that leads to the criterion increase for model orders higher than 30. What can be seen from the results in Fig. 5.6 and Fig. 5.7 is that both, the Akaike Information Criterion and singular values provide slightly less conclusive results than the residual analysis.
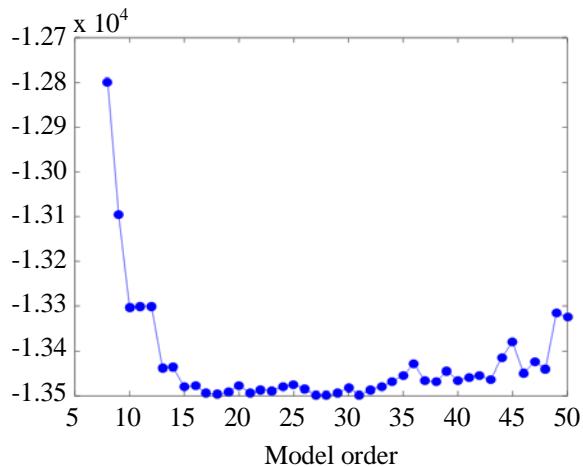

Fig. 5.7 Akaike Information Criterion (AIC) for different model orders (KTH Nordic 32 test system).

The next model order selection method that is applied is the Variance-Accounted-For (VAF). Four types of this indicator have been calculated and shown in Table 5.1. First, the VAF is computed using the data that are used for the identification process and the one-step ahead predictor (data obtained from the model). This value provides information on how good the fit is between the model and the dataset. Second, instead of using the data used during identification, an independent dataset is used (validation set). This value of VAF gives more information about the fit between the model and the actual underlying process. The third and fourth indicators are computed using fully simulated data in contrast to the one-step ahead predictor. These indicators say more about how good the model fit is over a longer period of time.

Table 5.1 Model fitting criteria for different model orders.

Model order	One step ahead VAF		Simulated VAF	
	Identif. data	Validation data	Identif. data	Validation data
6	96.94	96.84	82.07	81.21
12	98.02	97.99	94.97	94.63
18	98.04	97.84	95.44	94.36
22	98.06	98.03	95.01	94.71

The obtained results suggest that model orders higher than 18 do not contribute to better mode estimation (the validation data VAF does not increase significantly when the model order is higher than 18). In addition, it should be noted that smaller model orders are more appealing because they will result in a faster estimator response, as well as increased computational efficiency. Therefore, it can be concluded that a model order of 12 can be chosen without substantial change or improvements in the estimation accuracy.

5.3.2   *Study using the IEEE Test System with 145 buses and 50 generators*

In this subsection a test system with 145 buses and 50 generators is used to evaluate the performance of the model order selection methods [234],[235]. The reactive power injection at bus 111 is selected as input and the voltage magnitude of bus 59 is selected as output. Similar studies have been conducted as in the case of the KTH Nordic 32 test system, and the results are reported in Fig. 5.8-Fig. 5.12. and Table 5.2.
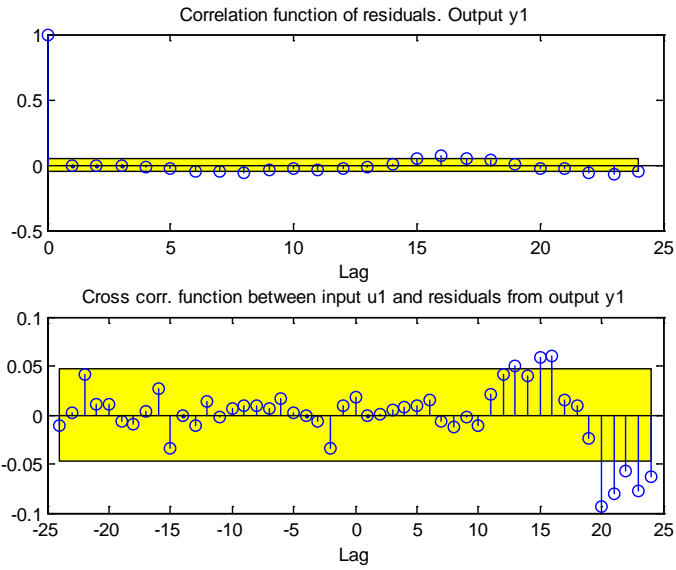
Fig. 5.8 Autocorrelation of $\varepsilon(t)$ and cross-correlation between $\varepsilon(t)$ and $u(t)$ for model order 18.
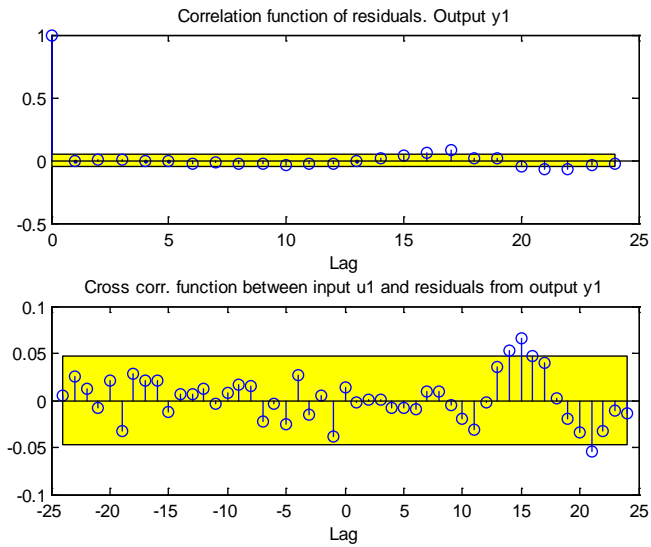

Fig. 5.9 Autocorrelation of $\varepsilon(t)$ and cross-correlation between $\varepsilon(t)$ and $u(t)$ for model order 22.
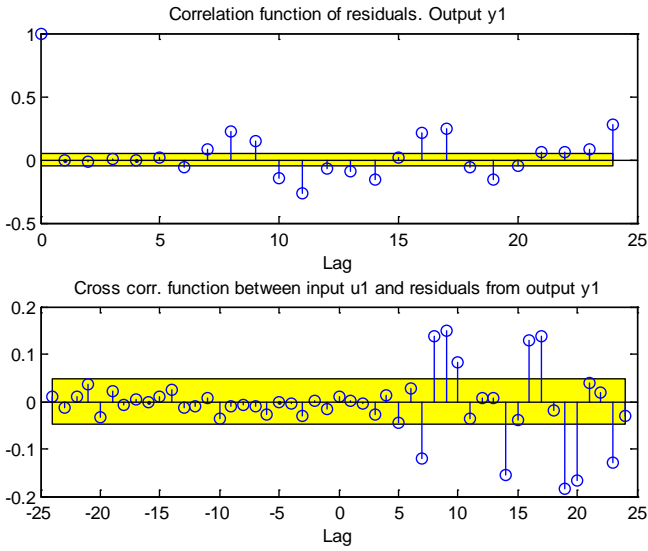
Fig. 5.10 Autocorrelation of $\varepsilon(t)$ and cross-correlation between $\varepsilon(t)$ and $u(t)$ for model order 6.
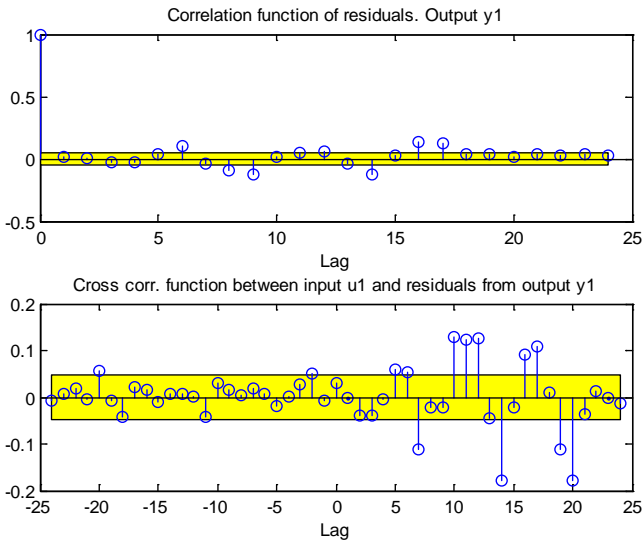

Fig. 5.11 Autocorrelation of $\varepsilon(t)$ and cross-correlation between $\varepsilon(t)$ and $u(t)$ for model order 12.
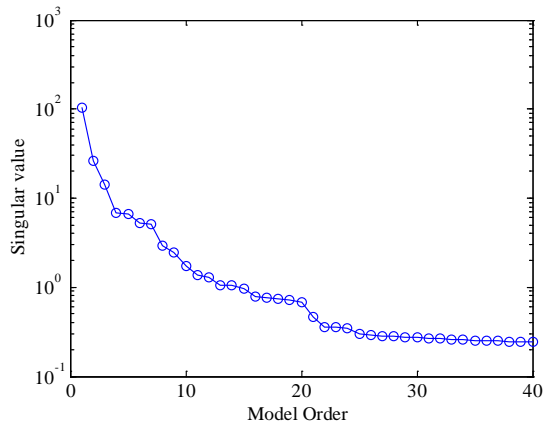
Fig. 5.12 Singular values obtained from the MOESP subspace identification algorithm (IEEE 145 bus test system).
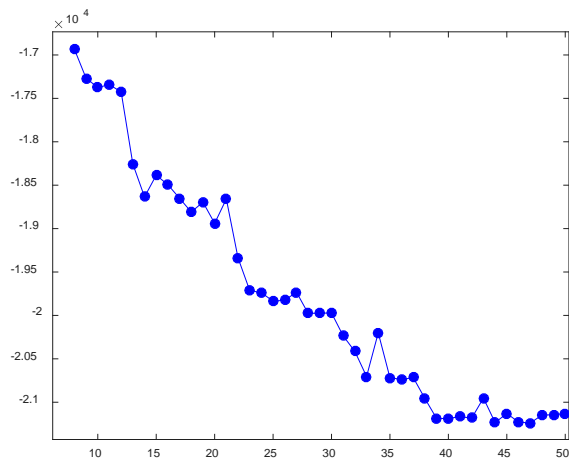

Fig. 5.13 Akaike Information Criterion (AIC) for different model orders (IEEE 145 bus test system).

Table 5.2 Model fitting criteria for different model orders

Model order	One step ahead VAF		Simulated VAF	
	Identif. data	Validation data	Identif. data	Validation data
6	97.89	97.75	87.23	86.52
12	98.44	98.35	87.91	84.55
18	98.89	98.82	93.92	93.18
22	98.86	98.85	94.41	94.37

As in the previous case, the Akaike Information Criterion generally provides less conclusive results. The results presented indicate that a model order of 20 describes sufficiently well the system dynamics, whereas a lower model orders (around 18) can be selected if faster mode estimation results are required. This is a bit higher model order in comparison to the KTH Nordic 32 test system. This result is understandable taking into account that the system is more complex (contains more dynamics).

5.4   Summary

This chapter presented the application of four methods for optimal model order selection for probing based mode estimation. A careful consideration of the results obtained by the described methods provides good insight into the nature of the process that generates low frequency oscillations in the system. However, none of the described methods provides a unique solution to select the best model order. Instead, each method contributes to a better understanding of the underlying process. Therefore, a detailed analysis of all the obtained results should lead to a set of rules that can be used to derive a fully automatized model order selection algorithm, which is a topic of future research.

Chapter 6

Implementation of a Real-Time Tool for Mode Estimation

6.1   Introduction

In addition to the theoretical development of methods for mode estimation [200], it is important to test an integrated solution for mode estimation including measurement data acquisition. This includes physical Phasor Measurement Units (PMUs) and the Information & Communication Technologies (ICT) systems that support the mode meter application.

This chapter presents a mode meter application that integrates the entire Wide Area Measurements Systems (WAMS) ICT infrastructure [215],[236]. Statnett's Synchrophasor Software Development Kit (SDK), which allows fast prototyping and testing of the integrated WAMS solution [237], is used here as a key software building block for developing the mode estimator. The SDK extracts synchrophasor data received in the IEEE C.37.118 protocol and converts them to a more convenient form (LabVIEW signals). The mode estimator is implemented in the LabVIEW environment using state machine logic [238]. This architecture enables easy modifications and further developments to the estimator.

6.2   Mode Estimation Algorithm

In order to demonstrate the real-time application of a mode estimation tool, a method based on the Yule-Walker's equations was used. In the sequel, this method is shortly described.

During (quasi) steady state operation, it can be assumed that the power system is mainly disturbed by small random load variations. These load variations are caused by the random behavior of individual consumers at different voltage levels. Because these random load changes are small in magnitude, the power system behavior can be described by a linear model. Therefore, the power system model can be written as follows:

$$\mathbf{Y}(j\omega) = \mathbf{H}(j\omega) \cdot \mathbf{U}(j\omega) , \qquad (6.1)$$

where:

$\mathbf{Y}(j\omega)$ – vector of measured electric variables;

$\mathbf{H}(j\omega)$ – transfer function matrix of the power system;

$\mathbf{U}(j\omega)$ – vector of inputs (load variations).

In order to demonstrate the mode estimation algorithm's principle, a single input-single output system is used [239]. Assuming that the individual load behavior is random and independent from other loads, the (input) load variations can be represented by white noise. Keeping in mind that the frequency spectrum of white noise is a constant function, it follows that the spectrum of the measured signal is proportional to the amplitude response of the system $(|H(j\omega)|)$. Therefore, the mode estimation algorithm determines the coefficients of a rational transfer function whose amplitude response is proportional to the spectrum of the measured signal. This can be written in the discrete time domain as:

$$y(k) = -\sum_{i=1}^{p} a_i \, y(k-i) + \sum_{j=0}^{q} b_j u(k-j) , \qquad (6.2)$$

where:

$y(k)$ – measured output signal at time point k;

$u(k)$ – random load input at time point k (assumed to be white noise);

a_i , b_j (i=1,…, p, and j=0,…, q) – unknown coefficients of the rational transfer function;

p, q – orders of the numerator and denumerator of the estimated rational transfer function, respectively.

Multiplying both sides of (6.2) by $y(k-n-l)$, taking the expected value and using the definition of autocorrelation (r) [218], the following matrix equation can be written (known as modified Yule-Walker equations) [240]:

$$
\begin{bmatrix} r(q) & \cdots & r(q-p+1) \\ \vdots & & \vdots \\ r(q+p-1) & \cdots & r(q) \end{bmatrix} \begin{bmatrix} a_1 \\ \vdots \\ a_p \end{bmatrix} = - \begin{bmatrix} r(q+1) \\ \vdots \\ r(q+p) \end{bmatrix}.
\tag{6.3}
$$

Note that the following property is used in the derivation:

$$
E\{u(k-j)\cdot y(k-j-l)\} = 0 \text{ , for } l=1,..,p.
\tag{6.4}
$$

The autocorrelations in (6.3) are estimated using (6.5):

$$
r(n) = \frac{1}{N} \sum_{k=0}^{N-n-1} y(k+n)y(k) \, .
\tag{6.5}
$$

The solutions of the equation system in (6.3) are the autoregressive (AR) coefficients of the model, which are sufficient to compute the modes of the system. In case that the moving average (MA) part is required, it can be computed using Durbin's method [48].

The characteristic equation of the system is defined by the computed AR coefficients as follows:

$$
1 + a_1 + ... + a_p = 0 \, .
\tag{6.6}
$$

The roots of the characteristic equation represent the modes of the system in the z-domain. These modes (denoted by $\mathbf{z}$) can be transformed easily to the s-domain using:

$$
\mathbf{s} = \boldsymbol{\sigma} + j\boldsymbol{\omega} = \frac{1}{T_s} \ln(\mathbf{z}) \, ,
\tag{6.7}
$$

where T_s is the signal's sampling period. $\boldsymbol{\sigma}$ and $\boldsymbol{\omega}$ are real and imaginary components of the modes in the s-domain ($\mathbf{s}$), respectively. Once the s-domain modes of the system are calculated, the damping ratio of the i-th pole (ζ_i) is computed using the following formula:

$$
\zeta_i = \frac{-\sigma_i}{\sqrt{\sigma_i^2 + \omega_i^2}} \, ,
\tag{6.8}
$$

where σ_i and ω_i are the *i*-th elements in $\boldsymbol{\sigma}$ and $\boldsymbol{\omega}$, respectively.

6.3   Synchrophasor Software Development Kit (SDK)

Statnett's Synchrophasor Software Development Kit (SDK) enables easy real-time access to PMU and Phasor Data Concentrator (PDC) data streams [237]. The LabVIEW platform provides easy integration with different hardware equipment as well as an intuitive graphical programing language (G language). The main benefit of the software development toolkit is that it exempts a developer of complicated synchrophasor data handling. Instead, the developer is required only to set the appropriate PDC connection parameters such as PDC ID, PDC host address and the port number to connect to the PDC stream.

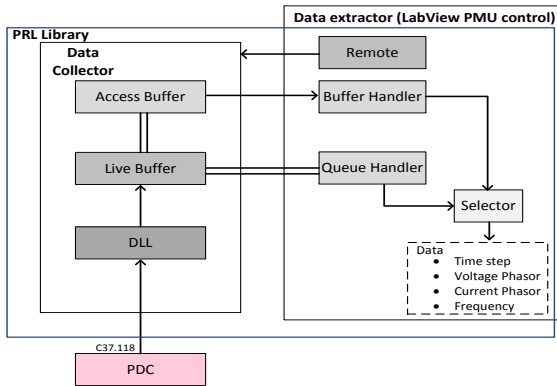The general architecture of the SDK is shown in Fig. 6.1.

Fig. 6.1 Statnett's SDK architecture.

The SDK has two major components, *Data Collector* and *Data Extractor*.

6.3.1   Data collector

The Data Collector reads the data from the PDC/PMU and stores them in configurable buffers. This component uses a Dynamic Link Library (DLL) developed in the C++ programming language to connect to the PDC stream via the IEEE C37.118.2 protocol. In addition, the DLL reads the configuration data of the PDC stream, such as channel names, scaling and number of the measured signals by type (analog, phasors or digital signals).

The incoming data from the DLL are received in the Live Buffer. When the Live buffer is full the data is put in the Access Buffer, where data of arbitrary length can be stored. The user (custom application) receives the data using the Queue Handler (which reads data directly from Live Buffer), or using the Buffer

Handler, which reads an arbitrary amount of data from the Access Buffer (this option is used in the mode meter application development).

6.3.2   Data extractor – LabVIEW PMU control

The data extractor is a collection of LabVIEW routines or Virtual Instruments (VIs) that allows the user to access the buffers and queues in the Data Collector. It reads the data from the buffers and provides the user with control over the data streams in a form suitable for further processing in the main application (as a signal data type in LabVIEW). The interface of this VI is shown in Fig. 6.2.

Other parameters such as PMU selection, data length, and others, are set in an auxiliary user interface. Additional LabVIEW VIs are provided in the SDK for data handling and processing.
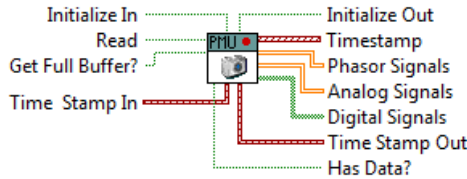

Fig. 6.2 LabVIEW PMU Control block.

6.4   Mode Meter Software Architecture

The state machine architecture [238] is chosen for the development of the mode meter application. This architecture allows to decouple different tasks and to develop them independently. The block diagram of the state machine is given in Fig. 6.3:
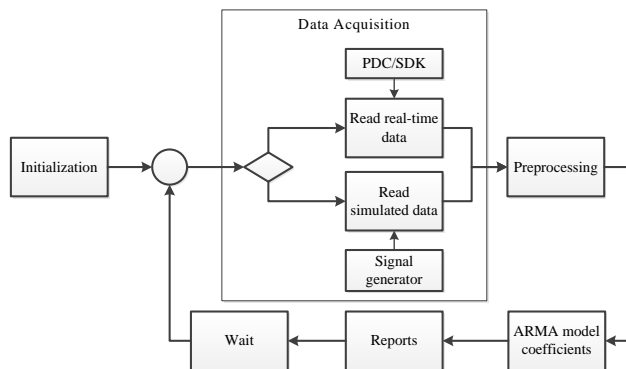

Fig. 6.3 Global block diagram of the implemented mode meter.

The software's structure, which is typical for real-time applications, consists of an initialization step and a main loop.

The initialization step is performed only once and it sets all variables to their initial values, as well as populating initial settings such as data source, refresh rate, etc. After the initialization step the program enters the main loop which consists of four blocks, namely: data acquisition, preprocessing, estimation of the ARMA coefficients and reports.

6.4.1   Data acquisition

Data acquisition imports a parcel of data which is used for mode estimation. The length of parcel is defined in the software's options and usually is in the range of 10-15 min. There are two operating modes of data acquisition:

1) Acquisition through a PDC and Statnett's SDK. The signal used for mode estimation is selected among the available real-time measurements in Statnett's SDK interface [237].

2) Acquisition from an internal data generator. The internal data generator provides Gaussian white noise filtered by a linear IIR filter. The coefficients of the IIR filter are set manually by the user in the *Testing* tab.

Software modularity is achieved through a standardized interface among the blocks. The following interface is adopted and implemented using a "type definition" LabVIEW structure (Fig. 6.4):
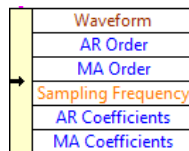

Fig. 6.4 Common data structure.

This user defined type consists of 6 elements, namely:

1) *Waveform* – Data parcel with corresponding time stamps;

2) *AR Order* – Order of the estimated autoregressive part of the model;

3) *MA Order* – Order of the estimated moving average part of the model;

4) *Sampling frequency* - Sampling frequency of the signal;

5) *AR Coefficients* – Calculated autoregressive coefficients;

6) *MA Coefficients* – Calculated moving average coefficients.

This user defined type is sufficient for the communication between different blocks. This means that the block's functionality is well defined and it is easy to

maintain the interfaces between blocks. This also means that each individual block can be developed independently, thus making software maintenance easier.

6.4.2   Preprocessing

After the data parcel is imported, the parcel is preprocessed in order to make it more adequate to apply the mode estimation algorithm. This includes signal downsampling, mean and outlier removal. Downsampling greatly improves the accuracy of the estimation algorithm because only the frequency range of interest is considered, i.e. the estimator is not constrained by fitting dynamics at higher frequencies. Also, in the case of high sampling frequency data, the modes in the *z*-domain tend to be grouped around point (1,0) in the complex plane, which creates numerical difficulties. More details can be found in [216].

6.4.3   Estimation of ARMA coefficients

A preprocessed signal is fed into the main computation block, which calculates the ARMA coefficients of the stochastic process. The algorithm used in this block was described before. This block does not perform any further computation because it is important to keep it independent from other blocks in order to make the core algorithm easy to update or replace. The computed ARMA coefficients are stored in the interface structure (Fig. 6.4.). The coefficients are later used to compute the estimation results presented to the user.

6.4.4   Reports

The computed ARMA coefficients are used in the Report block to present results to the user. This block computes the spectrum, and the poles in the discrete and continuous domain (described by (6.7) and (6.8)). Furthermore, this block buffers results from previous iterations. Each of these calculations are performed in sub-routines (sub VIs).

The algorithm described is executed in a timed loop, and paused after the *Report* block has been executed. The next iteration starts at the time specified in the settings of the timed loop.

Note that overlapping in the algorithm is defined by the loop period and the data parcel length.

6.5   User Interface

The user interface is designed to provide relevant information about the estimated modes of the system. There are two main parts of the interface: 1) Time domain signal plots (upper part) and 2) Computed results and estimator's settings (lower part).

In the upper part, the measured signal is shown in the time domain, as well as

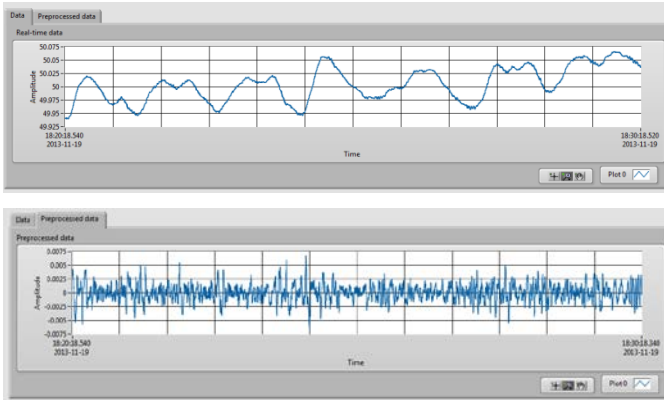the signal which is obtained after preprocessing (Fig. 6.5).

Fig. 6.5 Time domain signal presentation.

The lower part is composed of five parts (tabs), namely:

1) *Main Results* tab (Fig. 6.6). This tab shows the estimated location of the modes in the complex plane as well as the history of estimated damping ratios. In addition, the frequency and damping ratio of the most critical mode are shown.
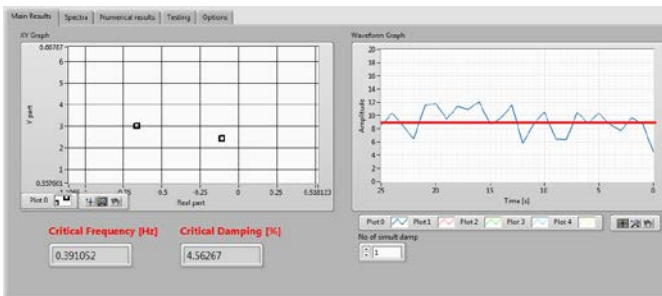

Fig. 6.6 Main results interface[14].

2) *Spectra* tab (Fig. 6.7). Shows the measured signal in the frequency domain. The spectrogram also gives information on how the spectrum has changed over time.

---

[14] The red lines in Fig. 6.6 and Fig. 6.7 were added to show important values (results) obtained from the tests and they are not part of the application interface.
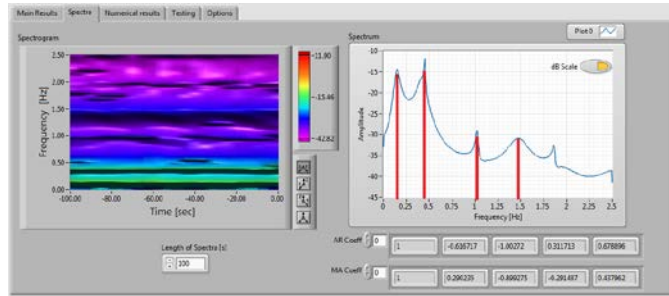
Fig. 6.7 Spectral estimation results

3) *Numerical results* tab. This tab presents numerical estimation results that are required for detailed analysis.

4) *Test* tab. Defines the parameters of the IIR filter of the data generator that is used in the simulation operating mode.

5) *Options* tab (Fig. 6.8). Defines the parameters of the estimator such as data length, etc.
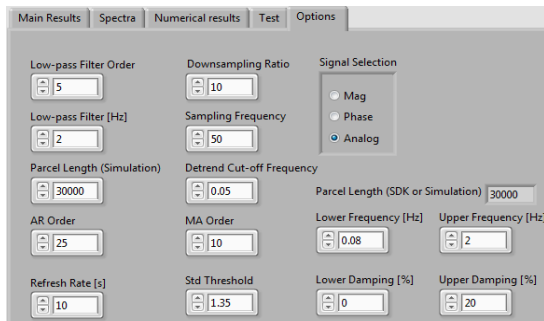
Fig. 6.8 Options tab of the mode estimator.

6.6   Experimental Results

The developed mode meter is first tested in the KTH SmartTS Lab using real-time hardware-in-the-loop simulation with Opal-RT's simulator and physical PMUs connected to it [241]. In the second test, a PMU connected to a low voltage grid is used for mode estimation in the Nordic grid.

6.6.1   Real-time hardware-in-the-loop test

Opal-RT's simulator is used for the hardware-in-the-loop (HIL) simulation of

the KTH Nordic 32 test system [212]. This system has a dominant mode at 0.4987 Hz with 3.5223 % damping ratio (computed using classical small signal stability analysis). The ambient response of the system is simulated by imposing random load variations in all load buses. It is assumed that these variations are described by Gaussian white noise. The phasor voltage magnitudes at bus No. 49 are chosen for mode estimation because that bus has the highest observability of the dominant mode [242]. The simulated signals (three-phase voltage waveforms) go through a digital to analog interface and are fed into a National Instruments PMU implemented in the CompactRIO platform [243]. The PMU is interfaced with a PDC that forwards the computed phasors to the application. The data parcel length used for estimation is chosen to be 10 minutes of the bus frequency as computed by the PMU.
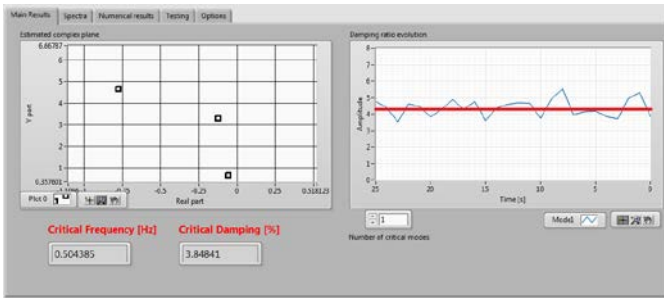
Fig. 6.9 Mode estimation results using signals generated through RT HIL simulation.

The results of this test are depicted in Fig. 6.8 and Fig. 6.9. It can be noticed that the estimator finds the 0.5 Hz mode to be the most critical with damping ratio oscillating around 4 %. Because this is a stochastic process (estimation), these results are not sufficient for a full assessment of the estimator's performance. To gain better insight into the estimator's performance, a large number of estimates (120 estimates obtained from 120 different 10-minutes data parcels) is recorded and the mean value and variance of the estimates are computed from:

$$\bar{x} = \frac{1}{N} \sum_{i=1}^{N} x_i \; ; \tag{6.9}$$

$$\text{var}(x) = \frac{1}{N-1} \sum_{i=1}^{N} (x_i - \bar{x})^2 \; ; \tag{6.10}$$

where $\bar{x}$ is the mean value of the all estimates and N is the number of estimates (N=120).

Fig. 6.10 Spectrum of the signal generated by the real-time hardware-in-the-loop simulation.

Further, these results are compared against an off-line mode estimator implementation in MATLAB, without physical PMUs involved (no HIL). This means that it is possible to discern between the error caused by the estimator itself and the errors from the measurement system (there are no measurement errors within the MATLAB (No HIL) simulation environment).
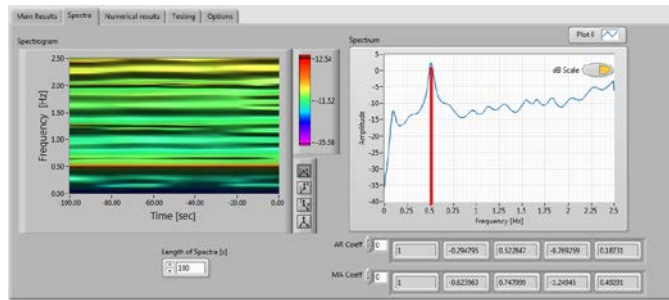
Table 6.1 Stochastic properties of the mode estimator.

	Hardware in the loop	Software simulation
Mean $\{f\}$ [Hz]	0.5073	0.4985
Mean $\{\xi\}$ [%]	4.0910	3.6905
Var $\{f\}$	1.1037e-04	7.5797e-05
Var $\{\xi\}$	1.9088	1.7184

It can be seen that the HIL test introduces additional error which can be explained by the imprecision of the HIL chain, including the limits of the PMU's accuracy.

6.6.2   Test using measurements from the Nordic grid

After having validated the software in the laboratory, the software was tested using real-time measurements from a PMU in the Nordic grid. The results from this test are shown in Fig. 6.5-Fig. 6.7, whereas the options used are shown in Fig. 6.8. Several oscillatory modes can be observed in Fig. 6.6 and Fig. 6.7. The most critical mode has a frequency of around 0.39 Hz and damping around 9 % (in average). Other modes that are observable appear at 0.2 Hz, 1 Hz and 1.4 Hz, while a 0.5 Hz mode sporadically appears as a poorly damped mode. These estimates are quite in accordance with the results reported in [244]. Also, the mode with frequency of 1 Hz has been reported in [245] and (presumably) it can be classified as a forced oscillation.

6.7   Summary

This chapter presented a real-time mode meter software implementation and its testing in real-life operating conditions. The mode meter uses the well-known methodology based on the Yule-Walker equations. The performed tests show that the tool provides results comparable to those obtained in the software simulation mode. In addition, this chapter demonstrates that with the tools used, a powerful real-time WAMS application can be developed in relatively short time.

In addition to intrinsic errors caused by estimation algorithms, mode estimates are affected by errors originating in the WAMS. The WAMS errors might have different effects depending on the mode estimation algorithm used. This is a reason why all mode estimators should be tested in an integrated environment (with WAMS) to better understand the actual mode estimation performance.

In order to make full use of the ambient data-based mode estimation approach, further improvements to the tool are necessary. In addition to the implementation of more sophisticated and precise mode estimation algorithms, one of the main requirements is that the algorithm provides confidence intervals for the estimates. Confidence intervals are necessary for operators to take corrective actions initiated by the mode estimator results. Furthermore, the tool should be able to use all the available synchrophasor signals.

Chapter 7

Conclusions

It is widely accepted that mode estimation is one of the most important applications of wide area monitoring systems. However, despite the fact that a large number of mode estimation methods have been developed, the results obtained are not sufficiently robust and reliable to be used as a critical decision support tool in every day operation. The main goal of this thesis was to improve the process of mode estimation by closely identifying the causes of possible errors in the overall process. The second goal was to provide a comprehensive guide for the implementation of the mode estimation tool by tackling implementation issues that are traditionally unjustifiably neglected in the literature, such as model order selection and optimal signal selection, as well as hardware and software design considerations for such tools.

The thesis is composed of six chapters, a list of references and conclusions. Introductory remarks, a detailed literature review and the main points of the thesis were provided in Chapter 1. Chapter 2 provided a solution for the first problem that the operators face in the implementation of mode estimation tools, i.e. the question of which signals should be used as the input. This chapter proposed a criterion for signal selection providing a tool for systematic and quantitative analyses. This is useful because the previous methods for signal selection were mostly based on heuristics or on observability analysis that has been proved to be inadequate. It has been shown that not only the power system model affects the decision on signal selection, but also the characteristics of the ambient noise excitation that is neglected in the observability based methods. In addition, it was shown that signal selection is similar to the PMU placement problem for this particular application, which means that the proposed solution

provides a way of including mode estimation requirements into the global PMU placement formulation.

The important phenomenon of forced oscillations and of random non-white noise load changes was addressed in Chapter 3. By exploiting the intrinsic power system property that the characteristics of electromechanical modes are predominately determined by the transmission part of the system, a new mode estimation algorithm was formulated. The proposed estimator is capable of minimizing the effect of forced oscillation on mode estimation results.

In Chapter 4, it was shown that the accuracy of probing methods can be radically improved simply by shaping the frequency spectrum of the probing signal, instead of giving the same importance to all the probing signal's frequencies. Namely, the results showed an improvement of 4-5 times in mode estimation accuracy when the probing signal was optimally shaped according to the proposed methodology. Also, it is important to note that improved accuracy comes without compromising the disturbance level or the cost of generating the probing signal. The proposed method for optimal probing signal design is formulated as a low order Linear Matrix Inequality optimization problem, which makes it numerically efficient. In addition, the probing signal with the optimal spectrum was generated considering arbitrary time domain signal constraints, which can be imposed by various probing signal generating devices.

Detailed models of power systems typically have a very large number of states/parameters and identifying such complex models from measurements is typically not feasible. This is the main reason for using reduced model orders for measurement based modeling. However, there is no unique answer to the problem of determining the optimal reduced model order because it represents a trade-off between the level of modeling detail and accuracy. In order to determine the best possible model order it is necessary to analyze different model reduction aspects. These analyzes were carried out in Chapter 5, where different methods for optimal model order selection were analyzed.

Finally, Chapter 6 has provided a description of the practical implementation of a real-time mode estimation tool. This includes a presentation of the used hardware for real-time hardware-in-the-loop testing of the software prototype, the software's architecture, graphical user interface, as well as details of the most important software components, such as the Statnett's SDK that allows easy access to synchrophasor data streams.

The basis for the presented methods and analyses was found in the theory of the prediction error system identification methods. Even though prediction error methods are generally not considered the most computationally efficient, they were selected as a basis because they provide deep insight in the system identification process through formal mathematical optimization.

The fundamental contributions of the thesis are mathematical expressions presented, which explain the nature of mode estimation uncertainty. These expressions were used throughout the thesis for solving different problems that affect classical mode estimators. This theory was used to derive a quality metric for each measured synchrophasor signal, which was later used as a solution for the signal selection problem. Furthermore, prediction error theory was used to establish a relationship between probing signals and mode estimation uncertainty, which allowed deriving a solution to determine the optimal spectrum of the probing signal. The same theory was also used to formulate a method to determine optimal order of the identified model.

In addition to these theoretical results, the thesis provides a clear guidance how the theory can be applied in practice. For instance, the signal selection problem was solved using efficient numerical algorithms that are suitable for real-time applications; probing signals were designed considering general time domain constraints that can be different for each probing device; and finally, a prototype software implementation of the mode estimation application that can be run using real-time measurements has been developed and described in detail.

Bibliography

[1]   U.S.-Canada Power System Outage Task Force, "Final report on the August 14, 2003, blackout in the United States and Canada: Causes and Recommendations", April, 2004.

[2]   D.N. Kosterev, C.W. Taylor and W.A. Mittelstadt, "Model validation for the August 10, 1996 WSCC system outage", *IEEE Transactions on Power Systems*, vol.14, no.3, pp.967-979, 1999.

[3]   www.naspi.org

[4]   Y. Yu, J. Yang and B. Chen, "The smart grids in China - A review", *Energies*, vol.5, no.5, pp.1321-1338, 2012.

[5]   J.F. Hauer, "Power system identification by fitting structured models to measured frequency response", *IEEE Transactions on Power Apparatus and Systems*, vol.PAS-101, no.4, pp.915-923, 1982.

[6]   J.F. Hauer, "Identification of power system models for large scale damping control", *in Proc. 28th IEEE Conference on Decision and Control*, 13-15 December, 1989.

[7]   J.F. Hauer and R.L. Cresap, "Measurement and modeling of Pacific AC Intertie response to random load switching", *IEEE Transactions on Power Apparatus and Systems*, vol.PAS-100, no.1, pp.353-359, 1981.

[8]   R.L. Cresap and J.F. Hauer, "Emergence of a new swing mode in the Western power system", *IEEE Transactions on Power Apparatus and Systems*, vol.PAS-100, no.4, pp.2037-2045, 1981.

[9]   C.E. Grund, J.F. Hauer, L.P. Crane, D.L. Carlson and S.E. Wright, "Square butte HVDC modulation system field tests", *IEEE Transaction on Power Delivery*, vol.5, no.1, pp.351-357, 1990.

[10]   J.F. Hauer and F. Vakili, "An oscillation detector used in the BPA power system disturbance monitor", *IEEE Transactions on Power Systems*, vol.5, no.1, pp.74-79, 1990.

[11]   J.F. Hauer, C.J. Demeure and L.L. Scharf, "Initial results in Prony analysis of power system response signals", *IEEE Transactions on Power Systems*, vol.5, no.1, pp.80-89, 1990.

[12] M.A. Magdy, K. Korzeniowski and H.M. Jones, "On-line estimation of low frequency modes in electric power systems", *Electric Power Systems Research*, vol.14, no.2, pp.149-153, 1988.

[13] J.R. Smith, F. Fatehi, C.S. Woods, J.F. Hauer and D.J. Trudnowski, "Transfer function identification in power system applications", *IEEE Transactions on Power Systems*, vol.8, no.3, pp.1282-1290, 1993.

[14] D.J. Trudnowski, M.K. Donnelly and J.F. Hauer, "A procedure for oscillatory parameter identification", *IEEE Transactions on Power Systems*, vol.9, no.4, pp.2049-2055, 1994.

[15] H. Saitoh, J. Toyoda and Y. Kobayashi, "Dominant mode filter for enhancing power system stability", *International Journal of Electrical Power and Energy Systems*, vol.15, no.1, pp.5-12, 1993.

[16] R. Doraiswami and W. Liu, "Real-time estimation of the parameters of power system small signal oscillations", *IEEE Transactions on Power Systems*, vol.8, no.1, pp.74-83, 1993.

[17] J.J. Sanchez-Gasca, K. Clark, N.W. Miller, H. Okamoto, A. Kurita and J.H. Chow, "Identifying linear models from time domain simulations", *IEEE Computer Applications in Power*, vol.10, no.2, pp.26-30, 1997.

[18] J.J. Sanchez-Gasca and J.H. Chow, "Performance comparison of three identification methods for the analysis of electromechanical oscillations", *IEEE Transactions on Power Systems*, vol.14, no.3, pp.995-1002, 1999.

[19] J.J. Sanchez-Gasca, "Toward the automated computation of electro-mechanical modes from transient simulations", *in Proc. IEEE PES General Meeting 2010*, 25-29 July, 2010.

[20] I. Kamwa, G. Trudel and L. Gerin-Lajoie, "Low-order black-box models for control system design in large power systems", *IEEE Transactions on Power Systems*, vol.11, no.1, pp.303-311, 1996.

[21] W. Gu and K.E. Bollinger, "A self-tuning power system stabilizer for wide-range synchronous generator operation", *IEEE Transactions on Power Systems*, vol.4, no.3, pp.1191-1199, 1989.

[22] N.R. Chaudhuri, A. Domahidi, R. Majumder, B. Chaudhuri, P. Korba, S. Ray and K. Uhlen, "Wide-area power oscillation damping control in Nordic equivalent system", *IET Generation, Transmission and Distribution*, vol.4, no.10, pp.1139-1150, 2010.

[23] P. Zhang, D.Y. Yang, K.W. Chan and G.W. Cai, "Adaptive wide-area damping control scheme with stochastic subspace identification and signal time delay compensation", *IET Generation, Transmission and Distribution*, vol.6, no.9, pp.844-852, 2012.

[24]   N. Kishor, L. Haarla and J. Turunen, "Controller design with model identification approach in wide area power system", *in Proc. PowerTech 2013*, 16-20 June, 2013.

[25]   J. Hauer, "Robust damping controls for large power systems", *IEEE Control System Magazine*, vol.9, no.1, pp.12-18, 1989.

[26]   Z. Huang, N. Zhou, F. Tuffner, Y. Chen, D. Trudnowski, W. Mittelstadt, J. Hauer and J. Dagle, "Improving small signal stability through operating point adjustment", *in Proc. IEEE PES General Meeting 2010*, 25-29 July, 2010.

[27]   H. Zhenyu, Z. Ning, F. Tuffner and D. Trudnowski, "Use of modal sensitivity to operating conditions for damping control in power systems", *in Proc. 44th Hawaii International Conference on System Sciences (HICSS)*, 4-7 January, 2011.

[28]   J.J. Sanchez-Gasca (Ed.), "Identification of electromechanical modes in power systems", IEEE Task Force Report, Special Publication TP462, 2012.

[29]   J. Hauer, D. Trudnowski and G. Rogers, "Keeping an eye on power system dynamics", *IEEE Computer Applications in Power*, vol. 10, no.4, pp. 50-54, 2002.

[30]   A. Marinakis and M. Larsson, "Survey of measurement- and intelligence-based applications in power systems", *in Proc. PowerTech 2013*, 16-20 June, 2013.

[31]   H. Lee, J. Burns, W. Mittelstadt, K. Martin and J. Hauer, "Integrated dynamic information for the Western power system: WAMS analysis in 2005", Chapter 14 in the *Power Stability and Control* volume of *The Electric Power Engineering Handbook*, edition 2, edited by L.L. Grigsby, CRC Press, 2007.

[32]   F.K. Tuffner, "Computationally efficient weighted updating of statistical parameter estimates for time varying signals with application to power system identification", University of Wyoming, PhD Thesis, 2008.

[33]   L.A. Dosiek, "Estimating power system electromechanical modes and mode shapes using modern system identification techniques", University of Wyoming, PhD Thesis, 2010.

[34]   J.F. Hauer and J.G. DeSteese, "A tutorial on detection and characterization of special behavior in large electric power systems", Pacific Northwest National Laboratory, Report PNL-14655, 2004.

[35]   V. Venkatasubramanian, X. Liu, G. Liu, Q. Zhang and M. Sherwood, "Overview of wide-area stability monitoring algorithms in power systems

using synchrophasors", *in Proc. American Control Conference (ACC2011),* 29 June-1 July, 2011.

[36] H. Cole, On-line failure detection and damping measurement of aerospace structures by random decrement signatures", Report NASA CR-2205, 1973.

[37] J.W. Pierre, D.J. Trudnowski and M.K. Donnelly, "Initial results in electromechanical mode identification from ambient data", *IEEE Transactions on Power Systems*, vol.12, no.3, pp.1245-1251, 1997.

[38]   J.F. Hauer, D. Trudnowski and J. G. DeSteese, "A perspective on WAMS analysis tools for tracking of oscillatory dynamics", *in Proc. IEEE PES General Meeting 2007*, 24-28 June, 2007.

[39] M. Verhaegen and V. Verdult, *Filtering and system identification: A least squares approach*, Cambridge University Press, 2007.

[40] N. Zhou, J.W. Pierre and R.W. Wies, "Estimation of low-frequency electromechanical modes of power systems from ambient measurements using a subspace method", *in Proc. North American Power Symposium (NAPS) 2003*, 20-21 October, 2003.

[41] H. Ghasemi and C. Cañizares, "Oscillatory stability limit prediction using stochastic subspace identification", *IEEE Transactions on Power Systems*, vol.21, no.2, pp.736-745, 2006.

[42] M. Anderson, N. Zhou, and J. Pierre, "Bootstrap-based confidence interval estimates for electromechanical modes from multiple output analysis of measured ambient data", *IEEE Transactions on Power Systems*, vol.20, no.2, pp. 943-950, 2005.

[43] N. Zhou, J.W. Pierre and D. Trudnowski, "A bootstrap method for statistical power system mode estimation and probing signal selection", *in Proc. Power Systems Conference and Exposition 2006*, 29 October- 1 November, 2006.

[44] S.A. Nezam Sarmadi and V. Venkatasubramanian, "Electromechanical mode estimation using recursive adaptive stochastic subspace identification", *IEEE Transactions on Power Systems*, vol. 29, no.1, pp.349-358, 2014.

[45] L. Dosiek and J.W. Pierre, "An improved bootstrap method for electromechanical mode estimation using multivariate probability distributions", *in Proc. IEEE PES General Meeting 2011*, 24-29 July, 2011.

[46] J. Ni, C. Shen and F. Liu, "Estimation of the electromechanical characteristics of power systems based on a revised stochastic subspace

method and the stabilization diagram", *Science China, Technological Sciences*, vol.55, no.6, pp.1677-1687, 2012.

[47]   A. Mohammadi, H. Khaloozadeh and R. Amjadifard, "Power system critical eigenvalue estimation using flexibility of subspace system identification", *Electric Power Components and Systems*, vol.40, no.13, pp. 1501-1521, 2012.

[48]   N. Sandgren, P. Stoica and P. Babu, "On moving average parameter estimation", *in Proc. European Signal Processing Conference (EUSIPCO)*, 27-31 August, 2012.

[49]   M. Hemmingsson, O. Samujelsson, K.O.H. Pedersen and A.H. Nielsen, "Estimation of electro-mechanical mode parameters using frequency measurements", *in Proc. IEEE PES Winter Meeting 2001*, 28 January-01 February, 2001.

[50]   R.W. Wies, J.W. Pierre and D.J. Trudnowski, "Use of ARMA block processing for estimating stationary low-frequency electromechanical modes of power systems", *IEEE Transactions on Power Systems*, vol.18, no.1, pp.167-173, 2003.

[51]   D.J. Trudnowski, J.W. Pierre and N. Zhou, "Performance of three mode-meter block-processing algorithms for automated dynamic stability assessment", *IEEE Transactions on Power Systems*, vol.23, no.2, pp.680-690, 2008.

[52]   N. Zhou, J.W. Pierre, D.J. Trudnowski and R.T. Guttromson, "Robust RLS methods for online estimation of power system electromechanical modes", *IEEE Transactions on Power Systems*, vol.22, no.3, pp.1240-1249, 2007.

[53]   N. Zhou, D.J. Trudnowski, J.W. Pierre and W.A. Mittelstadt, "Electro-mechanical mode online estimation using regularized robust RLS methods", *IEEE Transactions on Power Systems*, vol.23, pp.1670-1680, 2008.

[54]   N. Zhou, D. Trudnowski and J. Pierre, "Mode initialization for on-line estimation of power system electromechanical modes", *in Proc. IEEE PES Power Systems Conference and Exposition 2009*, 15-18 March, 2009.

[55]   F.J. De Marco, J.A Apolinario, P.C. Pellanda and N. Martins, "Efficient online estimation of electromechanical modes in large power systems", *in Proc. IEEE 4th Latin American Symposium on Circuits and Systems (LASCAS) 2013*, 27 February-1 March, 2013.

[56]   R.W. Wies, J.W. Pierre and D.J. Trudnowski, "Use of least-mean squares (LMS) adaptive filtering technique for estimating low-frequency electromechanical modes in power systems", *in Proc. PES General Meeting 2004*, 6-10 June, 2004.

[57]   R.W. Wies, A. Balasubramanian and J.W. Pierre, "Adaptive filtering techniques for estimating electromechanical modes in power systems", *in Proc. PES General Meeting 2007*. 24-28 June, 2007.

[58]   R.W. Wies, A. Balasubramanian and J.W. Pierre, "Using adaptive step-size last mean squares (ASLMS) for estimating low-frequency electromechanical modes in power systems", *in Proc. International Conference on Probabilistic Methods Applied to Power Systems (PMAPS) 2006*, 11-15 June 2006.

[59]   R.W. Wies, A. Balasubramanian and J. W. Pierre, "Combining least mean squares adaptive filter and auto-regressive block processing techniques for estimating the low frequency electromechanical modes in power systems", *in Proc. IEEE PES General Meeting 2006*, 18-22 June, 2006.

[60]   W. Chao, L. Chao, W. Tian and Y. Tongwei, "Ambient signals based power system oscillation modes identification considering model order selection", *in Proc. IEEE PES General Meeting 2009*, 26-29 July, 2009.

[61]   N. Sugawara, H. Saitoh, Y. Akiyama and K. Sakamoto, "Determination of whitening filter order for estimation of electromechanical mode by regression model representing power system damping characteristics", *Electronics and Communications in Japan*, vol.97, no.10, 2014.

[62]   J.M. Seppänen, J. Turunen and L.C. Haarla, "Modal analysis of power systems with eigendecomposition of multivariate autoregressive models", *in Proc. PowerTech 2013*, 16-20 June, 2013.

[63]   J.M. Seppanen, J. Turunen, L.C. Haarla, M. Koivisto and N. Kishor, "Analysis of electromechanical modes using multichannel Yule-Walker estimation of a multivariate autoregressive model", *in Proc. IEEE PES Innovative Smart Grid Technologies Europe (ISGT EUROPE) 2013*, 6-9 October, 2013.

[64]   I. Moreno and A.R. Messina, "Adaptive tracking of system oscillatory modes using an extended RLS algorithm", *Electric Power Systems Research*, vol.114, pp.28–38, 2014.

[65]   I. Moreno and A.R. Messina, "Adaptive tracking of ambient system oscillations by nonstationary RLS techniques", *in Proc. IEEE PES General Meeting 2011*, 24-29 July, 2011.

[66] C. Wu and J. Zhang, "Applicability comparison of three algorithms for electromechanical mode identification", *in Proc. IEEE PES General Meeting 2012*, 22-26 July, 2012.

[67] G.R. Gajjar and S.A. Soman, "Power system oscillation modes identifications from wide area frequency measurement system", *in Proc. IEEE International Conference on Power System Technology (POWERCON) 2012*, 30 October-2 November, 2012.

[68] G.R. Gajjar and S.A. Soman, "Power system oscillation modes identifications: Guidelines for applying TLS-ESPRIT method", *International Journal of Emerging Electric Power Systems*, vol.14, no.1, pp.57-66, 2013.

[69] D. Jones, "Estimation of power system parameters", *IEEE Transactions on Power Systems,* vol.19, no.4, pp.1980-1989, 2004.

[70] D.I. Jones, "Dynamic system parameters for the National Grid", *IEE Proceedings in Generation, Transmission and Distribution*, vol.152, no.1, pp.53-60, 2005.

[71] H. Ghasemi and C.A. Canizares, "Confidence intervals estimation in the identification of electromechanical modes from ambient noise", *IEEE Transactions on Power Systems*, vol.23, no.2, pp.641-648, 2008.

[72] L. Dosiek, J.W. Pierre and J. Follum, "A recursive maximum likelihood estimator for the online estimation for the online estimation of electromechanical modes with error bounds", *IEEE Transactions on Power Systems*, vol.28, no.1, pp.441-451, 2013.

[73] P. Korba, M. Larsson and C. Rehtanz, "Detection of oscillations in power systems using Kalman filtering techniques", *in Proc. IEEE Conference on Control Applications 2003*, 23-25 June, 2003

[74] P. Korba, "Real-time monitoring of electromechanical oscillations in power systems: first findings", *IET Generation, Transmission and Distribution*, vol.1, no.1, 2007.

[75] J.C.H. Peng, N.C. Nair, Z. Jian and A.K. Swain, "Detection of lightly damped inter-area power oscillations using extended complex Kalman filter", *in Proc. IEEE Region 10 Conference (TENCON) 2009*, 23-26 January, 2009.

[76] J.C.H. Peng, A. Meads and N.C. Nair, "Parallel computing for smart power oscillation monitoring using synchrophasor measurements", *in Proc. IEEE Region 10 Conference (TENCON)*, 21-24 November, 2010.

[77] R.A. Wiltshire, G. Ledwich and P. O'Shea, "A Kalman filtering approach to rapidly detecting modal changes in power systems", *IEEE Transactions on Power Systems*, vol.22, no.4, pp.1698-1706. 2007.

[78] N. Kakimoto, M. Sugumi, T. Makino and K. Tomiyama, "Monitoring of interarea oscillation mode by synchronized phasor measurement", *IEEE Transactions on Power Systems*, vol.21, no.1, pp.260-268, 2006.

[79] G. Ledwich, "Decoupling for improved Modal Estimation", *in Proc. IEEE PES General Meeting 2007*, 24-28 June, 2007.

[80] G. Liu and V. Venkatasubramanian, "Oscillation monitoring from ambient PMU measurements by Frequency Domain Decomposition", *in Proc. IEEE International Symposium on Circuits and Systems (ISCAS) 2008*, 18-21 May, 2008.

[81] J.A. Ning, L. Xing and V. Venkatasubramanian, "Distributed real-time stability monitoring algorithms using synchrophasors", *in Proc. IREP Symposium 2013*, 25-30 August, 2013.

[82] J. Ning, X. Pan and V. Venkatasubramanian, "Oscillation modal analysis from ambient synchrophasor data using distributed frequency domain optimization", *IEEE Transactions on Power Systems*, vol.28, no.2, pp.2556-2566, 2013.

[83] A. Subramanian and J.W. Pierre, "Basic frequency and time domain least squares methods for system identification", *in Proc. North American Power Symposium (NAPS) 2006*, 17-19 September, 2006.

[84] M. Jonsson, M. Begovic and J. Daalder, "A new method suitable for real-time generator coherency determination", *IEEE Transactions on Power Systems*, vol.19, no.3, pp.1473-1482, 2004.

[85] F.K. Tuffner and J.W. Pierre, "Electromechanical modal behavior during a 48 hour interval using nonparametric methods", *in Proc. North American Power Symposium (NAPS) 2006*, 17-19 September, 2006.

[86] J.H. Choi, K.S. Shim, H.K. Nam, Y.C. Lim and S.R. Nam, "Parameter estimation method of low-frequency oscillating signals using discrete Fourier transforms", *Journal of Electrical Engineering and Technology*, vol.7, no.2, pp.163-170, 2012.

[87] L. Vanfretti, S. Bengtsson, V.S. Perić and J.O. Gjerde, "Effects of forced oscillations in power system damping estimation", *in Proc. IEEE International Workshop on Applied Measurements for Power Systems (AMPS) 2012*, 26-28 September, 2012.

[88] M. Glickman, P. O'Shea and G. Ledwich, "Estimation of modal damping in power networks", *IEEE Transactions on Power Systems*, vol.22, no.3, pp.1340-1350, 2007.

[89] L. Vanfretti, L. Dosiek, J.W. Pierre, D. Trudnowski, J.H. Chow, R. Garcia-Valle and U. Aliyu "Application of ambient analysis techniques for the estimation of electromechanical oscillations from measured PMU data in four different power systems", *European Transactions on Electrical Power*, vol.21, no.4, pp.1640-1656, 2011.

[90] Q. Liu, D. Despa, M. Watanabe and Y Mitani, "Analysis of oscillation characteristics for Japan Eastern 50 Hz power system based on Campus WAMS", *in Proc. International Conference on Advanced Power System Automation and Protection (APAP) 2011,* 16-20 October, 2011.

[91] G. Ledwich and E. Palmer, "Modal estimates from normal operation of power systems", *in Proc. IEEE PES Winter Meeting 2000*, 23-27 January, 2000.

[92] J.M. Seppänen, J. Turunen, M. Koivisto, N. Kishor and L.C. Haarla, "Modal analysis of power systems through natural excitation technique", *IEEE Transactions on Power Systems*, vol.29, no.4, pp.1642-1652, 2014.

[93]   T. Rauhala, K. Saarinen, M. Latvala, M. Laasonen and M. Uusitalo, "Applications of phasor measurement units and wide-area measurement system in Finland", *in Proc. PowerTech 2011*, 19-23 June, 2011.

[94] J. Thambirajah, N.F. Thornhill and B.C. Pal, "A multivariate approach towards interarea oscillation damping estimation under ambient conditions via independent component analysis and random decrement", *IEEE Transactions on Power Systems*, vol.26, no.1, pp.315-322, 2011.

[95] A. Messina, *Inter-area oscillations in power systems: A nonlinear and nonstationary perspective*, Springer, 2009.

[96] A.R. Messina and V. Vittal, "Nonlinear, non-stationary analysis of interarea oscillations via Hilbert spectral analysis", *IEEE Transactions on Power Systems*, vol.21, no.3, pp.1234-1241, 2006.

[97] A.R. Messina, V. Vittal and D. Ruiz-Vega, "Interpretation and visualization of wide-area PMU measurements using Hilbert analysis", *IEEE Transactions on Power Systems*, vol.21, no.4, pp.1763-1771, 2006.

[98] D. Laila, A. Messina and B. Pal, "A refined Hilbert–Huang transform with applications to interarea oscillation monitoring", *IEEE Transactions on Power Systems*, vol.24, no.2, pp.610-620, 2009.

[99] D.S. Laila, M. Larsson, B.C. Pal and P. Korba, "Nonlinear damping computation and envelope detection using Hilbert transform and its

application to power systems wide area monitoring", *in Proc. IEEE PES General Meeting 2009*, 26-29 July, 2009.

[100] AR. Messina, V. Vittal, G.T. Heydt and T.J. Browne, "Nonstationary approaches to trend Identification and denoising of measured power system oscillations", *IEEE Transactions on Power Systems*, vol.24, no.4, pp.1798-1807, November, 2009.

[101] A. Prince, N. Senroy and R. Balasubramanian "Targeted approach to apply masking signal-based empirical mode decomposition for mode identification from dynamic power system wide area measurement signal data", *IET Generation, Transmission and Distribution*, vol.5, no.10, pp.1025-1032, 2011.

[102] F.L. Zarraga, A.L. Rios, P. Esquivel and A.R. Messina, "A Hilbert-Huang based approach for on-line extraction of modal behavior from PMU data", *in Proc. North American Power Symposium (NAPS) 2009*, 4-6 October, 2009.

[103] X. Wang and Z. Yan, "Multiple scale identification of power system oscillations using an improved Hilbert-Huang transform", *in Proc. Power Systems Conference and Exposition 2009*, 15-18 March, 2009.

[104] J. Li, A. Xue, J. Wang, L. Ding, M. Wang, T. Bi and F. Han, "A new node contribution factors for the low frequency oscillations of power system based on the PMU's data and HHT", *in Proc. 5th International Conference on Critical Infrastructure (CRIS)*, 20-22 September, 2010.

[105] J.C.H. Peng and J.L. Kirtley, "An improved Empirical Mode Decomposition method for monitoring electromechanical oscillations", *in Proc. IEEE PES Innovative Smart Grid Technologies (ISGT) 2014*, 19-22 February, 2014.

[106] D.C. Yang, C. Rehtanz and Y. Li, "Analysis of low frequency oscillations using improved Hilbert-Huang transform", *in Proc. International Conference on Power System Technology (POWERCON) 2010*, 24-28 October, 2010.

[107] D.C. Yang, C. Rehtanz, Y. Li and D. Yang, "A hybrid method and its applications to analyze the low frequency oscillations in the interconnected power system", *IET Generation, Transmission and Distribution*, vol.7, no.8, pp.874-884, 2013.

[108] A.R. Messina and V. Vittal, "Extraction of dynamic patterns from wide-area measurements using empirical orthogonal functions", *IEEE Transactions on Power Systems,* vol. 22, no.2, pp.682-692, 2007.

[109] N. Zhou, D. Trudnowski, J.W. Pierre, S. Sarawgi and N. Bhatt, "An algorithm for removing trends from power-system oscillation data", *in Proc. IEEE PES General Meeting 2008,* 20-24 July, 2008.

[110] E. Eng and T. Kitakyushu, "Application of HHT for Oscillation Mode Analysis in Power System Based on PMU", *in Proc. 2nd International Conference on Electric Power and Energy Conversion Systems (EPECS)*, 15-17 November, 2011.

[111] J. Turunen, L. Haarla and T. Rauhala, "Performance of wavelet-based damping estimation method under ambient conditions of the power system", *in Proc. IREP Symposium 2013*, 25-30 August, 2013.

[112] J.Turunen, T. Rauhala and L.Haarla, "Selecting wavelets for damping estimation of ambient-excited electromechanical oscillations", *in Proc. IEEE PES General Meeting 2010*, 25-29 July, 2010.

[113] J. Turunen, "A Wavelet-based method for estimating damping in power systems", Aalto University, PhD Thesis, 2011.

[114] AR. Messina, P. Esquivel and F. Lezama, "Wide-area PMU data monitoring using spatio-temporal statistical models", *in Proc. IEEE PES Power Systems Conference and Exposition*, 20-23 March 2011.

[115] N. Senroy, "Generator coherency using the Hilbert-Huang Transform", *IEEE Transactions on Power Systems*, vol.23, no.4, pp.1701-1708, 2008.

[116] J.L. Rueda, C.A. Juárez, and I. Erlich, "Wavelet-based analysis of power system low-frequency electromechanical oscillations," *IEEE Transactions on Power Systems*, vol.26, no.3, pp.1733-1743, 2011.

[117] J.L. Rueda and I. Erlich, "Enhanced wavelet-based method for modal identification from power system ringdowns", *in Proc. PowerTech 2011*, 19-23 June, 2011.

[118] D.J. Vowles, M.J. Gibbard, D.K. Geddey and D. Bones, "Benchmark testing methodology for continuous modal-estimation algorithms", *in Proc. IEEE PES General Meeting 2009*, 26-29 July, 2009.

[119] D.J. Trudnowski and J.W. Pierre, "Overview of algorithms for estimating swing modes from measured responses", *in Proc. IEEE PES. General Meeting 2009*, 26-30 July, 2009.

[120] J. Thambirajah, E. Barocio and N.F. Thornhill, "Comparative review of methods for stability monitoring in electrical power systems and vibrating structures", *IET Generation, Transmission and Distribution*, vol.4, no.10, pp.1086-1103, 2010.

[121] J. Turunen, M. Larsson, B.C. Pal, N. F. Thornhill, L.C. Haarla, W.W. Hung, A.M. Carter and T. Rauhala, "Comparison of three electromechanical oscillation damping estimation methods", *IEEE Transactions on Power Systems*, vol.26, no.4, pp. 2398-2407, 2011.

[122] J. Turunen, M. Larsson and J. Thambirajah, "Recent developments in modal estimation of power system electromechanical oscillations", *in Proc. PowerTech 2011*, 19-23 June, 2011.

[123] J.W. Pierre, D. Trudnowski, M. Donnelly, N. Zhou, F.K. Tuffner and L. Dosiek, "Overview of system identification for power systems from measured responses", *in Proc. 16th IFAC Symposium on System Identification*, 11-13 July, 2012.

[124] E. Barocio, B.C. Pal and A.R. Messina, "Real-time monitoring as enabler for smart transmission grids", *in Proc. IEEE PES General Meeting 2011*, 24-29 July 2011.

[125] D.A. Gray, M.J. Gibbard and D.J. Vowles, "Characterization of ambient noise in electricity power grids", *in Proc. 8th International Symposium on Signal Processing and Its Applications*, 28-31 August, 2005.

[126] P. Korba and K. Uhlen, "Wide-area monitoring of electromechanical oscillations in the Nordic power system: practical experience", *IET Generation, Transmission and Distribution*, vol.4, no.10, pp.1116-1126, 2010.

[127] J. Turunen, M. Larsson, P. Korba, J. Jyrinsalo and L. Haarla, "Experiences and future plans in monitoring the inter-area power oscillation damping", *in Proc. IEEE PES General Meeting 2008,* 20-24 July, 2008.

[128] P. Korba and M. Larsson, "Wide-area monitoring of electromechanical oscillations in large electric power systems", *in Proc. IEEE PES General Meeting 2012*, 22-26 July, 2012.

[129] F. Galvan, A. Abur, S. Kai, M. Thomas, V. Venkatasubramanian and K.C. Rubal, "Implementation of synchrophasor monitoring at Entergy: Tools, training and tribulations", *in Proc. IEEE PES General Meeting 2012*, 22-26 July, 2012.

[130] A. Chakrabortty and A. Salazar, "Building a dynamic electromechanical model for the pacific AC intertie using PMU measurements", *in Proc. IEEE PES General Meeting 2010*, 25-29 July, 2010.

[131] L. Guoping, N. Jiawei, Z. Tashman, V. Venkatasubramanian and P. Trachian, "Oscillation Monitoring System using synchrophasors", *in Proc. IEEE PES General Meeting 2012*, 22-26 July, 2012.

[132] C.W. Taylor, D.C. Erickson, K.E. Martin, R.E. Wilson and V. Venkatasubramanian, "WACS-Wide-area stability and voltage control system: R&D and online demonstration", *Proceedings of the IEEE*, vol.93, no.5, pp.892-906, 2005.

[133] I.C. Decker, A.S. e Silva, M.N. Agostini, F.B. Prioste, B.T. Mayer and D. Dotta, "Experience and applications of phasor measurements to the Brazilian interconnected power system", *European Transactions on Electrical Power*, vol.21, no.4, pp.1557-1573, 2011.

[134] I.C. Decker, A.S. e Silva, R.J.G. da Silva, M.N. Agostini, N. Martins and F.B. Prioste, "System wide model validation of the Brazilian interconnected power system", *in Proc. IEEE PES General Meeting 2010*, 25-29 July, 2010.

[135] F.B. Prioste, A.S. e Silva and I.C. Decker, "Monitoring oscillations modes of the Brazilian interconnected power system using ambient data", *in Proc. PowerTech 2011*, 19-23 June, 2011.

[136] L. Vanfretti, et al, "Estimation of Eastern Denmark's electromechanical modes from ambient phasor measurement data", *in Proc. IEEE PES General Meeting 2010*, 25-29 July, 2010.

[137] D. Despa, Y. Mitani, L. Changsong and M. Watanabe, "PMU based monitoring and estimation of interarea power oscillation for Singapore-Malaysia interconnection power system", *in Proc. International Power and Energy Conference (IPEC) 2010*, 27-29 October, 2010.

[138] M. Larsson, L.F. Santos, A. Suranyi, W. Sattinger and R. Notter, "Monitoring of oscillations in the continental European transmission grid", *39th Annual Conference of the IEEE Industrial Electronics Society (IECON)*, 10-13 November, 2013.

[139] Z. Zhong, X. Chunchun, B.J. Billian, Z. Li, S.S. Tsai, R.W. Conners, V.A. Centeno, A.G. Phadke and L. Yilu, "Power system frequency monitoring network (FNET) implementation", *IEEE Transactions on Power Systems*, vol.20, no.4, pp.1914-1921, 2005.

[140] J.K. Wang, R.M. Gardner and Y. Liu, "Analysis of system oscillations using wide-area measurements", *in Proc. IEEE PES General Meeting 2006*, 18-22 June, 2006.

[141] Y. Yanzhu, R.M. Gardner and Y. Liu, "Oscillation analysis in Western Interconnection using distribution-level phasor measurements", *in Proc. IEEE PES General Meeting 2011*, 24-29 July, 2011.

[142] K. Uhlen, L. Warland, J.O. Gjerde, O. Breidablik, M. Uusitalo, A.B. Leirbukt and P. Korba, "Monitoring amplitude, frequency and damping of

power system oscillations with PMU measurements", *in Proc. IEEE PES General Meeting 2008,* 20-24 July, 2008.

[143] D.H. Wilson, "Continuous damping measurement for power system analysis", *in Proc. IEEE Russia PowerTech 2005*, 27-30 June, 2005.

[144] J. Zhang; C.Y. Chung, S. Zhang and Y. Han, "Practical wide area damping controller design based on ambient signal analysis", *IEEE Transactions on Power Systems*, vol.28, no.2, pp.1687-1696, 2013.

[145] H.R. Ali and N. Hoonchareon, "Real-time monitoring of inter-area power oscillation using Phasor Measurement Unit", *in Proc. 10th International Conference on Electrical Engineering/Electronics, Computer, Telecommunications and Information Technology (ECTI-CON)*, 15-17 May, 2013.

[146] D. Trudnowski, "Estimating electromechanical mode shape from synchrophasor measurements", *IEEE Transactions on Power Systems*, vol.23, no.3, pp.1188-1195, 2008.

[147] L. Dosiek, D.J. Trudnowski and J.W. Pierre, "New algorithms for mode shape estimation using measured data", *in Proc. IEEE PES General Meeting 2008,* 20-24 July, 2008.

[148] L. Dosiek, J.W. Pierre, D. Trudnowski and N. Zhou, "A channel matching approach for estimating electromechanical mode shape and coherence", *in Proc. IEEE PES. General Meeting 2009*, 26-30 July 2009.

[149] N. Zhou, Z. Huang, L. Dosiek, D. Trudnowski and J.W. Pierre, "Electromechanical mode shape estimation based on transfer function identification using PMU measurements," *in Proc. IEEE PES. General Meeting 2009*, 26-30 July 2009.

[150] H. Koseki and K. Yoshimura, "Estimation of electromechanical modes of power system using ARMA model based on cross spectrum", *in Proc. 2nd IEEE International Power and Energy Conference (PECon)*, 1-3 December, 2008.

[151] F. Tuffner, L. Dosiek and J. Pierre, "Weighted update method for spectral mode shape estimation from PMU measurements," *in Proc. IEEE PES General Meeting 2010*, 25-29 July, 2010.

[152] S. Han, Z. Xu and C. Wu, "Mode shape estimation and mode checking for IAO using correlation analysis technique," *Electric Power Systems Research*, vol.81, no.6, pp.1181-1187, 2011.

[153] J. Follum and L. Dosiek, "The empirical transfer function estimate method for determining mode shape", *in Proc. North American Power Symposium (NAPS) 2011*, 4-6 August, 2011.

[154] L. Dosiek and J.W. Pierre, "Estimating electromechanical modes and mode shapes using the multichannel ARMAX model", *IEEE Transactions on Power Systems*, vol.28, no.2, pp.1950-1959, May 2013.

[155] F.D. Freitas, N. Martins and L. Fernandes, "Reliable mode-shapes for major system modes extracted from concentrated WAMS measurements processed by a SIMO identification algorithm", *in Proc. IEEE PES General Meeting 2008,* 20-24 July, 2008.

[156] X. Pan, F. Shang and S. Yuan, "Wavelet-based electromechanical mode shape online identification from ambient data", *in Proc. 4th International Conference on Electric Utility Deregulation and Restructuring and Power Technologies (DRPT)*, 6-9 July, 2011.

[157] L. Dosiek, N. Zhou and J.W. Pierre, "Mode shape estimation algorithms under ambient conditions: A comparative review", *IEEE Transactions Power Systems*, vol.28, no.2, pp.779-787, 2013.

[158] J.F. Hauer, W.A. Mittelstadt, K.E. Martin, J.W. Burns, H. Lee, J.W. Pierre and D.J. Trudnowski, "Use of the WECC WAMS in wide-area probing tests for validation of system performance and modeling", *IEEE Transactions on Power Systems*, vol.24, no.1, pp.250-257, 2009.

[159] N. Zhou, J.W. Pierre and J.F. Hauer, "Initial results in power system identification from injected probing signals using a subspace method", *IEEE Transactions on Power Systems*, vol.21, no.3, pp.1266-1302, 2006.

[160] J.W. Pierre, N. Zhou, F.K. Tuffner, J.F. Hauer, D.J. Trudnowski and W.A. Mittelstadt, "Probing signal design for power system identification", *IEEE Transactions on Power Systems*, vol.25, no.2, pp.835-843, 2010.

[161] J.W. Pierre, N. Zhou; F.K. Tuffner, J. Hauer, D. Trudnowski and W.A. Mittelstadt, "Probing signal design for power system identification", *in Proc. IEEE PES General Meeting 2010*, 25-29 July, 2010.

[162] J. Zhang, C. Lu, S. Zhang and Y. Han, "Enhance and assess wide area probing responses in low level probing tests", *in Proc. IEEE PES General Meeting 2013*, 21-25 July, 2013.

[163] J. Zhang, C. Lu and Y. Han, "MIMO identification of power system with low level probing tests: Applicability comparison of subspace methods", *IEEE Transactions on Power Systems*, vol.28, no.3, pp.2907-2917, 2013.

[164] B. Mohammadi-Ivatloo, M. Shiroei and M. Parniani, "Online small signal stability analysis of multi-machine systems based on synchronized phasor measurements", *Electric Power Systems Research*, vol.81, no.10, pp.1887-1896, 2011.

[165] A. Chakrabortty and A. Salazar, "Building a dynamic electro-mechanical model for the Pacific AC intertie using distributed synchrophasor measurements", *European Transactions on Electrical Power*, vol.21, no.4, pp.1657-1672, 2011.

[166] A. Vahidnia, G. Ledwich, E. Palmer and A. Ghosh, "Identification of reduced models of power system areas using phasor measurement units", *Australasian Universities Power Engineering Conference (AUPEC) 2013*, 29 September-3 October, 2013.

[167] I. Kamwa and L. Gerin-Lajoie, "State-space system identification-Toward MIMO models for modal analysis and optimization of bulk power systems", *IEEE Transactions on Power Systems*, vol.15, no.1, pp.326-334, 2000.

[168] A. Vahidnia, G. Ledwich, E. Palmer and A. Ghosh, "Identification and estimation of equivalent area parameters using synchronised phasor measurements", *IET Generation, Transmission and Distribution*, vol.8, no.4, pp.697-704, 2014.

[169] C. Wu, C. Lu and Y. Han, "Closed-loop identification of power system based on ambient data," *Mathematical Problems in Engineering*, vol.2012, pp. 1-16, 2012.

[170] C. Wu, C. Lu and Y. Han, "Research on ambient signals based closed-loop identification of power system", *in Proc. IEEE PES General Meeting 2011*, 24-29 July, 2011.

[171] D. Sidorov, D. Panasetsky and V. Šmídl, "Non-stationary autoregressive model for on-line detection of inter-area oscillations in power systems", *in Proc. IEEE PES Innovative Smart Grid Technologies Europe (ISGT EUROPE)*, 11-13 October, 2010.

[172] M. Dehghani and S.K.Y. Nikravesh, "State-space model parameter identification in large-scale power systems", *IEEE Transactions on Power Systems*, vol.23, no.3, pp.1449-1457, 2008.

[173] O. Antoine and J.C. Maun, "Inter-area oscillations: Identifying causes of poor damping using phasor measurement units", *in Proc. IEEE PES General Meeting 2012*, 22-26 July, 2012.

[174] O. Gomez, and M.A. Rios, "Inter-area stability prediction index based on phasorial measurement", *in Proc. IEEE PES Innovative Smart Grid Technologies (ISGT) 2012*, 16-20 January, 2012.

[175] A. Mohammadi, "Detection of hopf bifurcation using eigenvalue identification", *in Proc. IV International Conference Problems of Cybernetics and Informatics (PCI)*, 12-14 September, 2012.

[176] U. Kerin, E. Lerch and G. Bizjak, "Monitoring and reporting of security of power system low-frequency oscillations", *Electric Power Components and Systems*, vol.38, no.9, pp.1047-1060, 2010.

[177] H. Ghasemi and C. Canizares, "On-line damping torque estimation and oscillatory stability margin prediction"*, IEEE Transactions on Power Systems*, vol.22, no.2, pp.667-674, 2007.

[178] A.R. Messina and V. Vittal, "A structural time series approach to modeling dynamic trends in power system data", *in Proc. IEEE PES General Meeting 2012*, 22-26 July, 2012.

[179] D. Yang, C. Rehtanz, Y. Li and D. Cai, "Identification of dominant oscillation mode using complex singular value decomposition method", *Electric Power Systems Research*, vol.83, no.1, pp.227-236, 2012.

[180] E. Cotilla-Sanchez, P.D.H. Hines and C.M. Danforth, "Predicting critical transitions from time series synchrophasor data", *IEEE Transactions on Smart Grid*, vol.3, no.4, pp.1832-1840, 2012.

[181] A.R. Messina, N. Reyes, I. Moreno and M.A. Pérez G., "A statistical data-fusion-based framework for wide-area oscillation monitoring", *Electric Power Components and Systems*, vol. 42, no.3-4, pp.396-407, 2014.

[182] S. Backhaus and Y. Liu, "Electromechanical wave Green's function estimation from ambient electrical grid frequency noise", *in Proc. 45th Hawaii International Conference on System Sciences (HICSS)*, 4-7 January, 2012.

[183] B. Kokanos, "Power system mode estimation using associate hermite expansion", Arizona State University, PhD Thesis, 2010.

[184] B. Kokanos, "Associate hermite expansion small signal mode estimation," *IEEE Transactions on Power Systems*, vol.25, no.2, pp.999-1006, 2010.

[185] I. Kamwa, A.K. Pradhan and G. Joos, "Robust detection and analysis of power system oscillations using the Teager-Kaiser energy operator", *IEEE Transactions on Power Systems*, vol.26, no.1, pp.323-333, 2011.

[186] O. Samuelsson, M. Hemmingsson, A.H. Nielsen, K.O.H. Pedersen and J. Rasmussen, "Monitoring of power system events at transmission and distribution level", *IEEE Transactions on Power Systems*, vol.21, no.2, pp.1007-1008, 2006.

[187] D.J. Vowles and M.J. Gibbard, "Illustration of an analytical method for selecting signals and locations for power system modal-estimators", *in Proc. IEEE PES General Meeting 2010*, 25-29 July, 2010.

[188] J. Zhang, C. Wu and Y. Han, "A power spectrum density based signal selection approach for electromechanical mode estimation," *in Proc. IEEE PES General Meeting 2012*, 22-26 July, 2012.

[189] A. Chakrabortty and C.F. Martin, "Optimal measurement allocation algorithms for parametric model identification of power systems", *IEEE Transactions on Control Systems Technology*, vol.22, no.5, pp. 1801-1812, 2014.

[190] L.P. Kunjumuhammed, R. Singh and B. C. Pal, "Robust signal selection for damping of inter-area oscillations", *IET Generation, Transmission and Distribution*, vol.6, no.5, pp.404-416, 2012.

[191] J.V. Ness, "Response of large power systems to cyclic load variations", *IEEE Transactions on Power Apparatus and Systems*, vol.PAS-85, no.7, pp.723-727, 1966.

[192] W. Xuanyin, L. Xiaoxiao and L. Fushang, "Analysis on oscillation in electro-hydraulic regulating system of steam turbine and fault diagnosis based on PSOBP", *Expert Systems with Applications*, vol.37, no.5, pp.3887-3892, 2010.

[193] N. Rostamkolai and R. Piwko, "Evaluation of the impact of alarge cyclic load on the LILCO power system using time simulation and frequency domain techniques", *IEEE Transactions on Power Systems*, vol.9, no.3, pp.1411-1416, 1994.

[194] C. Vournas and N. Krassas, "Analysis of forced oscillations in a multimachine power system", *in Proc. International Conference on Control 1991*, 25-28 March, 1991.

[195] Y. Yu, Y. Min, L. Chen and P. Ju, "The disturbance source identification of forced power oscillation caused by continuous cyclical load", *in Proc. 4th International Conference on Electric Utility Deregulation and Restructuring and Power Technologies (DRPT)*, 6-9 July, 2011.

[196] T.R. Nudell and A. Chakrabortty, "A graph-theoretic algorithm for localization of forced harmonic oscillation inputs in power system networks", *in Proc. American Control Conference (ACC2014)*, 4-6 June, 2014.

[197] R.B. Myers and D.J. Trudnowski, "Effects of forced oscillations on spectral-based mode-shape estimation", *in Proc. IEEE PES General Meeting 2013*, 21-25 July, 2013.

[198] J. Ning, S.A.N Sarmadi and V.M. Venkatasubramanian, "Two-level ambient oscillation modal estimation from synchrophasor measurements", *IEEE Transactions on Power Systems*, vol.30, no.6, pp.2913-2922, 2015.

[199] V.S. Perić, X. Bombois and L. Vanfretti, "Optimal signal selection for power system ambient mode estimation using a prediction error criterion", accepted for publication in *IEEE Transactions on Power Systems*, available online, 2015.

[200] V.S. Perić and L. Vanfretti, "Power system ambient mode estimation considering spectral load properties", *IEEE Transactions on Power Systems*, vol.29, no.3, pp.1133-1143, 2014.

[201] V.S. Perić, T. Bogodorova, A.N. Mete and L. Vanfretti, "Model order selection for probing-based power system mode estimation", *in Proc. Power and Energy Conference at Illinois (PECI)*, 20-21 February, 2015.

[202] V.S. Perić, M. Baudette, L. Vanfretti, J.O. Gjerde and S. Løvlund, "Implementation and Testing of a Real-Time Mode Estimation Algorithm using Ambient PMU Data", *in Proc. Power System Conference at Clemson University 2014*, 11-14 March, 2014.

[203] M. Dehghani, B. Shayanfard and A.R. Khayatian, "PMU ranking based on singular value decomposition of dynamic stability matrix", *IEEE Transactions on Power Systems*, vol.28, no.3, pp.2263-2270, 2013.

[204] S. Ranjana, S.C. Srivastava and S.N. Singh, "Optimal PMU placement method for complete topological and numerical observability of power system", *Electric Power Systems Research*, vol.80, no.9, pp.1154-1159, 2010.

[205] P.W. Sauer and M.A. Pai, *Power System Dynamics and Stability*, Stipes Publishing, 2007.

[206] P. Kundur, *Power System Stability and Control*, McGraw-Hill, 1994.

[207] G. Rogers, *Power System Oscillations*, Kluwer Academic Publishers, 1999.

[208] N. Jacobsen, P. Andersen and R. Brincker, "Applications of frequency domain curve-fitting in the EFDD technique", *in Proc. IMAC-XXVI: Conference and Exposition on Structural Dynamics*, 4-7 February 2008.

[209] L. Ljung, *System identification theory for the user*, Prentice Hall, 1999.

[210] A.V. Oppenheim and R.W. Schafer, *Discrete-time signal processing, Third edition*, Prentice-Hall, 2009.

[211] C. Park and S. Ko, "The hopping discrete Fourier transform", *IEEE Signal Processing Magazine* , vol.31, no.2, pp.135-139, 2014.

[212] Y. Chompoobutrgool, W. Li and L. Vanfretti, "Development and implementation of a Nordic grid model for power system small-signal and

transient stability studies in a free and open source software", *in Proc. IEEE PES General Meeting 2012*, 22-26 July 2012.

[213] Y. Chompoobutrgool and L. Vanfretti, "Identification of power system dominant inter-area oscillation paths", *IEEE Transactions on Power Systems*, vol.28, no.3, pp.2798-2807, 2013.

[214] J. Turunen, J. Thambirajah, M. Larsson, B.C. Pal, N.F. Thornhill, L.C. Haarla, W.W. Hung, A.M. Carter and T. Rauhala, "Comparison of three electromechanical oscillation damping estimation methods", *IEEE Transactions on Power Systems*, vol.26, no.4, pp.2398-2407, November, 2011.

[215] F. Galvan and P. Overholt. "The intelligent grid enters a new dimension", *T&D World*, July 28, 2014.

[216] L. Vanfretti, S. Bengtsson and J.O. Gjerde, "Preprocessing synchronized phasor measurement data for spectral analysis of electromechanical oscillations in the Nordic Grid", *European Transactions on Electrical Power*, vol.25, no.2, pp.348-358, 2015.

[217] P. Dorato, "On the inverse of linear dynamical systems", *IEEE Transactions on Systems Science and Cybernetics*, vol.5, no.1, pp.43-48, 1969.

[218] M.H. Hayes, *Statistical Digital Signal Processing and Modeling*, John Wiley & Sons Inc., 1996.

[219] D. Bertsimas and J. Tsitsiklis, *Introduction to Linear Optimization*, Athena Scientific, 1997.

[220] X. Liu, D. McSwiggan, T.B. Littler and J. Kennedy, "Measurement-based method for wind farm power system oscillations monitoring", *IET Renewable Power Generation*, vol.4, no.2, pp.198-209, 2010.

[221] N. Zhou, J.W. Pierre and J.F. Hauer, "Initial results in power system identification from injected probing signals using a subspace method", *IEEE Transactions on Power Systems*, vol.21, no.3, pp.1296-1302, 2006.

[222] J.W. Pierre, Z. Ning, F.K. Tuffner, J.F. Hauer, D.J. Trudnowski and W.A. Mittelstadt, "Probing signal design for power system identification", *IEEE Transactions on Power Systems*, vol.25, no.2, pp.835-843, 2010.

[223] M. Gevers, X. Bombois, R. Hildebrand and G. Solari, "Optimal experiment design for open and closed-loop system identification", *Communications in Information and Systems,* vol.11, no.3, pp.197-224, 2011.

[224] C.R. Rojas, J.S. Welsh, G.C. Goodwin and A. Feuer, "Robust optimal experiment design for system identification", *Automatica*, vol.43, no.6, pp.993-1008, 2007.

[225] U. Forssell and L. Ljung, "Some results on optimal experiment design", *Automatica*, vol.36, no.5. pp.749-756, 2000.

[226] X. Bombois, G. Scorletti, M. Gevers, P.M.J. Van den Hof and R. Hildebrand, "Least costly identification experiment for control", *Automatica*, vol.42, no.10, pp.1651-1662, 2006.

[227] X. Bombois and G. Scorletti, "Design of least costly identification experiments", *Journal Européen des Systèmes Automatisés*, vol.46. no.6-7, pp.587-610, 2012.

[228] Z. Fuzhen (ed.), *The Schur complement and its applications*, Springer, 2005.

[229] C.R. Rojas, J.S. Welsh, G.C. Goodwin, "A receding horizon algorithm to generate binary signals with a prescribed autocovariance", *in Proc. American Control Conference (ACC2007)*, 9-13 July, 2007.

[230] C.A. Larsson, P. Hägg and H. Hjalmarsson, "Generation of excitation signals with prescribed autocorrelation for input and output constrained systems", *in Proc. American Control Conference (ACC2013)*, 17-19 June, 2013.

[231] B.D.O. Anderson, K. Hitz and N. Diem, "Recursive algorithm for spectral factorization", *IEEE Transactions on Circuits and Systems*, vol.21, no.6, pp.742-750, 1974.

[232] P. Stoica and Y. Selen, "Model-order selection: A review of information criterion rules", *IEEE Signal Processing Magazine*, vol.21, no.4, pp.36-47, 2004.

[233] P.M.T. Broersen, "Automatic spectral analysis with time series models", *IEEE Transactions Instrumentation and Measurement*, vol.51, no.2, pp. 211-2016, 2002.

[234] V.Vittal (chaiman), "Transient stability test systems for direct stability methods", *IEEE Transactions Power Systems*, vol.7, no.1, pp.37-43, 1992.

[235] X. Tu, L.A. Dessaint and I. Kamwa, "Fast approach for transient stability constrained optimal power flow based on dynamic reduction method", *IET Generation, Transmission and Distribution*, vol.8, no.7, pp.1293-1305, 2014.

[236] A.G. Phadke and J.S. Thorp, *Synchronized phasor measurements and their applications*, Springer, 2008.

[237] L. Vanfretti, V.H. Aarstrand, M.S. Almas, V.S. Perić and J.O. Gjerde, "A software development toolkit for real-time synchrophasor applications", *in Proc. PowerTech 2013*, 16-20 June 2013.

[238] F. Wagner, R. Schmuki, T. Wagner and P. Wolstenholme, *Modeling software with finite state machines: A practical approach*, CRC Press, 2006.

[239] B. Friedlander and B. Porat, "The Modified Yule-Walker Method of ARMA Spectral Estimation", *IEEE Transactions on Aerospace and Electronic. Systems*, vol.AES-20, no.2, pp.158-173, 1984.

[240] V.K. Madisetti (Ed.), *The digital signal processing handbook*, CRC Press, 2009.

[241] M.S. Almas, M. Baudette, L. Vanfretti, S. Lovlund and J.O. Gjerde, "Synchrophasor network, laboratory and software applications developed in the STRONg^{2}rid project", *in Proc. IEEE PES General Meeting* 2014, 27-31 July 2014.

[242] A.M. Almutairi and J.V. Milanović, "Comparison of different methods for optimal placement of PMUs", *in Proc. IEEE PowerTech 2009,* 28 June - 2 July, 2009.

[243] NI Advanced PMU Development System, www.ni.com.

[244] K. Uhlen, L. Vanfretti, M.M. de Oliveira, A.B. Leirbukt, V.H. Aarstrand and J.O. Gjerde, "Wide-area power oscillation damper implementation and testing in the Norwegian transmission network", *in Proc. IEEE PES General Meeting 2012*, 22-26 July, 2012.

[245] L. Vanfretti, S. Bengtsson, V.S. Perić and J.O. Gjerde, "Spectral estimation of low-frequency oscillations in the Nordic grid using ambient synchrophasor data under the presence of forced oscillations", *in Proc. IEEE PowerTech 2013*, 16-20 June, 2013.

List of Publications

Journal Papers:

1. <u>Vedran S. Perić</u>, Xavier Bombois and Luigi Vanfretti, "Optimal Signal Selection for Power System Ambient Mode Estimation using a Prediction Error Criterion", Accepted for publication in *IEEE Transactions on Power Systems* (available online).

2. <u>Vedran S. Perić</u> and Luigi Vanfretti, "Power System Ambient Mode Estimation Considering Spectral Load Properties", *IEEE Transactions on Power Systems*, vol.29, no.3, pp.1133-1143, May 2014.

3. <u>Vedran S. Perić</u>, Andrija T. Sarić and Dejan I. Grabež, "Coordinated Tuning of Power System Stabilizers based on Fourier Transformation and Neural Networks", *Electric Power Systems Research*, vol.88, iss.1, pp.78-88, July 2012.

Journal Papers in preparation:

4. <u>Vedran S. Perić</u>, Xavier Bombois and Luigi Vanfretti, "Least Costly Probing Signal Design for Power System Mode Estimation", to be submitted.

Other Journal Papers (without Impact Factor):

1. Tijana Šćuk, Pavle Savković and <u>Vedran S. Perić</u>, "Realization of simulation framework for Oasys SCADA application development using Simulink toolbox", *Zbornik radova FTN*, vol.25. iss.5, pp.1038-1041, 2010. (in Serbian).

2. <u>Vedran S. Perić</u> and Andrija T. Sarić, "Small signal stability enhancement using power system stabilizers", *Elelektroprivreda*, vol.63, iss.3, pp.272-283, 2010. (in Serbian).

Books:

1. Dragan S. Popović, Zvonko Gorečan, Jugoslav Dujić, Veran Vasić and Vedran S. Perić, "Power system modeling", book published by *DMS Group*, Novi Sad, Serbia, October 2011. (in Serbian).

Conference Papers:

1. Vedran S. Perić, Tetiana Bogodorova, Ahmet N. Mete, Luigi Vanfretti, "Model Order Selection For Probing-based Power System Mode Estimation", *Power and Energy Conference at Illinois*, Champaign, IL, USA, 20-21 February 2015 (Presenter).

2. Vedran S. Perić, Maxime Baudette, Luigi Vanfretti, Jan O. Gjerde and Stig Løvlund, "Implementation and Testing of a Real-Time Mode Estimation Algorithm using Ambient PMU Data", *Power System Conference 2014*, Clemson, SC, USA, 11-14 March 2014. (Presenter).

3. Luigi Vanfretti, Vedran S. Perić and Jan O. Gjerde, "Estimation of Electromechanical Oscillations in the Nordic Grid using Ambient Data Analysis", *IEEE PES General Meeting 2013*, Vancouver, Canada, 21-25 July 2013. (Presenter and panelist).

4. Luigi Vanfretti, Sebastian Bengtsson, Vedran S. Perić and Jan O. Gjerde, "Spectral Estimation of Low Frequency Oscillations in the Nordic Grid using Ambient Synchrophasor Data under the Presence of Forced Oscillations", *IEEE PowerTech 2013*, Grenoble, France, 16-20 June 2013. (Presenter).

5. Luigi Vanfretti, Vemund .H. Aarstrand, Muhammad S. Almas, Vedran S. Perić and Jan O. Gjerde, "A Software Development Toolkit for Real-Time Synchrophasor Applications", *IEEE PowerTech 2013*, Grenoble, France, 16-20 June 2013.

6. Luigi Vanfretti, Sebastian Bengtsson, Vedran S. Perić and J. O. Gjerde, "Effects of Forced Oscillations in Power System Damping Estimation", *IEEE International Workshop on Applied Measurements for Power Systems (AMPS)*, Aachen, Germany, 26-28 September 2012. (Presenter).

7. Vladimir Lj. Ljubojev, Vedran S. Perić, Veran Vasić and Andrija T. Sarić, "Integration of Distributed Generation Models in Distribution Management System", *30th Conference CIGRE Serbia*, Zlatibor, Serbia, 29 May-3 June 2011. (in Serbian).

8. Ljubomir Francuski, Aleksandar Selakov, Filip Kulić and Vedran S. Perić, "One Solution of Implementation and Visualisation of Automatic

Generation Control", *14th Symposium CIGRE Serbia* - Tara, Serbia, 16-18 June, 2008. (in Serbian) (Presenter).

9. <u>Vedran S. Perić</u> and Filip Kulić, "Matlab based Simulation of Interconnected Power Systems", 14th Symposium CIGRE Serbia - Tara, Serbia, 16-18 June, 2008. (in Serbian). (Presenter).